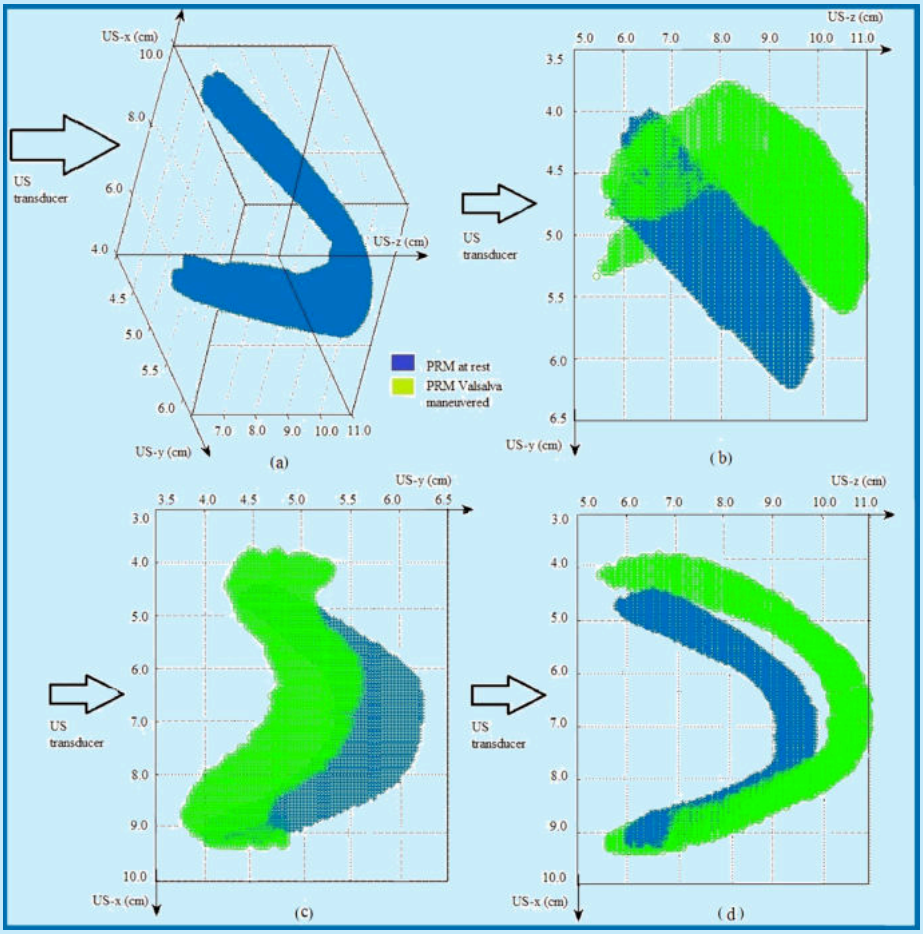

Deformation and strain imaging of puborectalis muscle using 3D ultrasound

Shreya Das

Deformation and strain imaging of puborectalis muscle using 3D ultrasound

Shreya Das

The research described in this thesis is carried out at the Medical Ultrasound Imaging Center, Radboud university medical center, Nijmegen, The Netherlands. The work presented in this thesis was carried out within the Radboudumc Research Institute for Medical Innovation. This research was financially supported by the project 'Gynecological Imaging using 3D Ultrasound (GYNIUS)' (Project No. 15301) from the Netherlands Organization for Scientific Research (NWO).

ISBN: 978-94-93330-90-0

Deformation and strain imaging of puborectalis muscle using 3D ultrasound

Proefschrift

ter verkrijging van de graad van doctor
aan de Radboud Universiteit Nijmegen
op gezag van de rector magnificus prof. dr. J. Sanders,
volgens besluit van het college voor promoties
in het openbaar te verdedigen op
maandag 1 juli 2024
om 14:30 uur precies

door

Shreya Das
geboren op 14 juli 1986
Kolkata, India

Promotoren

Prof. dr. ir. C.L. de Korte

Prof. dr. C.H. van der Vaart (UMC Utrecht)

Copromotor

Dr. ir. G.A.G.M. Hendriks

Manuscriptcommissie

Prof. dr. N. van Alfen

Prof. dr. J.P.W.R. Roovers (Amsterdam UMC)

Dr. ir. R.G.P. Lopata (Technische Universiteit Eindhoven)

Paranimfen

María Sofía Sappia

Joosje Marit Kee de Bakker

Dedicated to my mother

Contents

1 Introduction **13**

1.1 Brief description of female pelvic floor (PF) anatomy 14
1.1.1 Levator Ani muscles (LAM) 15
1.1.2 Puborectal muscle (PRM) 17
1.1.3 Female PF disorders 18

1.2 PF through the lens of evolution 20

1.3 Imaging of female PF 20
1.3.1 Transperineal ultrasound (TPUS) 21
1.3.2 Limitations of US imaging of PF muscles 23
1.3.3 Functional imaging of PRM: feasability using US 24
1.3.4 Strain imaging of PRM: clinical perspective 25
1.3.5 Pessary usage and strain imaging 26

1.4 Tissue characterization of PRM 26
1.4.1 Muscle trauma/damages in PRM through US 27
1.4.2 Statistical parameters 28

1.5 Outline of the thesis 28

Acknowledgements 31

References 32

2 3D ultrasound strain imaging of puborectalis muscle 37

2.1 Brief introduction . . . 39
2.1.1 Data acquisition . . . 39
2.1.2 Aim of the study . . . 40

2.2 Methods . . . 41
2.2.1 Volumetric data preparation . . . 41
2.2.2 Intervolume displacement estimations . . . 42
2.2.3 Tracking . . . 43
2.2.4 Strain calculations . . . 46

2.3 Results . . . 46
2.3.1 Acumulated displacement estimates . . . 47
2.3.2 Principal strain values . . . 48

2.4 Discussion . . . 52
2.4.1 Clinical significance . . . 57

2.5 Conclusion . . . 58

References . . . 59

Supplementary figures . . . 60

3 3D US strain imaging of PRM with & without unilateral avulsion 67

3.1 Brief introduction . . . 69
3.1.1 Data acquisition . . . 69
3.1.2 Aim of the study . . . 69

3.2 Methods . . . 70
3.2.1 Post-processing of US volumes . . . 70
3.2.2 Normalized ratio of strain percentage in PRM . . . 73
3.2.3 Statistical analysis . . . 74

3.3 Results . . . 75

3.4 Discussion . . . 78

3.4.1 Clinical significance 80
3.4.2 Limitations and future work 80

3.5 Conclusion 81

References 82

Supplementary figures 83

4 Functional assessment of ring pessary effect on avulsed PRM 93

4.1 Brief introduction 95
4.1.1 Data acquisition 96
4.1.2 Aim of the study 96

4.2 Methods 97
4.2.1 Post-processing of US volumes 97
4.2.2 Normalized ratio of median of strain percentages in PRM 97
4.2.3 Statistical methods 99

4.3 Results 99
4.3.1 Strain in unilateral avulsion of PRMs 101
4.3.2 Strain in bilateral avulsion of PRMs 102
4.3.3 Normalized strain ratio (NSR) 103

4.4 Discussion 104
4.4.1 Strain in avulsed PRMs prior to pessary fitting 105
4.4.2 Strain in avulsed PRMs post pessary fitting 106
4.4.3 Clinical significance 107
4.4.4 Limitations and future work 108

4.5 Conclusion 108

References 109

Supplementary figures 111

5 Tissue characterization of PRM from 3D US **119**

5.1 Brief introduction . . . 121
5.1.1 Data acquisition . . . 121
5.1.2 Aim of the study . . . 121

5.2 Materials and Methods . . . 122
5.2.1 Muscle segmentation and ROIs . . . 122
5.2.2 Mean echogenicity . . . 125
5.2.3 Shannon's entropy . . . 126
5.2.4 Statistical distribution of gray values . . . 127
5.2.5 Analysis procedure . . . 128

5.3 Results . . . 128
5.3.1 Mean echogenicity . . . 129
5.3.2 Entropy . . . 130
5.3.3 Shape parameter of Gamma distribution . . . 131

5.4 Discussion . . . 133
5.4.1 Physical interpretation . . . 134
5.4.2 Limitation and shortcomings . . . 135
5.4.3 Future directions . . . 136

5.5 Conclusion . . . 137

References . . . 138

Supplementary figures . . . 140

6 General discussion **147**

6.1 Research objectives . . . 148

6.2 Clinical and research workflows . . . 149

6.3 Brief background and contribution . . . 150
6.3.1 Contribution of the current work . . . 152

6.4 Clinical significance of functional information . . . 153

6.4.1 Implementation in clinic 154

6.5 Limitations 157

6.6 Future extensions 158

6.6.1 Clinical extensions 159

6.6.2 Algorithm improvement 160

6.7 Conclusion 160

References 161

7 Summary **163**

7.1 Summary in English 164

7.2 Samenvatting in Nederlands 167

Appendices of flowcharts 171

A. Volumetric data preparation 172

B. 'strainMUSIC' algorithm 174

C. Least Squared Strain Estimator (LSQSE) 176

D. Tracking (upgrade to the 'strainMUSIC' algorithm) 178

E. Filtering and principal strain 180

F. Displacement estimation (along muscle fibre direction) 182

G. Strain calculations (along muscle fibre direction) 185

H. Calculations for tissue characterization 187

List of Figures 189

List of Tables 199

List of Publications 200

Data management 202

PhD portfolio 204

Acknowledgements 206

About the author 210

Es gibt keinen Weg zum Glück,
Glücklichsein ist der Weg

Siddhartha Gautama Buddha

Knowledge can only be got in one
way, the way of experience;
there is no other way to know

Swami Vivekananda

Chapter 1

Introduction

1.1 Brief description of female pelvic floor (PF) anatomy

The earliest two scientific mentions about normal female pelvic floor (PF) anatomy which could be found from digital archives are from a graduation thesis from 1880, and a textbook of gynecology published in 1894 **[1-2]**. The authors described about the pelvic diaphragm and the levator ani muscle (LAM) among other anatomical structures of the PF. Actual mention of female PF disorder like prolapse and its treatment have also been found from historical documents from the Egyptian times **[3]**. It is interesting to ponder on the fact that there are still new discoveries to be made and studied on the female PF, just like human heart, brain etc.

The female PF can be divided into two compartments; the anterior and posterior compartment. The pubic bones and the pelvic sidewalls are the anterior and lateral boundaries. The posterior boundaries are the sacrum and the levator ani muscle (LAM), perineal body and the posterior vaginal wall. The organs which are included within these boundaries are the bladder and the urethra (within the anterior compartment) and the rectum and the anus (within the posterior compartment). The two compartments are shown in **Figure 1.1** and are divided by the flexible anterior vaginal wall. The anterior vaginal wall and the connective tissue that connects the pubovaginal portion of the LAM to the pubic bone and the LAM itself, all form the supportive system. Other than Besides the supportive system, otherPF muscles present in the PF consists of the urinary sphincter muscles located in the urethra and the anal sphincter muscles.

The external openings to the rectum and bladder are closed by the anal sphincter and the urethral sphincter muscles respectively. Increase in bladder pressure is counteracted by the urethral closure pressure to maintain continence. Urethral closure pressure is provided by the sphincter muscles of the urethra. This pressure must be more than the bladder pressure at all times to maintain continence. PF muscles are also active in counteracting the low atmospheric pressure with the higher PF pressure so as to maintain continence. That is why, these muscles maintain a constant tone **[4-6]**.

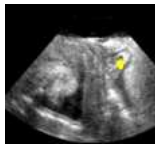

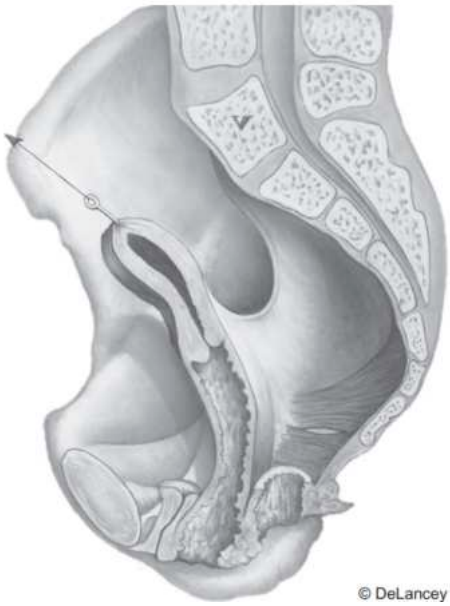

Figure 1.1: Sagittal view of the pelvic organs after removal of the bladder and rectum showing the anterior and posterior compartments separated by the uterus and vagina (deLancey book) [6]

1.1.1 Levator Ani muscles (LAM)

The individual muscles of the group of muscles called LAM is shown in **Figure 1.2** as well as in **Figure 1.3**.

The vagina and the entire pelvic cavity are closed by the LAM. Thus, the functions of the LAM come into play during rest as well as during activities like coughing, straining and jumping. Furthermore, LAM also have functions during pregnancy and childbirth, such as the following.

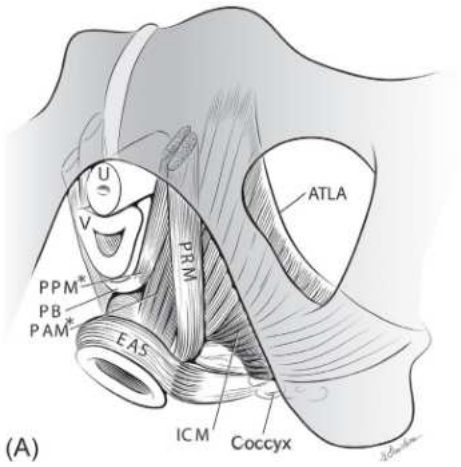

Figure 1.2: A schematic view of the levator ani muscles (LAM) from below after the vulvar structures and perineal membrane have been removed showing the urethra (U), vagina (V), external anal sphincter (EAS), puboanal muscle (PAM), perineal body (PB) uniting the two ends of the puboperineal muscle (PPM), iliococcygeal muscle (ICM) and puborectal muscle (PRM) [6]

- to support and counteract the weight of the overlying pelvic organs at rest
- to resist the forces created by the differences between atmospheric and abdominal pressures during activities. LAM maintains the pressures in the two compartments, namely the anterior and the posterior compartment. The lifting action of the LAM causes a balance of pressures between the two compartments making the pelvis an isobaric chamber
- to extend during vaginal delivery to allow for the passage of the baby

During rest, the baseline activity of intact LAM keeps the urogenital hiatus closed by compressing the vagina, urethra and rectum against the pubic bones, the PF organs in the cephalic direction. This continuous action closes the lumen of the vagina leading to support of the overlying PF organs **[11]**.

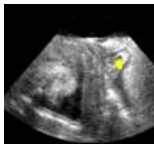

At maximum voluntary contraction of the LAM, the pubovisceral muscle and the PRM, further (additional to the baseline activity) compress the mid-urethra, distal vagina and rectum against the pubic bone distally and against abdominal pressure more proximally. It is this compressive force which is also detected by intra-vaginal palpation during maximum voluntary contraction **[11]**.

During pregnancy, the pelvic diaphragm extends support to the fetus. Thereafter, during vaginal delivery, LAM are extended, allowing the levator hiatus (LH) to widen during crowning **[7-10]**.

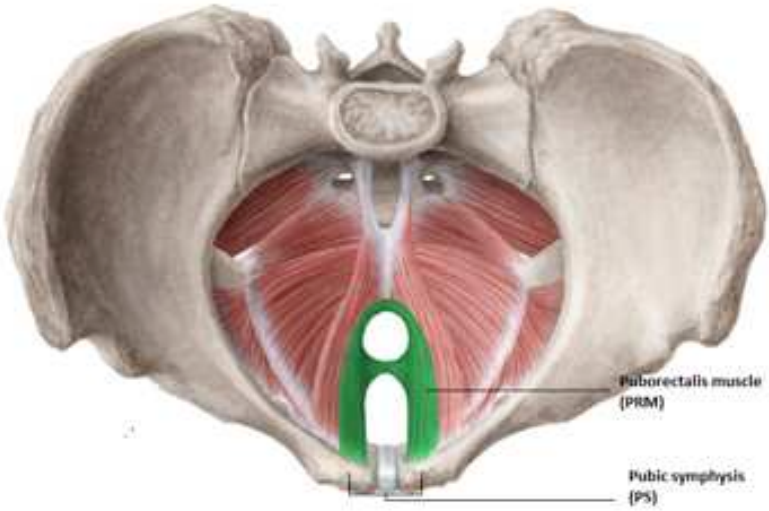

Figure 1.3: Female pelvic floor (PF) anatomy showing the surrounding pelvic bones and the levator ani muscle (LAM) forming the pelvic diaphragm. The puborectalis muscle (PRM) is highlighted in green [Kenhub (www.kenhub.com), illustrator: L. Znotina]

1.1.2 Puborectal muscle (PRM)

The supportive system of the PF, as mentioned earlier, consists of the connective tissues and LAM, forming the pelvic diaphragm. This pelvic diaphragm

as shown in **Figure 1.3** is located below the urethra and the vesical neck.

LAM can be sub-divided in three muscles; pubococcygeal or pubovisceral, iliococcygeal and puborectal muscle (PRM). PRM has its origin in the pubis and it forms the sling behind the rectum which is also its insertion point, as shown in green in **Figure 1.3**. The function of the PRM is to form the anorectal angle and thus closing of the PF. The posterior part of the LAM consisting of uterosacral ligaments and cardinal ligaments **[5]**.

Out of the three muscles of the LAM, the PRM has been chosen for strain analysis in this work because of the following reasons.

- During the second stage of labor the LAM extends and thus the PRM being part of the LAM also extends. The stretch ratio by which PRM extends have been determined by computer simulation and has been found to be 2.28 **[6]**. Since, the PRM consists of striated muscle fibers, it is susceptible to frequent damage when stretched to this extent **[6]**.

- In about half of all women after vaginal child delivery, there is substantial alteration of the functional anatomy affecting the PRM component of the LAM **[10, 12-14]**. The integrity of this structure, which encloses the largest potential hernial portal in the human body, is currently the best-defined etiological factor in the pathogenesis of prolapse **[12-13]**.

- PRM forms the outline of the LH when it is viewed in the top view in US data of the female PF **[53]**. Complete avulsion of the PRM, on one side or on both sides of the pubic symphysis (PS) can be reliably imaged in 3D US imaging.

1.1.3 Female PF disorders

LAM is extended by several times, allowing the LH to widen during crowning in vaginal delivery **[5-6, 7-9, 14]**. Vaginal delivery is associated with multiple LAM defects, all of which are risk factors for later-life pelvic floor dysfunction (PFD) **[7-9, 14-17]**. PFD comprises disorders that include stress urinary incontinence (SUI), overactive bladder, and pelvic organ prolapse (POP) **[17-18]**. SUI is involuntary urine leakage during physical exertion. When PF muscles are damaged or weakened, support for the pelvic organs is lost. Thus, the pelvic organs

descend **[6]**. This descent is known as prolapse or POP. It has been reported that the primary cause of these late-age PFD in women result from the damage of one or more muscles of the LAM **[10, 12-13]**. Damage and disconnection of PRM is known as avulsion. Avulsion is termed as unilateral when one of the connection of the PRM is disconnected and bilateral when both are disconnected.

The opening within the LAM, where the urethra and the vagina pass is known as the levator or urogenital hiatus, through which also prolapse occurs, as mentioned earlier. This hiatus is supported ventrally or anteriorly by the pubic bones and LAM and dorsally or posteriorly by the external anal sphincter muscle and perineal body.

The normal functioning of the PF muscles consists of prevention of urinary incontinence and pelvic organ prolapse (POP). Prevention of prolapse means uplifting of the load or pressure due to the PF organs. This is broadly the abdominal pressure, both during rest and contraction. When the muscles are damaged or weakened, the hiatus in the LAM can be pushed open and pelvic organs can descend to form different stages of prolapse. This leads to descend of one or both of the vaginal walls. The resultant misalignment creates a pressure differential between abdominal and atmospheric pressures. This difference is a deviation from the normal PF as an isobaric chamber.

As mentioned earlier, there are two compartments of the PF, anterior and posterior. Apical or central compartment is mentioned while describing POP. Dietz et al. mentions presence of this central compartment **[12]**. Thus, various forms of prolapse are briefly mentioned here according to their anatomical positions in the anterior, central (or apical) or posterior compartments. Descent of the anterior vaginal wall is associated with the anterior compartment. As a consequence, the bladder descends and is clinically termed as cystocele. Uterine prolapse is associated with the central compartment. And lastly, the descent of the posterior vaginal wall is clinically diagnosed as rectocele and is associated with the posterior compartment **[12]**.

1.2 PF through the lens of evolution

The problem of difficult childbirth and structure of the female PF cannot be overemphasized **[9, 12]**. Primates who are our evolutionary relatives, do not have to go through similar childbirth related difficulties. The question which arises is that why human childbirth is difficult, frequently leading to damage to maternal or baby's health. Thus, there are certain benefits to obstetrics and gynecology in understanding the evolutionary history of human traits and selective pressures that have shaped them **[76-81]**.

Anatomically, the human maternal birth canal is not uniformly shaped and vertical, unlike that of primates **[78]**. Due to humans' vertical PFs, it is believed that a small pelvic outlet and a narrow pelvis enhances support function of the PF. On the other hand, a broad pelvis is advantageous for childbirth but not suitable for carrying the heavy fetus throughout a long pregnancy **[76]**. Moreover, a study showing finite element analysis of lower birth canal also indicates that not only the size but also the shape of the birth canal plays a role **[76-77]**. Thus, humans have PFs and birth canals which are not uniform in orientation or in shape, due to the effects of evolution.

Both a broad pelvis during carrying the fetus and a narrow pelvis during parturition can lead to pelvic floor dysfunctions (PFDs). The source of PFD can be consequences of birth leading to injuries of the lower PF, as well as disorders expected to originate from strain to the muscles and connective tissues while carrying the heavy fetus. Although, these can also result from acute injuries during childbirth or otherwise **[77-78]**.

1.3 Imaging of female PF

Imaging plays a crucial role in diagnosis of PFD. Magnetic resonance imaging (MRI) and US are most frequently used to image the PF. These techniques are mainly used to image the anatomy to diagnose POP or stress urinary incontinence (SUI). Segmented organs in MRI or US images are used in biomechanical analysis to gain a better understanding of various pelvic organ disorders or specifically to diagnose POP **[19-22]**. Furthermore, biomechanical modeling

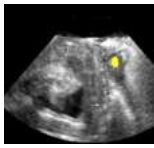

using imaging as input has been performed to enhance understanding of the anatomy of PF, aid in the diagnosis of various PF disorders and aid in surgical planning for corrective surgeries **[23-27]**. Diagnosis of POP and SUI is also performed using anatomically significant reference points (e.g., bladder neck and anorectal angle) **[28-29]**. Current studies also include deformation analysis of the PF, which has been performed using PF organs such as the bladder, uterus, and rectum **[30-32]**. Lastly, research on PF also includes vaginal tactile imaging, magnetic resonance defecography, and distribution representation of PF muscles in human motor cortex **[33-35]**. In summary, the PF as a whole has been investigated, however studies in the individual PF muscles remain scarce, especially considering the biomechanical behavior.

As mentioned before, current methods of detecting LAM damage involve imaging of it by US or MRI **[36-40]**. Dynamic imaging of PF muscles, enables characteristic measurements of certain anatomical structures. For example, by dynamic imaging of a healthy contraction, substantial shortening of the levator hiatus in the sagittal plane and a change in the angle between levator plane and pubic symphysis (PS) can be quantified. Other PF organs, including the uterus, bladder and urethra, will be displaced cranially as well as compression of the urethra, vagina and anorectal junction **[41]**. The deviations from these characteristic measurements of anatomical structures like the anorectal angle, perimeter of the PRM at contraction and hiatal area at Valsalva can be measured through imaging **[41-42]**. Diagnosis of PRM damage is dependent on these measurements together with the symptoms experienced by the woman **[46, 58]**. Imaging whether through US or MRI, is most effective when the damage in the muscle or the group of muscles is extensive and has been termed as macroscopically visible tears **[46]**. For example, unilateral or bilateral avulsions or disconnections from the bone are consequences of macroscopically visible tears in the PRM.

1.3.1 Transperineal ultrasound (TPUS)

Transperineal US (TPUS) is frequently used for female PF imaging because of its versatility and real time capabilities **[43]**. Moreover, many recent studies have tried to establish PFD through imaging methods, such as US, because of its ease of use, lack of ionizing radiation, minimal discomfort, the relatively short

period required for the acquisition of the required data, and low price **[7-10, 14, 36, 44-45]**. As mentioned earlier, US is chosen above MRI in this work, since good consistency between US and MRI in the imaging of PF muscles has been established as well as the fact that it allows deformation imaging **[44-45]**.

Minimum specifications for the US machine required to acquire transperineal US (TPUS) images is a B-mode capable 2D US system with cine-loop. For 3D or 4D images/volumes, these are required as well. The US transducer needed is usually a curved array transducer with the frequency range of 3.5 to 6 MHz **[65, 74]**.

TPUS can be obtained by placing the US transducer firmly against the symphysis pubis without causing significant discomfort, except in case of marked atrophy. Good contact of the transducer and tissues can be ensured by coughing which would part the labia, expel air bubbles and detritus **[65]**.

In 2D imaging of the PF, usually the mid-sagittal view is considered as a standard view. This view includes the symphysis anteriorly, the urethra, bladder neck, the vagina, cervix rectum and anal canal. **Figure 2.1c** show these organs as labeled. The position of the muscle of interest for this work, the PRM is situated beyond the anal canal. The orientation of the US image shown in this figure, with reference to anatomy is cranio-ventral aspects to the right and dorso-caudal to the left. The placement of the US transducer is shown below **[65]**.

However, it is not possible to image the LAM, and therefore the PRM reliably using only 2D US imaging because LAM lies in the axial plane. For visualization of the axial plane 3D US imaging is required. Furthermore, as in this work, we have focused on strain, we needed dynamic imaging. Thus 3D volumes over time or four dimensional (4D) imaging have been acquired. 4D imaging allows tracking of the PF muscles under contraction and under Valsalva maneuver **[74]**.

1.3.1.1 Three-dimensional (3D) US volumes showing PRM

Figure 1.4 and **Figure 1.5** illustrate US data acquired from a PF in the rest state, as imaged with TPUS. In this example, we can observe the PRM in the rest state. The US transducer was positioned against the PF while the women

were in supine position. Both the bone pubic symphysis (PS) and the PRM can be visualized with ease in the sagittal view, as can the surrounding PF organs. In **Figure 1.4a** and **Figure 1.5a** and **Figure 1.5b**, female PF can be seen in US in sagittal, axial and coronal views respectively. The intact PRM in these images can be seen as the yellow region bordering the anal canal. In **Figures 1.4c** the important organs like uterus and bladder and canals like urethra, vagina and anal canal have been outlined in colour.

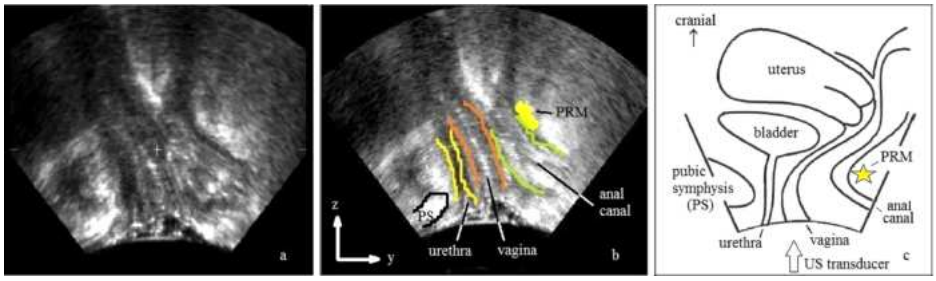

Figure 1.4: Pelvic floor (PF) anatomy and puborectalis muscle (PRM) as observed in transperineal ultrasound (US) data in sagittal view (z-y plane in US grid) (a) B-mode US image, (b) B-mode US image with labeling of the important PF organs, (c) Outline of the B-mode US in sagittal view with labeling of the PF organs [10, 57]

1.3.2 Limitations of US imaging of PF muscles

Macroscopically visible tears of the PF muscles like avulsion can be observed in US images, leading to altered functional properties. Although the presence of micro damages within the muscle can be indirectly assessed by observing the hiatal area during Valsalva maneuver, the change in contractile and functional properties cannot be derived **[46]**. This is due to the fact that in B-mode US, micro-structures like scar tissue within the muscle are difficult to image, without using any computational methods **[47–50]**.

To obtain information about the state of the PF muscles, US data are ac-

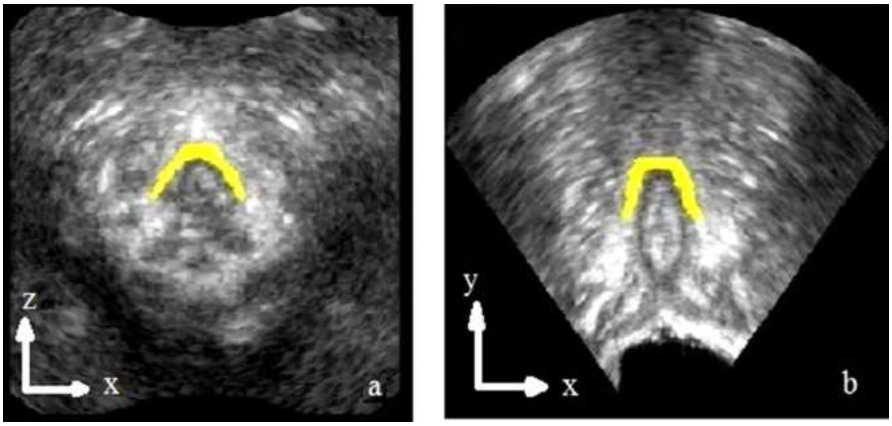

Figure 1.5: Transperineal ultrasound (US) data of the pelvic floor (puborectalis muscle in yellow) in; (a) axial view (z-x plane in US grid), (b) coronal view (y-x plane in US grid) [57]

quired of PF muscles from rest to contraction. Although information is obtained over the contraction cycle, only global geometrical changes can be determined from the static 2D images forming the 3D volumes. Therefore, the main limitation of the imaging of PRM through US is that only indirect information on the contractile properties can be deducted. Functional information cannot be deducted.

1.3.3 Functional imaging of PRM: feasability using US

US-based strain imaging can be used to investigate muscle movement and has been used extensively to understand and investigate the complex movements of the heart and skeletal muscles **[51-52]**. To date, US-based strain imaging is concentrated predominantly on two-dimensional (2D) US images, whereas the PF muscles are complex three-dimensional (3D) structures and their movements and deformations constitute an inherent 3D phenomenon. This means that the muscle has to be tracked over time in 3D as well. Furthermore, the deformation has to be quantified in multiple directions to fully characterize the deformation of the muscle and to be able to identify dysfunctional or dam-

aged parts of it. The hypothesis of this work state that it is possible to quantify strain 3D for the deforming PRM using a time series of volumetric US data. This work involved segmentation, displacement estimations, tracking and finally strain imaging of the PRM using 3D US data over time.

A certain analogy can be derived from cardiac strain imaging or echocardiography, to explain why deformation and strain imaging might be a good alternative to assess functional properties. Myocardial deformation is a result of contraction and relaxation of the cardiac muscle fibers in the longitudinal, circumferential and radial directions during a cardiac cycle along with a twisting motion. Therefore, the measurements of these deformations are typically made along these three axes, resulting in longitudinal, circumferential and radial strain, respectively. Strain is advantageous because it can assess regional as well as global function and is less susceptible to cardiac translation, imaging angle and measurement error than conventional systolic function measurements. 3D speckle tracking echocardiography allows for the simultaneous measurement of global and regional longitudinal, circumferential, and radial strains. Among these, global longitudinal strain is emerging as an important parameter of prognostic value in patients with (risk of) cardiovascular disease **[54-56]**.

In this work, strain has been calculated along the muscle fiber direction of the PRM. For the detection of PFD, it is crucial to have functional information on the PF muscles. Studies that have investigated the PF muscles conclude that the bio-mechanics of these muscles can be an indicator of PF disorders such as POP **[60-61]**. Quantifying the deformation of the muscle provides functional information of the PRM.

1.3.4 Strain imaging of PRM: clinical perspective

Computer simulation of vaginal birth shows that PRM has to stretch up to 2.28 times **[4-5]**. Due to this elongation, the entire LAM including the PRM can get damaged leading to pelvic floor dysfunction **[2-5, 25]**. The prevalence of PFD increases with age **[6]**. The extent of induced damage determines the inability of the LAM to provide support to the PF organs, which can lead to POP **[14-15]**.

It can be mentioned that the potential clinical value is two-fold. Firstly, in-

formation about the extent and the location of PRM damage would determine whether the first line of treatment, i.e., physiotherapy would be effective. It would also determine the necessity of training specific muscles like PRM, depending on whether it is functionally damaged. Also, recognizing that there is severe structural damage may well change the policy of having PF muscle training in every women with PF disorders. Secondly, when clinicians look at regenerative action for the muscle after delivery, it would be possible to determine if there has been functional improvement of the muscle after training. Functional improvement would show a change in strain in the muscle as observed from before to after training.

1.3.5 Pessary usage and strain imaging

POP is a common condition among women with defects in LAM. It is often observed that these women generate less vaginal closure force during a maximum contraction than controls **[5]**. Symptomatic POP is frequently treated by placement of a pessary. Pessaries are an inexpensive, simple, low risk, and effective conservative treatment for POP **[62–64]**. The effectiveness of pessary fitting is determined by a questionnaire which is answered by the woman, post pessary fitting and usage. This questionnaire is qualitative rather than quantitative. It has been previously shown that successful pessary fitting is associated with the size of the hiatal area. Thereafter, contractibility of the PRM improved after pessary fitting **[66-67]**. This improvement was shown by a strain ratio **[68]**. Although US is an accepted imaging modality used for visualizing female PF muscles for years, functional information about PF muscles after pessary fitting, through US remains limited **[36-37, 65, 75]**. Thus, strain imaging could be performed both prior to and post pessary fitting, in order to determine the effectiveness of the fitting by analyzing the actual quantitative functional information from the PRM.

1.4 Tissue characterization of PRM

PRM tissue composition also plays a role in it's functionality, thus alteration of this composition would also lead to altered functionality. Muscle damage to LAMs can be microscopic leading to changes in microstructural composition or

macroscopic damage. One of the most common forms of macroscopic damage of the LAMs is known as avulsion.

Unilateral or bilateral avulsion can be diagnosed according to Dietz (2010) by palpation or digital assessment of the PF muscle (PFM) via the vaginal or transanal route **[65]**. The alternative, more reproducible way of diagnosing such trauma is with the aid of US imaging. Avulsion of the PRM from the bone can occur with or without microdamage within the muscle. This microdamage could be indicative of the extent of damage of the PRM. This is due to the fact that in B-mode US, only the macrostructures are imaged and the microstructures, such as scar tissue, within the PRM are difficult to image without using computational methods **[47]**.

1.4.1 Muscle trauma/damages in PRM through US

Woodhouse and McNally (2011) have presented that strains, tears, and lacerations are muscle injuries which are most commonly caused by over-elongation of muscles in the body **[69]**. These indirect muscle injuries have altered microstructural composition. Recurrent and/or severe muscle injury can also leave behind intramuscular scars which appear as hyperreflective foci or hyper-echogenic areas. These injuries can alter the functional dynamics of the surrounding muscle **[69]**. Such an example of a hyperechogenic region due to muscle injury can be seen in **Figure 1.6**.

The presence of an avulsion of the PRM could result in a change in the statistical distribution of gray values in a B-mode US image of the PRM. Thus apart from strain analysis, statistical analysis on the gray values in the US volumes, might be a suitable tool to examine whether differences between intact and avulsed PRMs can be quantified.

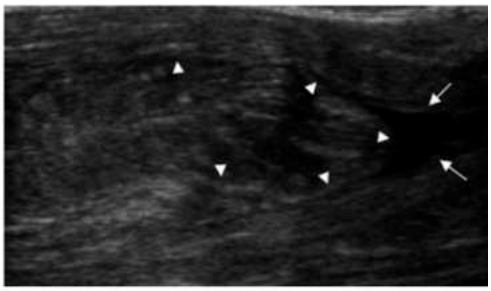

Figure 1.6: Rectus femoris showing partial tears (arrowheads) and a small hematoma (arrows). Permission has been granted by the publisher to use this image [69]

1.4.2 Statistical parameters

In US imaging, US waves are absorbed, reflected, or scattered by structures in the human body. The brightness of the pixels in a B-mode US image depends on the strength of the returning echo **[49, 70]**. Microstructural composition of muscle tissue can be assessed indirectly by measuring echogenicity as representation of the reflective properties of the tissue **[71]**. It has already been found that there are changes in the mean echogenicity (MEP) and levator hiatal area after vaginal delivery using 2D US images at rest and at contraction **[59, 72]**. In the current work, we will investigate if MEP, Shannon's entropy as well as shape parameter of Gamma distribution calculated from 3D images, can be used for characterizing tissue damage of the PRM **[73]**.

1.5 Outline of the thesis

The principal aim of the entire work is to derive functional information about the deforming PRM through quantifying tissue strain. This functional information is intended as an aid to the clinician to assess the condition of the muscle. Presence of avulsion can already be detected by the clinician from US images. Yet, additional functional information would show how functional the PRM still is in the avulsed end, as well as its effect on the entire PRM.

US data which has been used in this work is acquired in the same way as is needed for clinical diagnosis. Thus, to be able to implement this work in the clinic, additional apparatus or ethical approval would not be required. Patient consent is only required to be able to use the acquired data for research purposes. This consent have been acquired from all the women whose US images have been included in this work. The algorithm in its current form can provide strain results one day after the calculations have been started. This can be achieved due to the usage of a graphics card for the calculations.

Chapter 1

This **Introduction** is **Chapter 1** of the thesis and it is the general introduction to the topic of female PF muscles and strain imaging to derive functional information about the muscle, particularly PRM.

Chapter 2

In **Chapter 2**, the algorithm to calculate strain, including tracking have been explained. This algorithm has been utilized to estimate displacement estimates from the deforming intact PRMs. Deformations of the muscle include rest and contraction as well as rest and Valsalva maneuver. Principal strain has been calculated for these two deformations. The methods to obtain the results have been explained both in Chapter 2 and the respective flowcharts have been shown in **Appendix A, B, C, D** and **E**.

Chapter 3

In **Chapter 3**, improvement of the previously mentioned algorithm has been described calculating the strain in the muscle fiber direction. Women with intact PRMs and PRMs with unilateral avulsions were included and strain during contraction of the PRMs were investigated. The methods to obtain the results of **Chapter 3** have been explained both in the chapter itself and the respective flowcharts have been shown in **Appendix F** and **G**.

Chapter 4

Chapter 4 is about strain in avulsed PRMs before and after pessary fitting. Women with both unilateral and bilateral avulsions have been included. The methods to obtain the results have been briefly explained in **Chapter 4** and the flowcharts have been shown in **Appendix F** and **G**.

Chapter 5

The results of tissue characterization have been shown in **Chapter 5**. In this chapter, women with intact PRMs and PRMs with unilateral avulsion have been included. The methods to obtain the results have been explained in **Chapter 5** and the flowchart have been shown in **Appendix H**.

Chapter 6 and 7

Finally, in **Chapter 6**, a general discussion have been provided. This chapter decribes the research objectives, developed methods and future prospectives for the entire work.

General discussion of the thesis is followed by a short summary of the entire thesis, in English followed by in Dutch. This summary forms **Chapter 7**; the final chapter of this thesis.

Acknowledgements

Research leading to all the publications as mentioned in **List of Publications** has been supported by the project ”Gynecological Imaging using 3D Ultrasound **(GYNIUS)**” (Project No. 15301) from the Netherlands Organization for Scientific Research (NWO).

We thank Philips Healthcare (Bothell, WA, USA) for providing the EPIQ 7G US system and license for the proprietary software QLAB (Philips Healthcare, Andover, MA, USA) for data acquisition and conversion respectively.

We would also like to thank NVIDIA (Santa Clara, CA, USA) for donating a Titan V graphics card for our work.

References

[1] D. B. Hart, The structural anatomy of the female pelvic floor, vol. 20. Maclachlan; Stewart, 1880.

[2] J. C. Wood, A text-book of gynecology. Boericke & Tafel, 1894.

[3] S. M. Shah, A. H. Sultan, and R. Thakar, "The history and evolution of pessaries for pelvic organ prolapse," International Urogynecology Journal, vol. 17, pp. 170–175, 2006.

[4] K.-C. Lien, B. Mooney, J. O. DeLancey, and J. A. Ashton-Miller, "Levator ani muscle stretch induced by simulated vaginal birth," Obstetrics and gynecology, vol. 103, no. 1, p. 31, 2004.

[5] J. O. DeLancey et al., "Comparison of levator ani muscle defects and function in women with and without pelvic organ prolapse," Obstetrics & gynecology, vol. 109, no. 2 Part 1, pp. 295–302, 2007.

[6] J. DeLancey, L. Hoyte, and M. Damaser, "Biomechanics of the female pelvic floor," 2016.

[7] A. Tubaro, H. Koelbl, R. Laterza, V. Khullar, and C. de Nunzio, "Ultrasound imaging of the pelvic floor: Where are we going?" Neurourology and Urodynamics, vol. 30, no. 5, pp. 729–734, 2011.

[8] A. A. Dieter, M. F. Wilkins, and J. M. Wu, "Epidemiological trends and future care needs for pelvic floor disorders," Current opinion in obstetrics & gynecology, vol. 27, no. 5, p. 380, 2015.

[9] P. Dixit, K. Shek, and H. Dietz, "How common is pelvic floor muscle atrophy after vaginal childbirth?" Ultrasound in Obstetrics & Gynecology, vol. 43, no. 1, pp. 83–88, 2014.

[10] K. Shek and H. Dietz, "Pelvic floor ultrasonography: An update," Minerva Ginecol, vol. 65, no. 1, pp. 1–20, 2013.

[11] J. A. Ashton-Miller and J. O. DeLancey, "On the biomechanics of vaginal birth and common sequelae," Annual review of biomedical engineering, vol. 11, pp. 163–176, 2009.

[12] H. P. Dietz, "Pelvic floor trauma in childbirth," Australian and New Zealand Journal of Obstetrics and Gynaecology, vol. 53, no. 3, pp. 220–230, 2013.

[13] H. Dietz and J. Simpson, "Levator trauma is associated with pelvic organ prolapse," BJOG: An International Journal of Obstetrics & Gynaecology, vol. 115, no. 8, pp. 979–984, 2008.

[14] K. Shek and H. Dietz, "Intrapartum risk factors for levator trauma," BJOG: An International Journal of Obstetrics & Gynaecology, vol. 117, no. 12, pp. 1485–1492, 2010.

[15] O. Dalpiaz and P. Curti, "Role of perineal ultrasound in the evaluation of urinary stress incontinence and pelvic organ prolapse: A systematic review," Neurourology and Urodynamics: Official Journal of the International Continence Society, vol. 25, no. 4, pp. 301–306, 2006.

[16] K. J. Notten, T. F. Vergeldt, S. M. van Kuijk, M. Weemhoff, and J.-P. W. Roovers, "Diagnostic accuracy and clinical implications of translabial ultrasound for the assessment of levator ani defects and levator ani biometry in women with pelvic organ prolapse: A systematic review," Urogynecology, vol. 23, no. 6, pp. 420–428, 2017.

[17] D. Bedretdinova, X. Fritel, H. Panjo, and V. Ringa, "Prevalence of female urinary incontinence in the general population according to different definitions and study designs," European urology, vol. 69, no. 2, pp. 256–264, 2016.

[18] C. C. de Araujo, S. A. Coelho, P. Stahlschmidt, and C. R. Juliato, "Does vaginal delivery cause more damage to the pelvic floor than cesarean section as determined by 3D ultrasound evaluation? A systematic review," International urogynecology journal, vol. 29, pp. 639–645, 2018.

[19] A. Akhondi-Asl, L. Hoyte, M. E. Lockhart, and S. K. Warfield, "A logarithmic opinion pool based STAPLE algorithm for the fusion of segmentations with associated reliability weights," IEEE transactions on medical imaging, vol. 33, no. 10, pp. 1997–2009, 2014.

[20] S. Onal, S. K. Lai-Yuen, P. Bao, A. Weitzenfeld, and S. Hart, "MRI-based segmentation of pubic bone for evaluation of pelvic organ prolapse," IEEE Journal of Biomedical and Health Informatics, vol. 18, no. 4, pp. 1370–1378, 2014.

[21] S. Onal, X. Chen, S. Lai-Yuen, and S. Hart, "Segmentation of sacral curve on dynamic MRI for diagnosis of pelvic organ prolapse," in 2016 IEEE-EMBS international conference on biomedical and health informatics (BHI), 2016, pp. 90–93.

[22] I. Nekooeimehr, S. Lai-Yuen, P. Bao, A. Weitzenfeld, and S. Hart, "Automated tracking, segmentation and trajectory classification of pelvic organs on dynamic MRI," in 2016 38th annual international conference of the IEEE engineering in medicine and biology society (EMBC), 2016, pp. 2403–2406.

[23] N. Wang, Y. Wang, H. Wang, B. Lei, T. Wang, and D. Ni, "Auto-context fully convolutional network for levator hiatus segmentation in ultrasoudn images," in 2018 IEEE 15th international symposium on biomedical imaging (ISBI 2018), 2018, pp. 1479–1482.

[24] M. Damser et al., "Development of a virtual reality model of the normal female pelvic floor," in Proceedings of the second joint 24th annual conference and the annual fall meeting of the biomedical engineering society][engineering in medicine and biology, 2002, vol. 3, pp. 2395–2396.

[25] M. Parikh et al., "Methods of development of a three dimensional model of the normal female pelvic floor," in Proceedings of the second joint 24th annual conference and the annual fall meeting of the biomedical engineering society][engineering in medicine and biology, 2002, vol. 3, pp. 2414–2415.

[26] M.-E. Bellemare, N. Pirro, L. Marsac, and O. Durieux, "Toward the simulation of the strain of female pelvic organs," in 2007 29th annual international conference of the IEEE engineering in medicine and biology society, 2007, pp. 2752–2755.

[27] F. Pu et al., "Reconstruction of three-dimensional model of normal female pelvic cavity based on magnetic resonance imaging," in 2007 IEEE/ICME international conference on complex medical engineering, 2007, pp. 732–735.

[28] S.-L. Lee, E. Tan, V. Khullar, W. Gedroyc, A. Darzi, and G.-Z. Yang, "Physical-based statistical shape modeling of the levator ani," IEEE transactions on medical imaging, vol. 28, no. 6, pp. 926–936, 2009.

[29] A. Basarab et al., "Motion estimation in ultrasound imaging applied to the diagnostic of pelvic floor disorders," in 2011 annual international conference of the IEEE engineering in medicine and biology society, 2011, pp. 8058–8061.

[30] C. Czyrnyj, M. Labrosse, and L. McLean, "Urogenital kinematics mesaured in the sagittal plane using a novel ultrasound image processing approach," in 2016 IEEE EMBS international student conference (ISC), 2016, pp. 1–4.

[31] M. Rahim, M.-E. Bellemare, N. Pirró, and R. Bulot, "A shape descriptors comparison for organs deformation sequence characterization in mri sequences," in 2009 16th IEEE international conference on image processing (ICIP), 2009, pp. 1069–1072.

[32] A. C. Ogier, S. Rapacchi, A. Le Troter, and M.-E. Bellemare, "3D dynamic MRI for pelvis observation-a first step," in 2019 IEEE 16th international symposium on biomedical imaging (ISBI 2019), 2019, pp. 1801–1804.

[33] V. Egorov, H. Van Raalte, and A. P. Sarvazyan, "Vaginal tactile imaging," IEEE Transactions on Biomedical Engineering, vol. 57, no. 7, pp. 1736–1744, 2010.

[34] C. L. Costa, M. A. Batista, D. Guliato, T. A. Macedo, and C. Z. Barcelos, "MR defecography registration for computer-aided diagnosis of pelvic floor disorder," in 2014 IEEE international conference on systems, man, and cybernetics (SMC), 2014, pp. 1039–1044.

[35] M. S. Yani et al., "Distributed representation of pelvic floor muscles in human motor cortex," Scientific reports, vol. 8, no. 1, p. 7213, 2018.

[36] H. Dietz, "Ultrasound imaging of the pelvic floor. Part i: Two-dimensional aspects," Ultrasound in Obstetrics and Gynecology, vol. 23, no. 1, pp. 80–92, 2004.

[37] H. Dietz, "Ultrasound imaging of the pelvic floor. Part II: Three-dimensional or volume imaging," Ultrasound in Obstetrics and Gynecology: The Official Journal of the International Society of Ultrasound in Obstetrics and Gynecology, vol. 23, no. 6, pp. 615–625, 2004.

[38] S. A. Taylor, "Imaging pelvic floor dysfunction," Best Practice & Research Clinical Gastroenterology, vol. 23, no. 4, pp. 487–503, 2009.

[39] Y. Ozog, J. Deprest, K. Haest, F. Claus, D. De Ridder, and E. Mazza, "Calculation of membrane tension in selected sections of the pelvic floor," International urogynecology journal, vol. 25, pp. 499–506, 2014.

[40] K. J. Notten et al., "Translabial three-dimensional ultrasonography compared with magnetic resonance imaging in detecting levator ani defects," Obstetrics & Gynecology, vol. 124, no. 6, pp. 1190–1197, 2014.

[41] X. Wang, M. Ren, Y. Liu, T. Zhang, and J. Tian, "Perineal ultrasound versus magnetic resonance imaging (MRI) detection for evaluation of pelvic diaphragm in resting state," Medical Science Monitor: International Medical Journal of Experimental and Clinical Research, vol. 24, p. 4449, 2018.

[42] C. S. Calderwood, A. Thurmond, A. Holland, B. Osmundsen, and W. T. Gregory, "Comparing 3D ultrasound to 3D MRI in the detection of levator ani defects," Female pelvic medicine & reconstructive surgery, vol. 24, no. 4, p. 295, 2018.

[43] H. P. Dietz, "Female pelvic floor dysfunction—an imaging perspective," Nature Reviews Gastroenterology & Hepatology, vol. 9, no. 2, pp. 113–121, 2012.

[44] Y. Yan et al., "Combination of tomographic ultrasound imaging and three-dimensional magnetic resonance imaging-based model to diagnose postpartum levator avulsion," Scientific Reports, vol. 7, no. 1, p. 11235, 2017.

[45] C. A. Unger, M. M. Weinstein, and D. H. Pretorius, "Pelvic floor imaging," Obstetrics and Gynecology Clinics, vol. 38, no. 1, pp. 23–43, 2011.

[46] H. Dietz, "Clinical consequences of levator trauma," Ultrasound in obstetrics & gynecology, vol. 39. Wiley Online Library, pp. 367–371, 2012.

[47] B. Van Hooren, P. Teratsias, and E. F. Hodson-Tole, "Ultrasound imaging to assess skeletal muscle architecture during movements: A systematic review of methods, reliability, and challenges," Journal of Applied Physiology, vol. 128, no. 4, pp. 978–999, 2020.

[48] F. Sarto, J. Spörri, D. P. Fitze, J. I. Quinlan, M. V. Narici, and M. V. Franchi, "Implementing ultrasound imaging for the assessment of muscle and tendon properties in elite sports: Practical aspects, methodological considerations and future directions," Sports Medicine, vol. 51, pp. 1151–1170, 2021.

[49] J. L. Whittaker and M. Stokes, "Ultrasound imaging and muscle function," Journal of Orthopaedic & Sports Physical Therapy, vol. 41, no. 8, pp. 572–580, 2011.

[50] J. M. Scott et al., "Teleguided self-ultrasound scanning for longitudinal monitoring of muscle mass during spaceflight," IScience, vol. 24, no. 4, p. 102344, 2021.

[51] K. Kalam, P. Otahal, and T. H. Marwick, "Prognostic implications of global LV dysfunction: A systematic review and meta-analysis of global longitudinal strain and ejection fraction," Heart, vol. 100, no. 21, pp. 1673–1680, 2014.

[52] K. Gijsbertse et al., "Ultrasound imaging of muscle contraction of the tibialis anterior in patients with facioscapulohumeral dystrophy," Ultrasound in medicine & biology, vol. 43, no. 11, pp. 2537–2545, 2017.

[53] A. Grob, A. Veen, K. Schweitzer, M. Withagen, G. van Veelen, and C. van der Vaart, "Measuring echogenicity and area of the puborectalis muscle: Method and reliability," Ultrasound in obstetrics & gynecology, vol. 44, no. 4, pp. 481–485, 2014.

[54] J. K. Dave, M. E. Mc Donald, P. Mehrotra, A. R. Kohut, J. R. Eisenbrey, and F. Forsberg, "Recent technological advancements in cardiac ultrasound imaging," Ultrasonics, vol. 84, pp. 329–340, 2018.

[55] M. S. Amzulescu et al., "Myocardial strain imaging: Review of general principles, validation, and sources of discrepancies," European Heart Journal-Cardiovascular Imaging, vol. 20, no. 6, pp. 605–619, 2019.

[56] E. K. Oikonomou et al., "Assessment of prognostic value of left ventricular global longitudinal strain for early prediction of chemotherapy-induced cardiotoxicity: A systematic review and meta-analysis," JAMA cardiology, vol. 4, no. 10, pp. 1007–1018, 2019.

[57] S. Das et al., "3D ultrasound strain imaging of puborectalis muscle," Ultrasound in Medicine & Biology, vol. 47, no. 3, pp. 569–581, 2021.

[58] J. M. Wu, A. F. Hundley, R. G. Fulton, and E. R. Myers, "Forecasting the prevalence of pelvic floor disorders in US women: 2010 to 2050," Obstetrics & Gynecology, vol. 114, no. 6, pp. 1278–1283, 2009.

[59] M. Van de Waarsenburg, C. Van der Vaart, and M. Withagen, "Structural changes in puborectalis muscle after vaginal delivery," Ultrasound in Obstetrics & Gynecology, vol. 53, no. 2, pp. 256–261, 2019.

[60] E. Silva, M. Parente, R. N. Jorge, and T. Mascarenhas, "Characterization of the biomechanical properties of the pubovisceralis muscle of two women—one with pelvic organ prolapse and other without pathology," in 2017 IEEE 5th portuguese meeting on bioengineering (ENBENG), 2017, pp. 1–4.

[61] L. Hu, L. Li, H. Wang, Z. Bi, X. Zhang, and M. Lu, "Quantitative evaluation of female pelvic floor muscle biomechanics using ultrasound elastography," IEEE Access, vol. 7, pp. 60940–60946, 2019.

[62] S. D. Atnip, "Pessary use and management for pelvic organ prolapse," Obstetrics and Gynecology Clinics, vol. 36, no. 3, pp. 541–563, 2009.

[63] R. Oliver, R. Thakar, and A. H. Sultan, "The history and usage of the vaginal pessary: A review," European journal of obstetrics & gynecology and reproductive biology, vol. 156, no. 2, pp. 125–130, 2011.

[64] E. Pott-Grinstein and J. R. Newcomer, "Gynecologists' patterns of prescribing pessaries." The Journal of reproductive medicine, vol. 46, no. 3, pp. 205–208, 2001.

[65] H. P. Dietz, "Pelvic floor muscle trauma," Expert review of obstetrics & gynecology, vol. 5, no. 4, pp. 479–492, 2010.

[66] C. Manzini, F. van den Noort, A. T. Grob, M. I. Withagen, and C. H. van der Vaart, "The effect of pessary treatment on puborectalis muscle function," International Urogynecology Journal, vol. 32, pp. 1409–1417, 2021.

[67] C. Manzini, F. van den Noort, A. T. Grob, M. I. Withagen, C. H. Slump, and C. H. van der Vaart, "Appearance of the levator ani muscle subdivisions on 3D transperineal ultrasound," Insights into imaging, vol. 12, pp. 1–8, 2021.

[68] S. Das, G. A. Hendriks, F. van den Noort, C. Manzini, C. H. van der Vaart, and C. L. de Korte, "3D ultrasound strain imaging of puborectal muscle with and without unilateral avulsion," International urogynecology journal, vol. 34, no. 9, pp. 2225–2233, 2023.

[69] J. B. Woodhouse and E. G. McNally, "Ultrasound of skeletal muscle injury: An update," in Seminars in ultrasound, CT and MRI, 2011, vol. 32, pp. 91–100.

[70] M. Van Holsbeeck and J. Introcaso, "Sonography of muscle," Musculoskeletal ultrasound, vol. 2, pp. 23–75, 2001.

[71] A. T. Grob, "Structural and functional ultrasound imaging of the pelvic floor during pregnancy and postpartum," PhD thesis, Utrecht University, 2016.

[72] A. Grob, N. Hitschrich, M. K. van de Waarsenburg, M. I. Withagen, K. J. Schweitzer, and C. H. van der Vaart, "Changes in global strain of puborectalis muscle during pregnancy and postpartum," Ultrasound in obstetrics & gynecology, vol. 51, no. 4, pp. 537–542, 2018.

[73] J.-R. Chen et al., "Clinical value of information entropy compared with deep learning for ultrasound grading of hepatic steatosis," Entropy, vol. 22, no. 9, p. 1006, 2020.

[74] G. Salsi et al., "Three-dimensional/four-dimensional transperineal ultrasound: Clinical utility and future prospects," International journal of women's health, pp. 643–656, 2017.

[75] C. Manzini, C. H. van der Vaart, F. van den Noort, A. T. Grob, and M. I. Withagen, "Pessary fitting for pelvic organ prolapse: Parameters associated with specific reasons for failure," International urogynecology journal, vol. 33, no. 7, pp. 2037–2046, 2022.

[76] A. Huseynov et al., "Developmental evidence for obstetric adaptation of the human female pelvis," Proceedings of the National Academy of Sciences, vol. 113, no. 19, pp. 5227–5232, 2016.

[77] M. Pavličev, R. Romero, and P. Mitteroecker, "Evolution of the human pelvis and obstructed labor: New explanations of an old obstetrical dilemma," American journal of obstetrics and gynecology, vol. 222, no. 1, pp. 3–16, 2020.

[78] E. Stansfield, B. Fischer, N. D. Grunstra, M. V. Pouca, and P. Mitteroecker, "The evolution of pelvic canal shape and rotational birth in humans," BMC biology, vol. 19, pp. 1–11, 2021.

[79] S. L. Washburn, "Tools and human evolution," Scientific American, vol. 203, no. 3, pp. 62–75, 1960.

[80] B. Fischer and P. Mitteroecker, "Allometry and sexual dimorphism in the human pelvis," The Anatomical Record, vol. 300, no. 4, pp. 698–705, 2017.

[81] P. Mitteroecker, S. M. Huttegger, B. Fischer, and M. Pavlicev, "Cliff-edge model of obstetric selection in humans," Proceedings of the National Academy of Sciences, vol. 113, no. 51, pp. 14680–14685, 2016.

Chapter 2

3D ultrasound strain imaging of puborectalis muscle

This chapter is based on the publication:
S. Das, H. H. G. Hansen, G. A. G. M. Hendriks, F. van den Noort, C. Manzini, C. H. van der Vaart & C. L. de Korte, **3D ultrasound strain imaging of puborectalis muscle**. *Ultrasound in medicine and biology*, vol. 47, no. 3, pp. 569-581, 2021.

Abstract

The female pelvic floor (PF) muscles provide support to the pelvic organs. During delivery, some of these muscles have to stretch up to three times their original length to allow passage of the baby, leading frequently to damage and consequently later-life PF dysfunction (PFD). Three-dimensional (3D) ultrasound (US) imaging can be used to image these muscles and to diagnose the damage by assessing quantitative, geometric and functional information of the muscles through strain imaging. In this study we developed 3D US strain imaging of the PF muscles and explored its application to the puborectalis muscle (PRM), which is one of the major PF muscles.

Keywords - Puborectalis, Ultrasound, Strain imaging, Pelvic floor, Obstetrics, 3D imaging

2.1 Brief introduction

In this chapter, principal strain have been calculated for the puborectal muscles (PRMs) of four women. Initially, displacement estimates from the tracked PRMs have been estimated and thereafter principal strain. Strain calculations are from contracting PRMs as well as PRM showing Valsalva maneuver. The results shown in this chapter demonstrate that strain imaging of PRM using three-dimensional (3D) ultrasound (US) is feasible.

2.1.1 Data acquisition

Data acquisition from the women for which the results of principal strain have been shown can be briefly mentioned in the **Table 2.1**.

Dynamic 3D TPUS volumes were acquired using a Philips X6-1 matrix transducer connected to an EPIQ 7G US machine (Philips Healthcare, Bothell, WA, USA), at the University Medical Centre (UMC), Utrecht, The Netherlands. The transducer was fitted with a gel pad and a glove to permit the full PRM within it's field of view. All data were acquired by one clinician minimizing any intra-observer variability.

In each of the acquired datasets, one volume consists of 352 x 229 x 277 pixels (in the X, Y and Z directions respectively). The physical size of the volume is 14.78cm x 13.74cm x 9.41cm. The volumetric data were acquired at a rate of approximately 1.5 volumes/sec resulting in 22 volumes which span over 11-15 seconds. The data were stored in the Digital Imaging and Communications in Medicine (DICOM) format.

Data from all women were acquired with the same preset in the US machine. The time gain compensation (TGC) and other settings like filtering, contrast, gain, power, gray map or processing were identical for all acquisitions. Since, the US machine and the matrix transducer were identical for all acquisitions, the B-mode log compression, normalization etc. were also the same. That is why, two different scans for the same woman/subject will not show different levels of brightness. Two different scans from different women/subjects, will indeed

show similar or different levels of echogenicity regarding difference in the state of the tissue.

The Medical Research Ethics Committee of UMC Utrecht exempted the project from approval, since all these women came to the clinic for treatment, as part of routine diagnostic procedures and standard care from the clinic. All women signed appropriate research consent forms.

2.1.1.1 Intact PRMs

US data were obtained over time from women (n = 4) who had never given birth (nulliparous). These women had overactive PFs, which is chronically raised pelvic muscle tone. The PRMs in these women were intact and undamaged, as confirmed by the clinician. US volumes were recorded during two types of exercise (in supine position with empty bladder). During the first exercise, contraction, the women were asked to actively contract their PF muscles, commencing and ending with the muscles in a state of rest.

During the second exercise, they performed a Valsalva maneuver. A Valsalva maneuver is performed by a moderately forceful exhalation against a closed airway. It is used to increase the abdominal pressure, which causes LAM distension and allows the clinician to assess the full extent of a POP. Data acquisition commenced with rest and ended at maximum Valsalva maneuver.

To ensure that the women could perform contraction or Valsalva maneuver of their PF muscles, the clinician acquired the data while the US images were being observed on the screen of the US machine. Positive bio-feedbacks were provided to the women if she could properly contract her PF muscles or do Valsalva maneuver. Thus it was ensured that all included women in this study could change the state of their PF muscles during data acquisition.

2.1.2 Aim of the study

We hypothesized in this work that it is possible to quantify strain in three dimensions for the deforming PRM using a time series of volumetric US data. Strain imaging was performed in four nulliparous women (n = 4), who were asked

to contract (n = 4) their PF muscles or perform both a contraction and a Valsalva maneuver (n = 1). We chose nulliparous women, that is, women who have not yet given birth because these women are considered to have intact PF muscles. Therefore, this study provides insight into how the undamaged muscle strains in three dimensions during activation. Summarized, the aim of this study was to develop 3D US strain imaging of the PF muscles and to explore its application to the PRM, which is one of the PF muscles.

2.2 Methods

The block diagram in **Figure 2.1** illustrates the processing steps performed to calculate strain in the acquired volumes of the PRM. The input comprised the recorded dynamic US volumes and the region of interest (ROI) for which strain was calculated. To obtain the ROI, the PRM was manually segmented by an experienced clinician in the initial US volume (rest before exercise) **[1]**. The output was a set of accumulated echo volumes as a function of time. The influence of segmentation of the ROI was varied by decreasing the ROI, and displacement estimates were calculated using these volumes. The difference in the values obtained at these different sizes was identical for corresponding voxels. The processing sequence can be divided into four steps: volumetric data preparation, intervolume displacement estimations, tracking (involving an update of the ROI) and strain calculations.

Each processing step is explained in detail hereafter. Each block of the block diagram shown in **Figure 2.1** have been detailed with flowcharts, shown in **Appendices A - E**.

2.2.1 Volumetric data preparation

The first of the two inputs for the work was the data from the US machine, which were in DICOM format. These data were first converted to a rectilinear format with ".fld" extension using a proprietary software called QLAB, Version 10.8 (Philips Healthcare, Andover, MA, USA). Conversion of the data was performed to allow import in MATLAB R2018 a (The MathWorks, Inc., Natick, MA, USA), which was the program we used to develop our 3D strain analysis soft-

ware. The total number of volumes per data set was 22, and each of the 3D volumes contained 352 x 229 x 277 (X x Y x Z) pixels which were uniformly sampled at distances of 0.42 x 0.60 x 0.34 mm (dx x dy x dz).

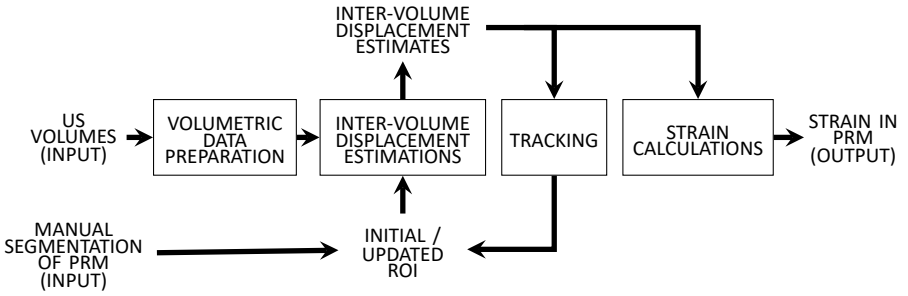

Figure 2.1: Block diagram of the processing steps involved to obtain 3D strain output from the 3D ultrasound data sequence (PRM = puborectalis muscle; ROI = region of interest)

2.2.2 Intervolume displacement estimations

The next step was to calculate intervolumetric displacements. Therefore, displacements were estimated between the first two volumes within the initial ROI (illustrated in **Figures 2.4** and **2.5** for volunteer 1). Intervolumetric displacements for each pair of subsequent volumes were estimated with a 3D normalized cross-correlation algorithm optimized for PF muscles and the US system used in this study **[2-3]**.

In this algorithm, two subsequently recorded volumes were subdivided into 3D blocks called kernels and templates. The kernel and template sizes used for those volumes were (111 x 81 x 41) and (51 x 51 x 11) pixels, respectively. The kernels were matched on the templates, and the locations of the 3D cross-correlation peaks were calculated. These locations of peaks indicated the displacements between the two blocks. To estimate subsample displacements, the cross-correlation peaks were interpolated (parabolic fit) **[3]**. The displacement

estimates were finally filtered using a 3D median filter.

2.2.3 Tracking

As the PRM changes (position and shape) from volume to volume, that is, changes with time, the position and shape of the ROI for displacement estimation also needs to be updated over time. Otherwise, displacement estimation would no longer be performed for PRM tissue only, but would gradually shift to the surrounding tissue. The ROI coordinates (position of the manually segmented PRM) of the next volume were updated using the displacement estimates as calculated in the previous step. In the next step, displacements were calculated between the next two subsequently acquired volumes, and the ROI was updated. The process of estimating intervolumetric displacements and updating ROI is called tracking **[4-5]**. Tracking began after the displacement estimations between the first two subsequently acquired volumes were estimated using the initial ROI.

The input to this processing step was the filtered intervolume displacement estimates from the previous step. Filtering was done using a median filter (2 x 2 x 2 cm) to smoothe the displacement estimates and remove outliers **[5-6]**. This was required for tracking.

Accumulation of the filtered displacement estimates was performed using the equation shown below:

$$accum\_disp\_estmts(n+1) = \sum_{n=1}^{n+1} inter\_vol\_disp\_estmts(n, n+1) \tag{2.1}$$

where,

accum_disp_estmts = accumulated displacement estimates in z, x or y direction,
inter_vol_disp_estmts = intervolume displacement estimates in z, x or y direction and

n = number of US volumes.

The accumulated displacement estimates were the total movement of the muscle up to the (n + 1)th volume or time point. These displacement estimates were obtained in number of US grid points that a certain index had passed. The indexes were updated with these accumulated displacement estimates.

Because the updated indexes are subsample values, displacement estimates were calculated from the eight surrounding sample points, and the displacement estimates of the subsample points were arrived at by linear interpolation (**Figure 2.2**). In this way, the muscle could be tracked throughout its complete deformation cycle. After each update of the ROI, it was checked visually on the respective US volume to ensure whether it was at the same position as the displaced muscle.

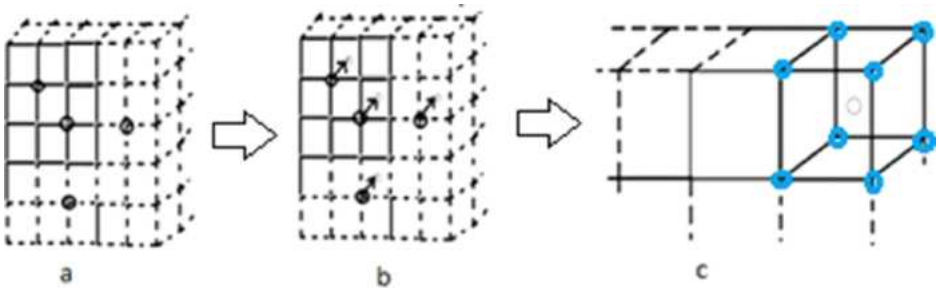

Figure 2.2: Visual explanation of the temporary surrounding eight-point grid; (a) Part of the ultrasound grid, where the circled corners represent the positions or indices forming part of the region of interest (black circles), (b) Changes in positions of the indexes when updated by accumulated z, x and y displacement estimates to positions that are out of grid (gray circles), (c) One example of surrounding eight points in the ultrasound grid (blue circles) to follow a certain updated out of grid position or index (gray circle)

Therefore, for this processing step, the inputs were the intervolume displacement estimates, and the outputs were the updated ROIs.

2.2.3.1 Validation of tracking

The tracked muscle was superimposed on each of the acquired US volumes from rest to maximum contraction or Valsalva maneuver. Thereafter all these 22 volumes for all four women were visually checked. This was performed to validate whether the tracking of the deforming muscle matched with the expected position of the muscle.

An example each of the PRM at rest, at contraction and at Valsalva maneuver for one of the volunteers have been shown in **Figure 2.3a, b and c**. In **Figure 2.3a** the PRM at rest has been shown in yellow. As the muscle moved away from the rest position to maximum contraction, it can be observed that it moved towards the PS. This is shown in **Figure 2.3b**. The PRM at rest is dark gray and the actual contracted position of the PRM is in yellow. The same is shown in **Figure 2.3c**, except it is for Valsalva maneuver. In this last sub-figure, the deformed PRM can be seen as moved away from the PS.

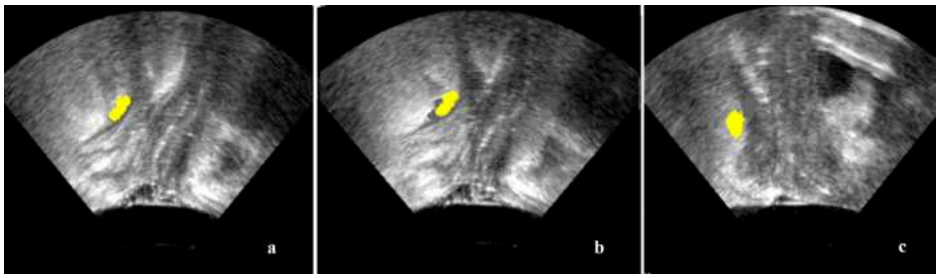

Figure 2.3: Puborectalis muscle (PRM) as observed in transperineal ultrasound (US) data in sagittal view (z-y plane in US grid) (a) B-mode US image, showing PRM at rest in yellow (b) B-mode US image, showing PRM at max. contraction in yellow and the position at rest in dark gray (c) B-mode US image, showing PRM at Valsalva maneuver in yellow and the position at rest in dark gray

2.2.4 Strain calculations

Strain calculation was the last processing step. Accumulated displacements were calculated by summing intervolumetric displacements up to each time point. The non-filtered intervolumetric displacements were used and filtered with a median filter kernel (1 x 1 x 1 cm) before accumulation **[3, 6]**. A kernel size smaller than that in the tracking step was applied to avoid too much smoothing of the displacements, which would result in the absence of a gradient in the strain calculations. As the displacement estimates were filtered using a different kernel, interpolation was again performed, now for the updated indexes. In the next step, the interpolated displacement estimates were accumulated using **Equation** . These accumulated displacement estimates were used to calculate the 3D strain tensor using a 3D least-squares strain estimator (LSQSE) **[7]**.

The contraction direction of the PRM is not coaligned with the rectilinear coordinate system. To determine the major or principal component of the strain that is induced in the contraction or Valsalva maneuver of PRM, principal strains were calculated from the individual strain values in the z, x and y directions **[8]**. As we have observed from the LSQSE strain that strain for contraction is negative and strain for Valsalva maneuver is positive, we chose the largest negative principal strain component for data during contraction and the largest positive strain component for data during the Valsalva maneuver.

2.3 Results

Accumulated displacement estimates are illustrated in **Figures 2.4** and **2.5**, and principal strain results, in **Figures 2.6** and **2.7**, for two of four volunteers (**Figures S2.1**, **S2.3** and **S2.5** in the supplementary figures show the results for the other three volunteers for contraction). These time points are, respectively, muscle at rest, muscle at maximum contraction and muscle at rest post contraction, for volunteer 1. In the case of volunteer 4, the time points are rest and maximum Valsalva maneuver. The principal strain magnitudes and principal strain directions are illustrated in the figures. The demographic characteristics of all the women included in the study are shown in **Table 2.1**.

Table 2.1: Demographic information about all the inclusions

	Volunteer 1	Volunteer 2	Volunteer 3	Volunteer 4	Volunteer 5
Age (yrs)	52	38	61	23	23
Body mass index (Kg/m^2)	26.9	19.0	24.8	19.2	19.2
Exercise performed	Contraction	Contraction	Contraction	Contraction	Valsalva maneuver

2.3.1 Acumulated displacement estimates

In volunteer 1, at the time point at which the muscle is at rest (**Figure 2.4a, 2.4d, 2.4g**, first column), the estimated displacements between the first two volumes are quite low in all directions, which is expected at rest. We observed this for displacement estimates of all volunteers. In **Figure 2.4b,2.4e, 2.4h** (second column) are the accumulated displacement results for maximum contraction. The displacement estimates in the z-direction are the highest, followed by displacement estimates in the y-direction. In the x-direction, we see that displacement estimates are almost zero.

During contraction, in the z-direction, negative displacement estimates mean that the PRM is moving toward the bone PS and, thus, toward the US transducer. In the y-direction, displacement estimates are positive, which means that in this direction, the muscle is moving away from the US transducer. There is very little lateral or side-to-side movement of the muscle, that is, in the x-direction. These movements or lack of movement with respect to the muscle at rest are illustrated in **Figure 2.8b-d**.

In **Figure 2.4c, 2.4f, 2.4g** (third column), we see that the muscle is almost back at rest, and so the accumulated displacement estimates are again back to

approximately zero values. The muscle does not completely return to the rest position, because these data sets were acquired in women who have overactive PFs. Thus, these women might take longer to return to the rest position post-contraction.

In the data sets acquired during the Valsalva maneuver, data acquisition was stopped when the muscle reached maximum Valsalva maneuver. The accumulated displacement results are illustrated in **Figure 2.5**. We observe that displacements are initially close to zero, as the muscle is at rest.

During the maximum Valsalva maneuver the accumulated displacements are predominantly positive in the z-direction and negative in the x- and y-directions. This indicates elongation of the muscle in Valsalva maneuver as opposed to shortening during contraction. This deformation with respect to the muscle at rest is illustrated in **Figure 2.9b-d**.

The movements of the PRM during contraction and Valsalva maneuver, axial, sagittal and coronal views, are illustrated in the supplementary videos in the Supplementary Data (online only). In these videos, the dark gray area represents the position of the muscle during rest, and the yellow area, the muscle during contraction/ Valsalva maneuver. We can observe that the movement during contraction with respect with the bone PS is complementary in direction compared with that of Valsalva maneuver.

2.3.2 Principal strain values

During contraction, as illustrated in **Figure 2.6**, it is observed that the major principal strain becomes more negative with increasing contraction. As the muscle returns to the rest position, the negative strain decreases but does not become zero. The principal strain component directions change for all volunteers when the muscle contracts from rest and becomes predominantly aligned with muscle fiber direction at maximum contraction. In **Figure 2.6e, 2.6f**, it can be seen that the direction of strain further changes when the muscle returns to the rest state after contraction (**Figures S2.2**, **S2.4** and **S2.6** in the supplementary figures show principal strains and directions for the other three volunteers).

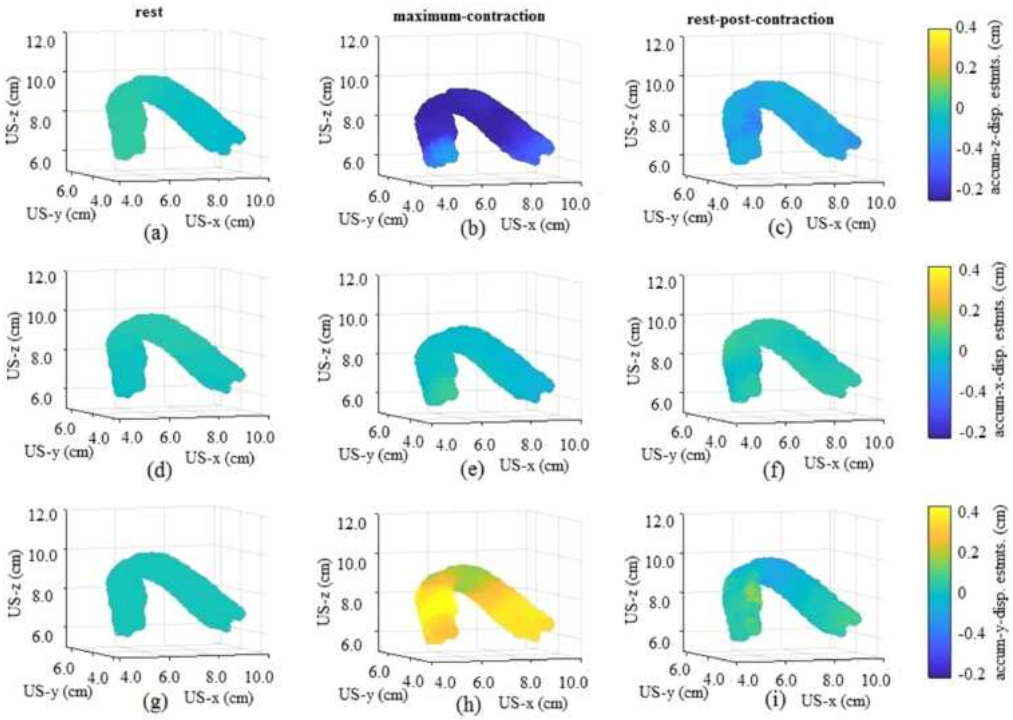

Figure 2.4: Accumulated displacement estimates at three time points during the rest-contraction-rest sequence of volunteer 1; (a-c) Accumulated z-direction displacement estimates, (d-f) Accumulated x-direction displacement estimates, (g-i) Accumulated y-direction displacement estimates)

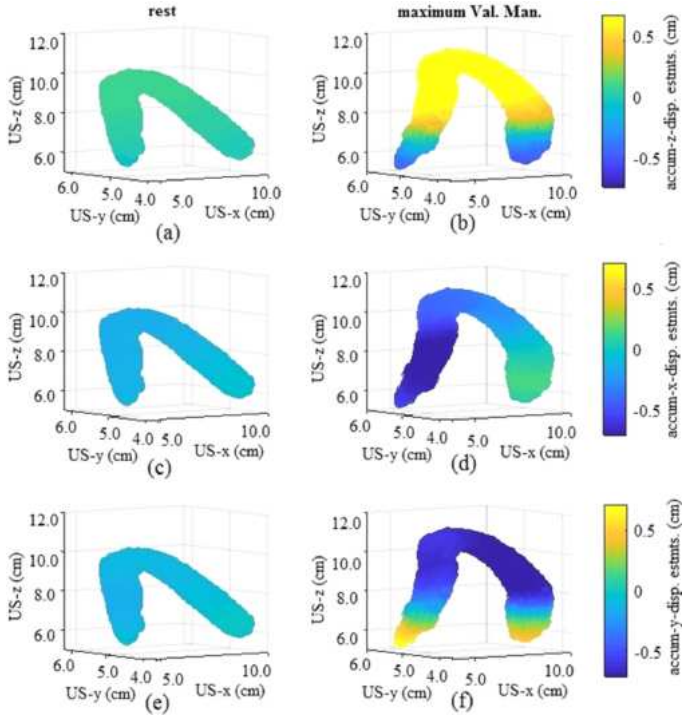

Figure 2.5: Accumulated displacement estimates at two time points during the rest-Valsalva maneuver sequence of volunteer 4; (a-c) Accumulated z-direction displacement estimates, (d-f) Accumulated x-direction displacement estimates, (g-i) Accumulated y-direction displacement estimates

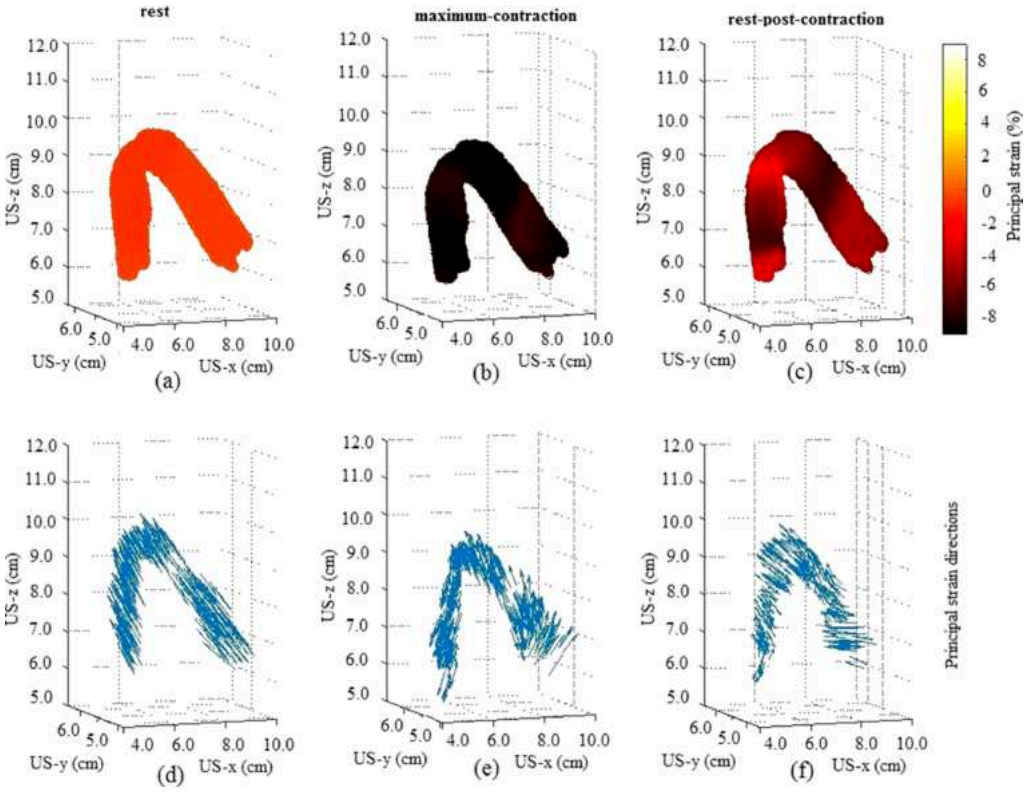

Figure 2.6: Accumulated principal strain (%) magnitudes (first row) and their respective directions (second row) for volunteer 1 (US = ultrasound)

As illustrated in **Figure 2.7**, the data for volunteer 4 contain a Valsalva maneuver. In this case, rest remains the same as the rest during contraction, whereas during maximum Valsalva maneuver, strain is positive with a peak value of 60% strain.

The bottom row of **Figure 2.7** illustrates the principal strain component directions. Once again it is observed that the directions change when the muscle changes from rest to maximum Valsalva maneuver.

Table 2.2 lists the spatial means of the principal strain (%) values over the PRM for all data sets. Mean principal strain (%) values in the rest position for all

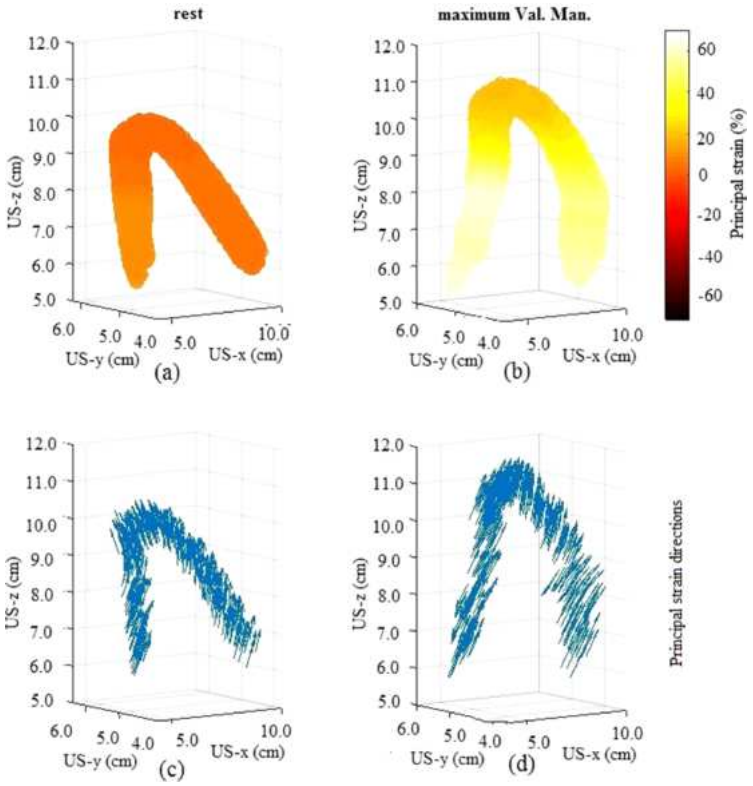

Figure 2.7: Accumulated principal strain (%) magnitudes (first row) and their respective directions (second row) for volunteer 4 (US = ultrasound; Val. Man. = Valsalva maneuver)

five volunteers were less than 3%. The principal strains at maximum contraction ranged between -8.9% and -41.5%. For the data set for the Valsalva maneuver, the maximum principal strain was 38.6%. At the last time point, namely, rest post-contraction, strain had decreased with respect to earlier time points before but was not equal to that before contraction.

2.4 Discussion

To our knowledge, this is the first study in which 3D displacement and strain

Table 2.2: Mean principal strain values of the four volunteers included in the study

Time point	Mean principal strain (%)				
	Volunteer 1	Volunteer 2	Volunteer 3	Volunteer 4	Volunteer 4
Rest	-0.9	-1.6	-2.0	-1.1	3.1
Maximum contraction \Valsalva maneuver	-8.9	-13.7	-33.4	-41.5	38.6
Rest post-contraction	-5.2	-7.5	-28.8	-21.8	-

were estimated in the PRM. Normally, when clinicians examine the PF with TPUS, they can only visually examine the motion of the PF and measure the (relative) motion for certain specific anatomic landmarks. In other words, a qualitative assessment can be made. As can be observed, the proposed algorithm allows quantitative determination of strain, locally within the PRM.

We observe from the obtained results that the strain during contraction and the strain during Valsalva maneuver are complementary, which allows the algorithm to distinguish between these two opposite movements of the muscle. We also observe that there are changes in the deformation of the muscle. These deformations are different for contraction compared with Valsalva maneuver. Because of the short data acquisition time, we can observe the muscle returning to almost rest but not complete rest post-contraction.

For this initial study, we focused on strain estimation in the undamaged and intact PRM of nulliparous women undergoing voluntary contraction or Valsalva maneuver before focusing on strain estimation in patients with a complex pathology, for example, avulsions.

We observe in the last column of displacement estimates in Figure 5 that the muscle does not return to the exact rest position post-contraction. There are three possible explanations for this: a clinical one, an explanation related to

the hardware and a technical explanation. The clinical explanation is that the volunteers from whom the data were acquired had overactive PFs. Therefore, it might be that the PRM will take more time to return to its rest position post-contraction. For example, in volunteer 1, we find the maximum contraction is at volumes 13 and 14, which means that 7 of the 11sec of total data acquisition time had already passed. The PRM does not return to rest within the remaining approximately 4sec. As the volunteers were supine and contracting their PF muscles only during data acquisition, motion of the volunteer or global motion can be ignored. This can also mean a hardware limitation; the time for data acquisition was too short and ended before the muscle had returned to its rest position. Lastly, the technical explanation is that tracking might not be ideal. Small inaccuracies in the displacement estimates accumulate over time to introduce error in tracking.

The complementary sign is visible in the displacement estimates and strain during Valsalva maneuver (**Figures 2.7** and **2.8**), compared with those observed during contraction (**Figures 2.5** and **2.6**). It can be observed that the muscle has moved away from the US transducer in the z-direction, and there is clearly a change in shape of the muscle. In the x-direction, we can observe that one end of the muscle has moved more than the other end. This differs from the results for contraction, where there is little or no movement in the x-direction. This might be because the contracting muscle is expected to move toward the bone PS (in effect the US transducer) to which it is attached. It is not expected to move laterally or from side to side in contraction. In the Valsalva maneuver, while the muscle is elongating, we observe that deformation is occurring in all three z, x and y directions. In this volunteer, in the x-direction, one arm of the muscle is manifesting more displacement than the other. In the y-direction, we observe that the muscle has moved toward the transducer. Because we studied the Valsalva maneuver in only one volunteer, these observations cannot be generalized. The presence of these trends needs to be investigated in a large sample size.

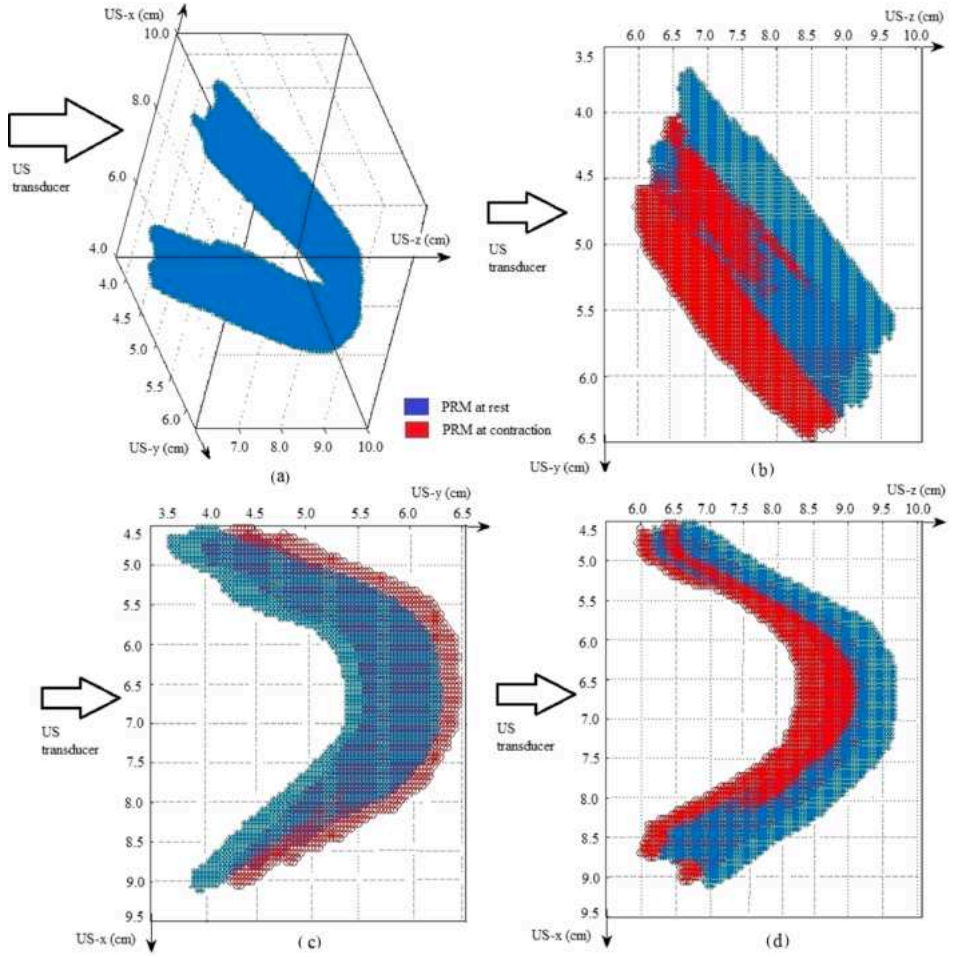

Figure 2.8: Deformation of the puborectalis muscle (PRM) at contracted state (red) when compared with the rest state (blue) for volunteer 1; (a) The undeformed PRM at rest state in the ultrasound grid, (b) Deformation of the PRM in z-y plane, (c) Deformation of PRM in y-x plane, (d) Deformation of PRM in z-x plane (US = ultrasound)

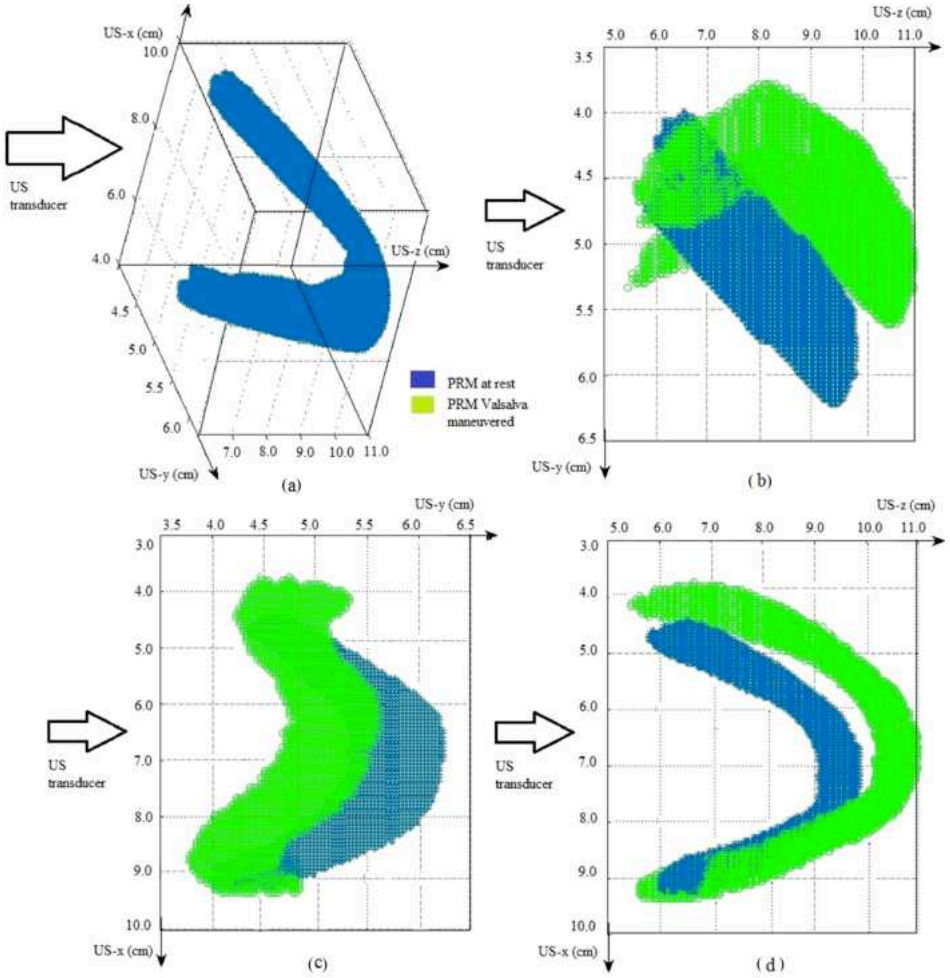

Figure 2.9: Deformation of the puborectalis muscle (PRM) at Valsalva maneuver state (green) compared with the rest state (blue) for volunteer 4; (a) The undeformed PRM in rest state in the ultrasound (US) grid, (b) Deformation of PRM in z-y plane, (c) Deformation of PRM in y-x plane, (d) Deformation of PRM in z-x plane

The PRM is almost uniformly strained (**Figures 2.6a-c**, first row), indicating contraction, whereas it manifests non-uniform strain when it returns to rest after contraction. A possible explanation might be that in the case of an overactive PF, different parts of the muscle take longer to return to zero strain. As the sample size was small in this study, it should be extended in future studies to investigate whether this trend is present in a large group of women.

Also, there is a large variation between the strain (%) values obtained during contraction from the four volunteers in contraction, as illustrated in **Table 2**. A possible reason could be that different women have different levels of control over their PRMs during contraction. Additionally, deformation of the muscle during contraction might also vary per woman. Larger sample sizes in future studies could provide a range of strain from minimum to maximum for undamaged PRM.

We can observe the directions of the principal strains in **Figures 2.7** and **2.8d-f**, second row. It can be observed that the strains are in the direction of muscle fiber orientation.

2.4.1 Clinical significance

First, knowledge of the exact length by which the muscle has moved and deformed is beneficial in that we can assess numerically how far the woman can move her muscle voluntarily. Thereafter, we can compare how much movement is expected in a normal undamaged muscle compared with a damaged muscle. Moreover, it would provide clinicians and pelvic physiotherapists with a quantitative tool to follow patients' improvements during treatment (e.g., PF muscle training).

Second, when the muscle is observed in the image displayed in the US machine, it is difficult to assess quantitatively which part of the muscle is displaced more and which is displaced less. As illustrated in the results, for undamaged muscles, it is possible to know which part of the muscle is displaced more from the different colors of the displacement estimates in the figures. For example, in the case of displacement estimates in the z-direction, for volunteer 1 (**Figure**

2.5e), the “sling” of the PRM moved more than the two ends that are attached to the bone PS. In the results for volunteer 4 (**Figure 2.6**), in the Valsalva maneuver, we observe that different parts of the PRM move dissimilarly in all three z, x and y directions. These observations of the figures can give us an idea about how the undamaged muscle moves. Thereafter, a comparison can be made with damaged muscle movement.

Lastly is the exact time point, or more specifically the volume, at which the muscle, for certain data at maximum contraction/Valsalva maneuver, can be determined. It can be useful in TPUS as a means of automatically arriving at the specific volume for maximum contraction/Valsalva maneuver, thus reducing a source of variability in TPUS assessments.

In this study, the primary reason for calculating strain induced in the PRM was to quantify the deformation and strain in undamaged PRM. When there is damage or scar tissue formation in the muscle, it might be of clinical significance to assess the exact position of the damage through the different strain (%) values in different parts of the muscle along with the directions of the strain values. Thereafter, it might also be possible to quantify in three dimensions which part of the muscle is damaged.

To further investigate PF muscles through 3D strain, future studies should include larger sample sizes for both undamaged PRM and complex PRM pathologies. Other LAMs should also be investigated to learn how the muscles behave in relation to each other.

2.5 Conclusion

Strain imaging of PRM is possible as it deforms from rest to maximum contraction or Valsalva maneuver from acquired 3D US volumes of the muscle.

References

[1] F. van den Noort, A. T. Grob, C. H. Slump, C. H. van der Vaart, and M. van Stralen, "Automatic segmentation of puborectalis muscle on three-dimensional transperineal ultrasound," Ultrasound in obstetrics & gynecology, vol. 52, no. 1, pp. 97–102, 2018.

[2] K. Gijsbertse et al., "Three-dimensional ultrasound strain imaging of skeletal muscles," Physics in Medicine & Biology, vol. 62, no. 2, p. 596, 2016.

[3] G. A. Hendriks, B. Holländer, J. Menssen, A. Milkowski, H. H. Hansen, and C. L. de Korte, "Automated 3D ultrasound elastography of the breast: A phantom validation study," Physics in Medicine & Biology, vol. 61, no. 7, p. 2665, 2016.

[4] R. Lopata et al., "3D cardiac strain imaging using a novel tracking method," in 4th european conference of the international federation for medical and biological engineering: ECIFMBE 2008 23–27 november 2008 antwerp, belgium, 2009, pp. 697–700.

[5] R. G. Lopata et al., "Dynamic imaging of skeletal muscle contraction in three orthogonal directions," Journal of Applied Physiology, vol. 109, no. 3, pp. 906–915, 2010.

[6] H. Hansen, R. Lopata, T. Idzenga, and C. L. de Korte, "Full 2D displacement vector and strain tensor estimation for superficial tissue using beam-steered ultrasound imaging," Physics in Medicine & Biology, vol. 55, no. 11, p. 3201, 2010.

[7] F. Kallel and J. Ophir, "A least-squares strain estimator for elastography," Ultrasonic imaging, vol. 19, no. 3, pp. 195–208, 1997.

[8] M. E. Tuttle, Structural analysis of polymeric composite materials. CRC Press, 2012.

Supplementary figures

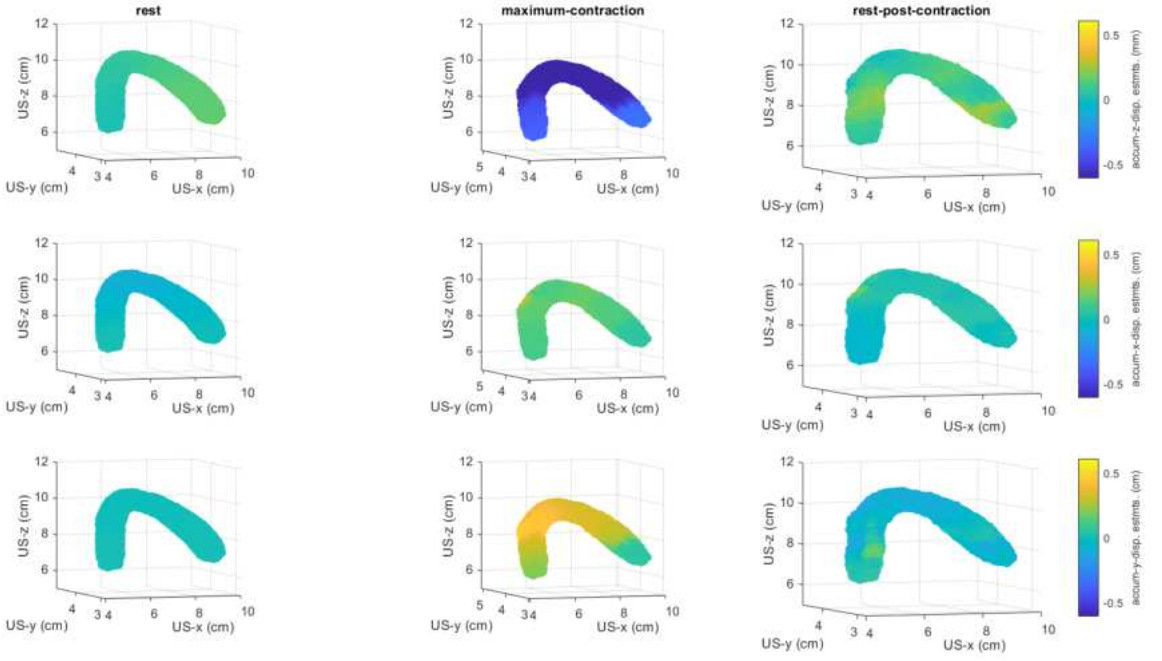

Figure S2.1: Accumulated displacement estimates at three time points during the rest-contraction-rest sequence of volunteer 2; (a-c) Accumulated z-direction displacement estimates, (d-f) Accumulated x-direction displacement estimates, (g-i) Accumulated y-direction displacement estimates)

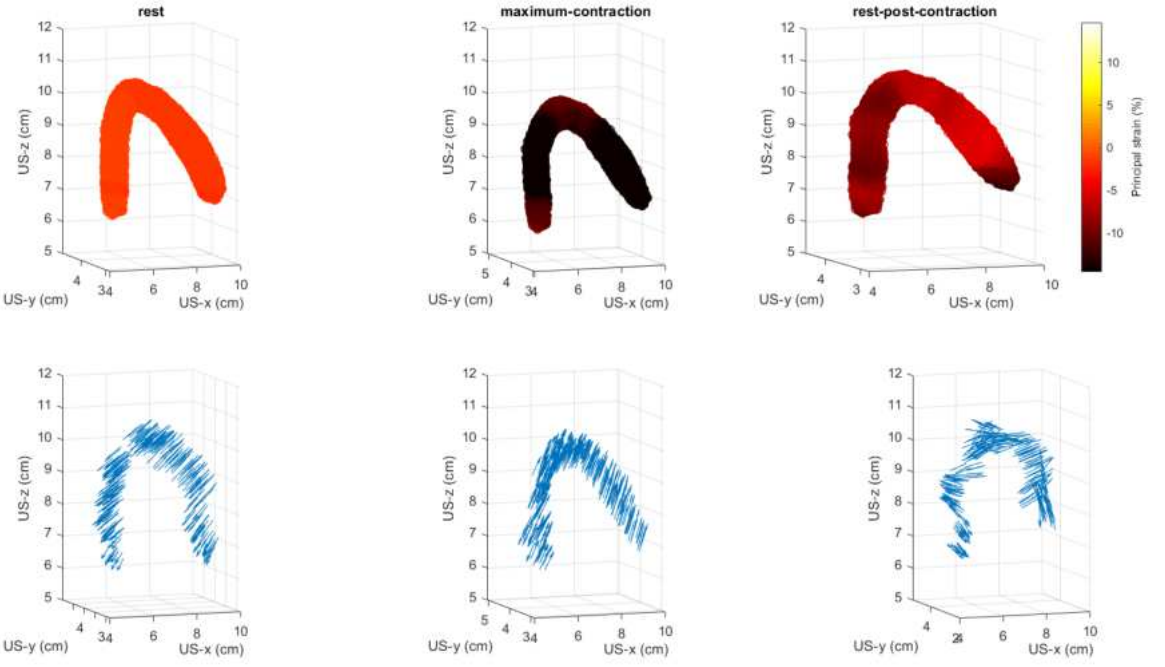

Figure S2.2: Accumulated principal strain (%) magnitudes (first row) and their respective directions (second row) for volunteer 2 (US = ultrasound)

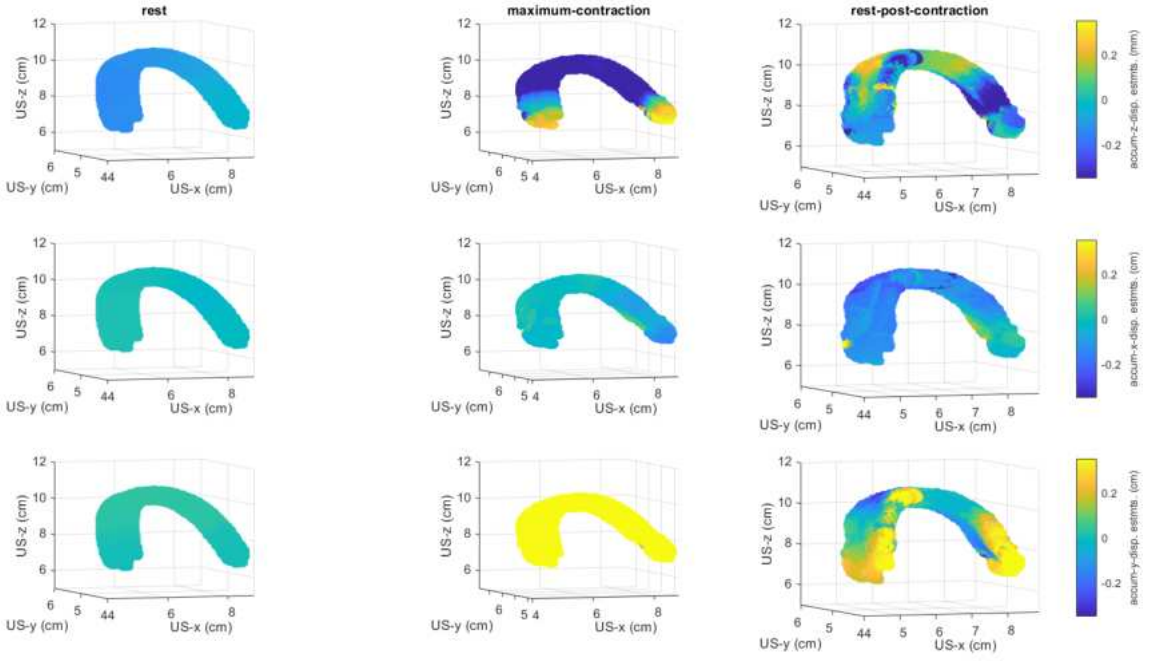

Figure S2.3: Accumulated displacement estimates at three time points during the rest-contraction-rest sequence of volunteer 3; (a-c) Accumulated z-direction displacement estimates, (d-f) Accumulated x-direction displacement estimates, (g-i) Accumulated y-direction displacement estimates)

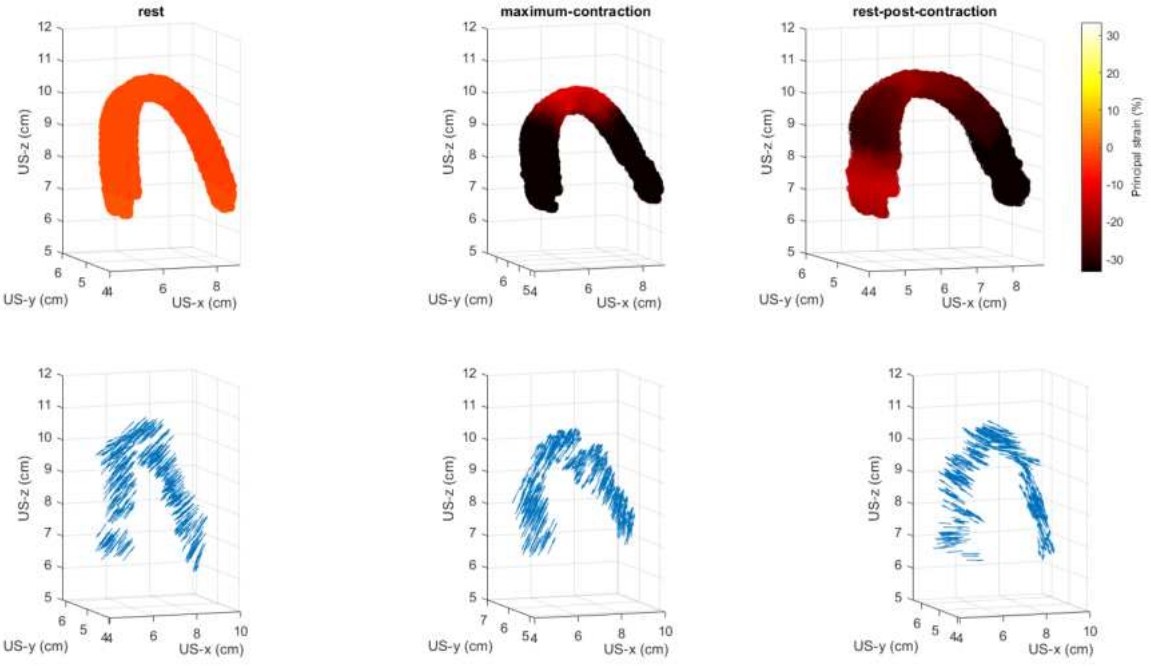

Figure S2.4: Accumulated principal strain (%) magnitudes (first row) and their respective directions (second row) for volunteer 3 (US = ultrasound)

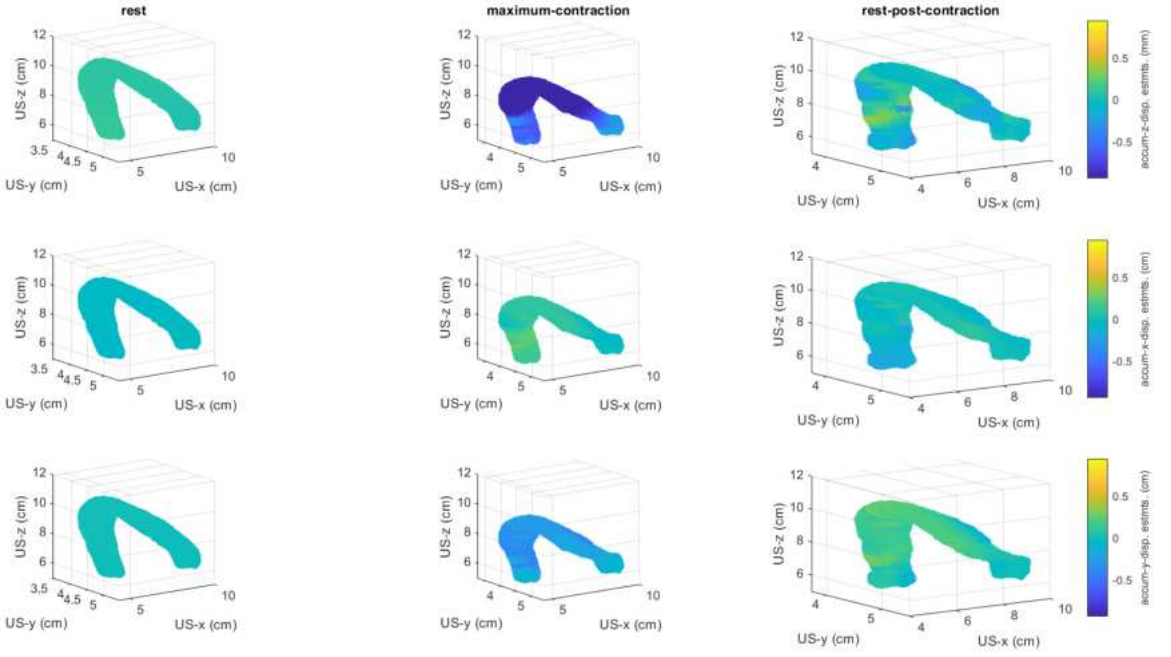

Figure S2.5: Accumulated displacement estimates at three time points during the rest-contraction-rest sequence of volunteer 4; (a-c) Accumulated z-direction displacement estimates, (d-f) Accumulated x-direction displacement estimates, (g-i) Accumulated y-direction displacement estimates)

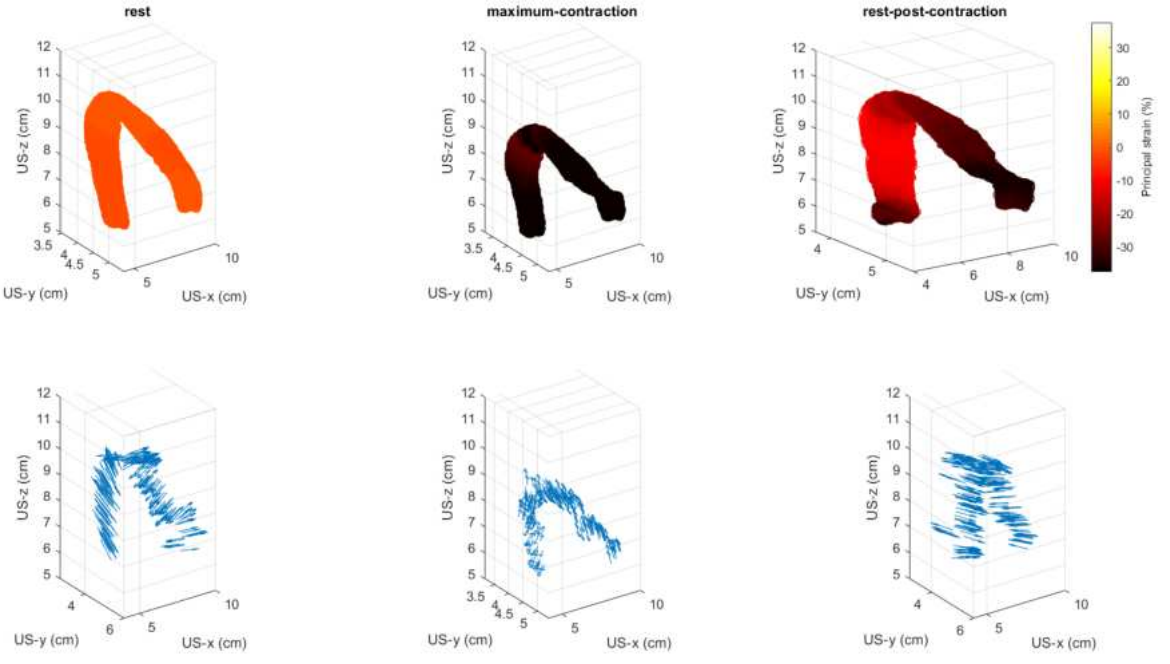

Figure S2.6: Accumulated principal strain (%) magnitudes (first row) and their respective directions (second row) for volunteer 4 (US = ultrasound)

Chapter 3

3D US strain imaging of PRM with & without unilateral avulsion

This chapter is based on the publication:
S. Das, G. A. G. M. Hendriks, F. van den Noort, C. Manzini, C. H. van der Vaart & C. L. de Korte, **3D ultrasound strain imaging of puborectal muscle with and without unilateral avulsion**. *International urogynecology journal*, vol. 34, no. 9, pp. 2225-2233, 2023.

Abstract

The puborectal muscle (PRM), one of the female pelvic floor (PF) muscles, can get damaged during vaginal delivery leading to disorders like pelvic organ prolapse. Current diagnosis involves ultrasound (US) imaging of the female PF muscles but functional information is limited. Previously, we developed a method for strain imaging of the PRM, from US images to obtain functional information. In this article, we hypothesize that functional information like strain in the PRM could be used to distinguish between intact PRMs from PRMs with unilateral avulsion. We calculated strain in PRMs at maximum contraction, along their muscle fiber direction, from US images of two groups of women, which consisted of women with intact (n_1 = 8) and avulsed PRMs (unilateral) (n_2 = 10). Normalized strain ratios between both ends of the PRM (avulsed or intact) and the mid region were calculated. Subsequently, the difference in ratio between the avulsed and intact PRMs was determined. We observe from the obtained results that the contraction/strain pattern of intact and undamaged PRMs is different from PRMs with unilateral avulsion. Normalized strain ratio's between avulsed and intact PRMs were statistically significant (p = 0.04). US strain imaging of PRMs can shows differences between intact PRMs and PRMs with unilateral avulsion.

Keywords - ultrasound, puborectal muscle, unilateral avulsion

3.1 Brief introduction

In this chapter, calculations for projected strain have been introduced for the puborectal muscles (PRMs) of women. Initially, displacement estimates in the muscle fiber direction from the tracked PRMs have been estimated and thereafter strain have been calculated in the same direction, which is called as projected strain. Strain calculations are from women with intact PRMs as well as from women with unilateral avulsions of PRMs. The results shown in this chapter demonstrate that projected strain imaging of PRMs can be used to assess the state of the muscle.

3.1.1 Data acquisition

Data acquisition from all the women (intact PRMs as well as unilateral avulsion of PRMs) for which the results of projected strain have been shown is briefly mentioned in the **Table 3.1**.

3.1.1.1 Intact and unilateral avulsion of PRMs

US data were obtained over time from women who had intact and undamaged PRMs (n_1 = 8) and from women who had unilateral avulsion (n_2 = 10). In all women, US volumes were recorded from rest to maximum contraction. Details of data acquisition have already been explained in **Chapter 2**, **Section 2.1.1**, for women with intact PRMs. For women with unilateral avulsions of PRMs, data acquisition was the same. The criteria for determining avulsion had been levator–urethra gap of ≤ 25 mm on the three central slices on either right or left side as unilateral or both sides as bilateral **[16]**.

3.1.2 Aim of the study

The aim of the work is to investigate if contraction/strain patterns of undamaged PRMs and PRMs with unilateral avulsion show differences. Our hypothesis is that intact or undamaged PRMs will have different contraction patterns than PRMs with unilateral avulsion in which scar or connective tissue formation can be present.

3.2 Methods

The next step, after data acquisition is to calculate strain in the PRMs using the obtained US volumes (DICOM). The method to calculate strain is explained thoroughly in our previous publication and is summarized in **Figure 3.1 [1]**. In short, inter-volume displacements were calculated between subsequent recorded volumes and used to update the segmentations of the PRMs. Those intervolume displacements were accumulated to calculate strain during muscle contraction.

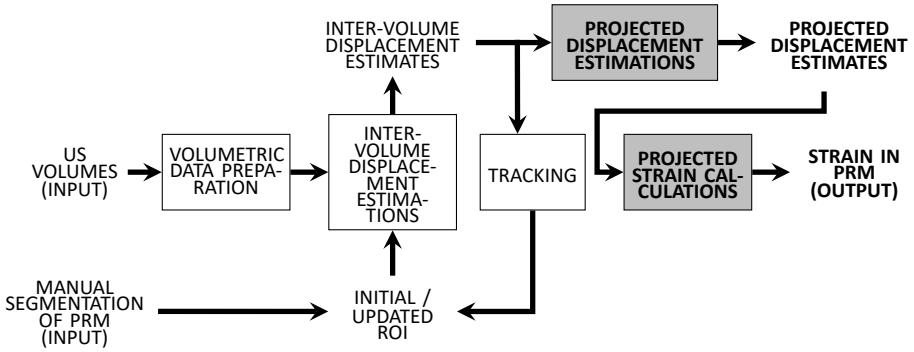

Figure 3.1: Block diagram 1; the blocks in white have been explained in our previous publication [1] (The blocks in grey with bold letters have been explained in the current section)

3.2.1 Post-processing of US volumes

Since the objective of this work is to detect whether there might be differences in the contraction pattern of the PRM, the strain in the muscle fiber direction is determined. However, since the muscle fiber direction is dependent on the location, the displacement estimates were determined in the x, y and z directions. From that, strain along the muscle fiber direction have been obtained.

Information about the muscle fiber direction is not provided by studies on gross anatomy **[2]**. However, this information has been determined by MR fiber tractography **[3]**. According to MR tractography of female PF, the fiber directions are such, that the individual fibers are connected to the two parts of the bone pubic symphysis (PS), and they curve around to form the sling of the muscle as shown in **Figures 3.2a** and **3.2b**.

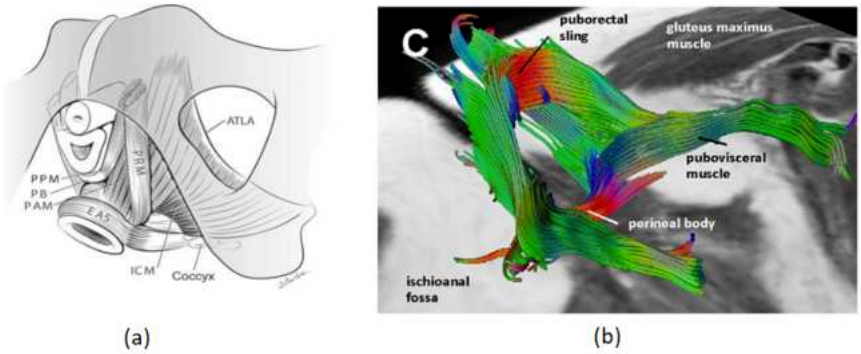

Figure 3.2: (a) Pelvic floor anatomy showing PRM [2] (Permission granted by the publisher to use this image), (b) MR tractography showing the muscle fiber orientation of the PRM and the puborectal sling [3] (Permission granted by the publisher to use this image)

Therefore, we modified the original method to assess strain along the fiber direction (gray blocks of the block diagram in **Figure 3.1**). These gray blocks have been detailed with flowcharts, shown in **Appendices F - G**.

As shown in this block diagram, the **'inter-volume displacement estimates'** at a certain time point or volume number were used to calculate the **'projected displacements'** along the fiber direction. Therefore, the center line of the PRM was calculated which acted as reference for the muscle fiber direction.

The center line of the muscle was obtained in three steps. In the first step, the **'manual segmentation of PRM'**, or **'updated ROI'** as shown in **Figure 3.3**

was eroded over its entire length. This allowed us to obtain a connected curve or center line over the length of PRM. In the second step, this connected curve was fitted to a polynomial curve to smooth the obtained curve and to remove outliers. In the third step, the accumulated displacements (x, y and z directions) were projected to the closest point on this central axis using vector projections **[4]**. Finally, strain was calculated by the projected displacements using a 2x2x2 least-squared strain estimator (LSQSE) **[5]**. These calculations were performed while correcting for the change in angle or direction of the previously calculated center line of the PRM. Thus, we obtain the projected strain values for the PRM at a certain volume. These projected displacements were calculated for all volumes, from rest to contraction.

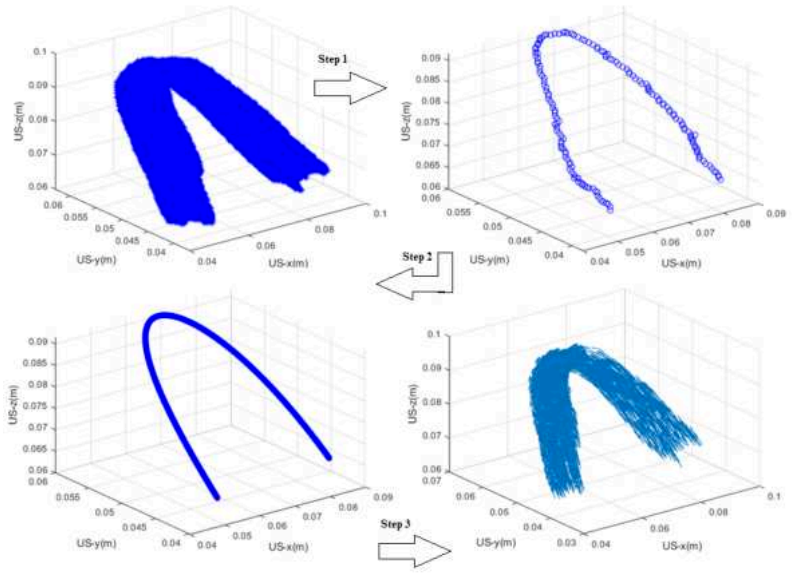

Figure 3.3: An example of a segmented PRM (in 3D), showing the center line through it and center line after curve fitting and scaling (Steps 1-3). The last figure shows the displacement estimates projected on the center line

3.2.2 Normalized ratio of strain percentage in PRM

Anatomically, the muscle fibers in the PRM are approximately parallel to the US transducer direction in the two connected ends, when imaged in TPUS. The muscle fibers in the mid region or 'sling' of the PRM are approximately perpendicular to the US transducer direction. Since we are interested in the effect of avulsion on the local contraction properties of the PRM, we have divided the whole PRM into three parts: the two ends, that are in undamaged condition connected to the PS and the mid region between these two ends, containing the 'sling'. The reason for choosing three regions in the PRM is based on the observation (later shown in Results section, **Figure 3.5b**) that in case of intact PRMs, the two regions near the bone show similar strain and the mid-region show different strain. The division of the muscle into three regions enable us to relate the strain in the ends of the PRM with that of the mid-region through normalized strain ratio.

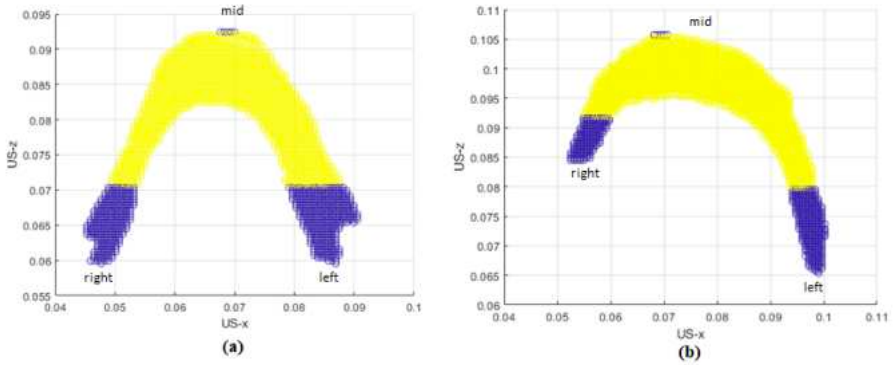

Figure 3.4: Three regions (shown in XZ plane, axial view) within the PRM with the right, left (blue) and mid regions (yellow) labeled; (a) example showing intact PRM, (b) example showing PRM with unilateral avulsion

Since the PRM for each woman has slightly different size and volume; each PRM has been individually divided into three subdivisions. The combined vol-

ume of both the subdivisions of the PRMs which includes the connection to the PS (shown in blue in **Figure 3.4a** and **Figure 3.4b**), was approximately one-third of the total volume of the PRM. These three subdivisions have been done for both intact PRMs and PRMs with unilateral avulsion. Examples of these subdivisions or regions are shown in **Figure 3.4a** and **Figure 3.4b**, for both intact PRM and unilateral avulsion of PRM.

For the analysis, the strain values in the three regions were used. As a first step, medians of the strain values were obtained for the three regions for all the women. Since the contraction of the PRM was widely variable among women, a wide range of strain values was obtained. To correct for this effect, the difference in strain values for both ends was normalized by relating it to average difference in strain between the mid region and the average of both ends according to **Equation** .

$$\textit{Normalized strain ratio} = \frac{[abs(\varepsilon_{right} - \varepsilon_{left})]}{[abs(\varepsilon_{mid} – avg(\varepsilon_{right}, \varepsilon_{left}))]} \tag{3.1}$$

where,

$\varepsilon_{right} =$ median of the percentage of strain in right region of PRM,
$\varepsilon_{left} =$ median of the percentage of strain in left region of PRM,
$\varepsilon_{mid} =$ median of the percentage of strain in mid region of PRM

and *abs* and *avg* indicate *absolute* and *average* values respectively.

3.2.3 Statistical analysis

The normalized strain ratio was calculated for all women with and without unilateral avulsion (two independent and non-paired groups). Since the normalized strain ratios were not normally distributed, non-parametric statistical analysis had been performed. Shapiro-Wilk test of normality was used to verify non-normality. Statistical significance has been calculated using Mann-Whitney U-test and a p-value < 0.05 was considered significant **[6]**.

P-values and medians for the two groups, for age, BMI and parity have been calculated and shown in **Table 3.1**. Since, ages and BMIs for the two groups followed normal distribution, t-tests were used for calculating p-values. To calculate the p-value for parity, Mann-Whitney U test was used since parity values for the two groups did not follow normal distribution.

3.3 Results

The developed method had been applied on all the datasets acquired from women with intact and undamaged PRMs (n_1 = 8) and women with unilateral avulsion (n_2 = 10). The demographic characteristics of all these women is shown in table 1. The median values of age, BMI, parity and additional information about delivery for all the women included are listed as indicators of the health of their PF muscles. Women with intact PRMs are in general, younger and have less parity, as shown in the medians. The median of BMI between the two groups show lower median for the group with intact PRMs although were not significantly different. In this work, the effects of different age, parity and BMI have not been analyzed and can be only done on a large scale study. Thus statistical significance for these parameters between the two groups have also been not considered.

Figures 3.5a and **3.5b** show typical projected strains of an intact PRM and a PRM with unilateral avulsion, respectively (**Figures S3.1** to **S3.8** in the supplementary figures show projected strains for the rest of the included women). The projection of the strain on the central axis resembles the strain in and along the muscle fiber direction. The intact PRM shows that high negative strain values (indicating high levels of contraction) are present in the mid region and the strain values at both ends show positive strain values. In case of PRM with unilateral avulsion, it can be observed that the strain pattern differs from the intact and undamaged PRM. Here, strains in the avulsed end and the mid region are negative. In the intact end of the PRM, strain is positive similar to the two intact ends in case of an intact PRM. We observed similar findings for the strain values in all women in the two groups, as observed in these two examples.

Table 3.1: Demographic information about all the inclusions

	Women with intact PRMs (n_1 = 8)	Women with unilateral avulsion of PRMs (n_2 = 10)	P-values
Median of age	34	58	0.01
Median of BMI	20.9	24.4	0.07
Parity	0-1	1-3	$<$0.01
Additional information	7 women nulliparous, 1 woman vaginally nulliparous (with primary C-section)	1 woman with 1 vaginal delivery (and 1 vacuum extraction), 6 women with 2 vaginal deliveries, 2 women with 3 vaginal deliveries	-

In **Figure 3.6** two boxplots are shown of the normalized strain ratio obtained using equation 1 in women with intact PRMs and women with unilateral avulsion. In case of women who do not have an avulsion, the ratios are in general less than 1, which means that the two ends of the PRMs show similar strain values which are larger than the strain in the mid-section. In case of women with unilateral avulsion, the ratio in general is larger than 1. Values more than 1 means that the difference between the two ends is greater than the difference between the strain of the mid region and the strain in the two ends. In other words, it means that these particular PRMs have a large difference in strain values between the two ends.

In case of women with intact or undamaged PRMs, the median of the normalized strain percentage ratio is 0.36, with the upper and lower limits being 3.07 and 0.13 respectively. In case of women with unilateral avulsion the median is 1.54, with upper and lower limits being 14.59 and 0.95 respectively. The

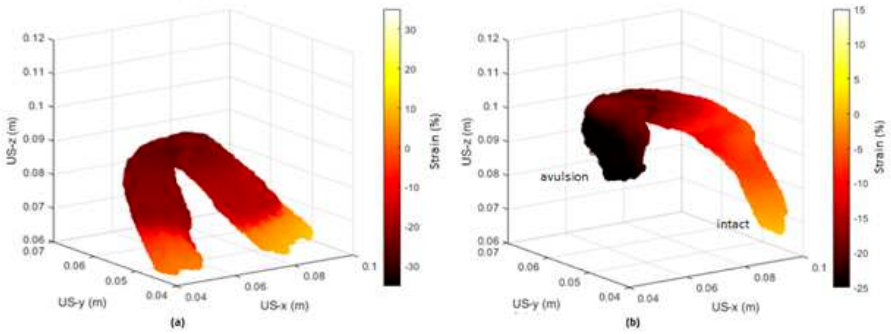

Figure 3.5: Percentage of strain at maximum contraction (shown in 3D) in two women with; (a) intact PRM, (b) unilateral avulsion of PRM (The avulsed and intact ends of the avulsed PRM are labeled. X, Y and Z axes are in meter and the color bars show percentage of strain from negative (dark red) to positive (yellow))

difference in the medians between these two groups of women is represented in the boxplots.

The normalized strain ratio is within 1, for six out of the eight women with undamaged PRMs. For two women, in this group, we found that the normalized strain ratio is more than one (1.96 and 3.07).

In the group of women with unilateral avulsion, the normalized strain ratio is larger than 1 for nine out of ten women. For one of the women, the ratio is 0.95.

Non-parametric statistical analysis using Mann-Whitney U-test shows a significant difference ($p = 0.04$) demonstrating that women with unilateral avulsion have a higher ratio than women with intact PRMs.

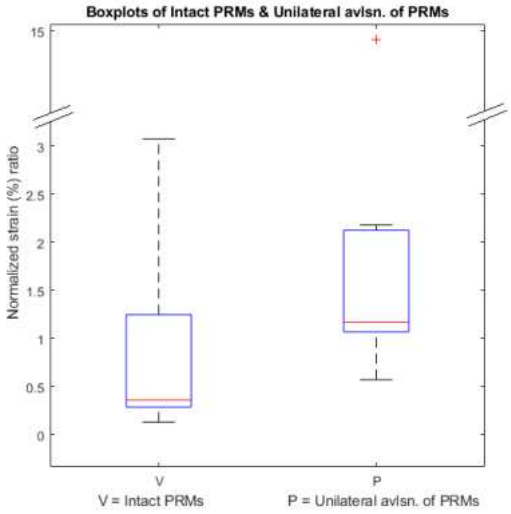

Figure 3.6: Boxplots showing normalized strain ratio for women with intact PRMs and women with unilateral avulsion

3.4 Discussion

The principal finding of this pilot study is that the strain pattern at contraction in the avulsed end of the PRM, is different from the intact end, whereas strain patterns were similar in both ends of intact and undamaged PRMs.

PRM is part of LAM. Function of the LAM is to maintain equilibrium by balancing the hydrostatic pressure of the overlying pelvic organs and also adjust to variations in posture **[12-13, 7]**. LAM consists of type 1 striated muscle fibers. Striated muscles are most prone to injury when they are forcibly lengthened, such as vaginal birth **[12-13]**. Earlier studies have demonstrated that LAM defects occur after vaginal birth which can confer a four-to eleven-fold increase in risk for developing prolapse among parous women **[13]**. LAM damage is avulsion of the PRM **[14]**. This damage can be imaged by functional imaging.

Current literature already explains the term functional imaging using MRI **[8]**. Functional US imaging of the female PF can be defined as US imaging of

the PF while the woman voluntarily contracts or undergoes Valsalva maneuver (VM) of their PF muscles. In recent functional studies of the PF, shear wave elastography (SWE) has been studied and it has been reported that it is possible to measure the shear modulus of the LAM, at rest and at VM **[9]**. Another method reported in literature is representative finite element model (FEM) of the PF based on anatomy from a 2D or 3D level **[10-11]**. These studies have used MRI imaging of PF at VM instead of contraction of the LAM. Since, we used 3D strain as measure for contraction we could not directly compare our results with already published results.

In the obtained results, in case of the group of women with intact and undamaged PRMs, it can be observed in **Figure 3.5a** that the contraction started at the mid region or slings of the PRMs. The negative strain in the sling shows contraction of this part of the PRM. The two ends which are connected to the PS show positive strain which indicate elongation of these two parts. This indicates that the contraction of the PRM is dominated by the central area, whereas both connected ends appear to elongate as indicated by the positive strain values.

Our results, as shown in **Figure 3.5b**, showed that in case of strain in PRMs in women with unilateral avulsion, negative strain was obtained in the mid-regions as well as the avulsed ends of the PRMs. The possible explanation for this is that the avulsed end could contract along with the mid region to which it was connected and not elongate since it was not connected to the bone. The intact ends of these PRMs still showed positive strain indicating elongation. This revealed a different contraction pattern when compared with strain images of PRMs with no damage, where both the intact ends of the muscle showed positive strain or elongation. Thus, we obtained different contraction patterns in the two groups of women.

In our work, data was acquired from women only at rest and contraction, since the primary objective was to investigate about the active component of PRM functionality shown during contraction. A future extension of this work could also be used to investigate about the passive component of PRM functionality, shown during Valsalva maneuver. The boxplots in **Figure 3.6** showed a difference in the medians of the normalized strains in these two groups of women. Furthermore, although we had to perform a non-parametric statistical

test due to small sample sizes, we still could show that the strain ratio is significantly ($p = 0.04$) different between avulsed and intact PRMs.

The normalized strain ratio is within 1, for six out of the eight women with undamaged PRMs. This indicates that the strain in the two connected ends of the PRM are similar. This is also expected because the ends of the muscle are intact and undamaged, resulting in similar strain. For two women, in this group, we found that the normalized strain ratio is more than one (1.96 and 3.07). Since, our study is a pilot study, the cause for this higher ratio could not be determined.

In the group of women with unilateral avulsion, the normalized strain ratio is larger than 1 for nine out of ten women. This indicates that the strain in the avulsed end of the muscle is more negative than strain in the intact end. For one of these women, the ratio is marginally less than 1.

Although we had to perform a non-parametric statistical test due to small sample sizes, we still could show that the strain ratio is significantly ($p = 0.04$) different between avulsed and intact PRMs.

3.4.1 Clinical significance

Potential clinical significance of our work can be stated as two-fold. Firstly, recognizing which part of the muscle is dysfunctional may be of benefit for physiotherapists treating women with pelvic floor disorders. Also, recognizing that there is presence of severe structural damage may well change the policy of having PF muscle training in every women with PF disorders.

Secondly, when clinicians look at regenerative action for the muscle after delivery, it would be possible to determine if there has been functional improvement of the muscle after training. Changes in strain in the muscle as observed from before to after training could tailor the training to obtain optimal benefit.

3.4.2 Limitations and future work

There are three limitations of the work. Firstly, the tracking of the PRM that

was integral part of the method, was only visually verified on B-mode US volumes. However, since the technology is based on similar principles as applied for extensively validated cardiac strain imaging techniques, and the contraction patterns are in accordance with physiologic assumptions, it can be concluded that the performed analysis is valid. Secondly, currently our method is based on in house developed software for displacement estimation which makes the method computationally extensive. However, since 3D cardiac strain estimation is feasible almost online, we expect our analysis can also be made nearly real-time. Thirdly, the segmentation of the PRMs at rest have been performed manually, which could be extended to automated as is demonstrated in literature **[15]**.

To further investigate PF muscles through 3D strain, future studies should include larger sample sizes and effort to reduce the computation time for calculation of the strain values. Also, other muscles of the LAM apart from PRM should be studied to learn how the surrounding muscles behave in relation to each other, in both groups of women.

3.5 Conclusion

We could show in this pilot study that women with unilateral avulsion of their PRMs show different strain pattern than women with intact PRMs.

References

[1] S. Das et al., "3D ultrasound strain imaging of puborectalis muscle," Ultrasound in Medicine & Biology, vol. 47, no. 3, pp. 569–581, 2021.

[2] J. A. Ashton-Miller and J. O. DeLancey, "Functional anatomy of the female pelvic floor," Annals of the New York Academy of Sciences, vol. 1101, no. 1, pp. 266–296, 2007.

[3] F. M. Zijta, M. Froeling, A. J. Nederveen, and J. Stoker, "Diffusion tensor imaging and fiber tractography for the visualization of the female pelvic floor," Clinical anatomy, vol. 26, no. 1, pp. 110–114, 2013.

[4] M. Hausner, A vector space approach to geometry. Courier Corporation, 1998.

[5] F. Kallel and J. Ophir, "A least-squares strain estimator for elastography," Ultrasonic imaging, vol. 19, no. 3, pp. 195–208, 1997.

[6] D. G. Altman, Practical statistics for medical research. CRC press, 1990.

[7] J. A. Ashton-Miller and J. O. DeLancey, "On the biomechanics of vaginal birth and common sequelae," Annual review of biomedical engineering, vol. 11, pp. 163–176, 2009.

[8] A. Lienemann and T. Fischer, "Functional imaging of the pelvic floor," European journal of radiology, vol. 47, no. 2, pp. 117–122, 2003.

[9] B. Gachon, X. Fritel, F. Pierre, and A. Nordez, "Transperineal ultrasound shear-wave elastography is a reliable tool for assessment of the elastic properties of the levator ani muscle in women," Scientific Reports, vol. 11, no. 1, pp. 1–9, 2021.

[10] J. Xie, S. Li, T. Yao, and J. Shen, "A 2D equivalent mechanical model of the whole pelvic floor and impairment simulation," International Journal for Numerical Methods in Biomedical Engineering, vol. 39, no. 1, p. e3659, 2023.

[11] Z. Yang, J. Hayes, S. Krishnamurty, and I. R. Grosse, "3D finite element modeling of pelvic organ prolapse," Computer methods in biomechanics and biomedical engineering, vol. 19, no. 16, pp. 1772–1784, 2016.

[12] F. van den Noort, A. T. Grob, C. H. Slump, C. H. van der Vaart, and M. van Stralen, "Automatic segmentation of puborectalis muscle on three-dimensional transperineal ultrasound," Ultrasound in obstetrics & gynecology, vol. 52, no. 1, pp. 97–102, 2018.

[13] K.-C. Lien, B. Mooney, J. O. DeLancey, and J. A. Ashton-Miller, "Levator ani muscle stretch induced by simulated vaginal birth," Obstetrics and gynecology, vol. 103, no. 1, p. 31, 2004.

[14] J. O. DeLancey et al., "Comparison of levator ani muscle defects and function in women with and without pelvic organ prolapse," Obstetrics & gynecology, vol. 109, no. 2 Part 1, pp. 295–302, 2007.

[15] H. Dietz, "Clinical consequences of levator trauma," Ultrasound in obstetrics & gynecology, vol. 39. Wiley Online Library, pp. 367–371, 2012.

[16] C. Manzini, C. H. van der Vaart, F. van den Noort, A. T. Grob, and M. I. Withagen, "Pessary fitting for pelvic organ prolapse: Parameters associated with specific reasons for failure," International urogynecology journal, vol. 33, no. 7, pp. 2037–2046, 2022.

Supplementary figures

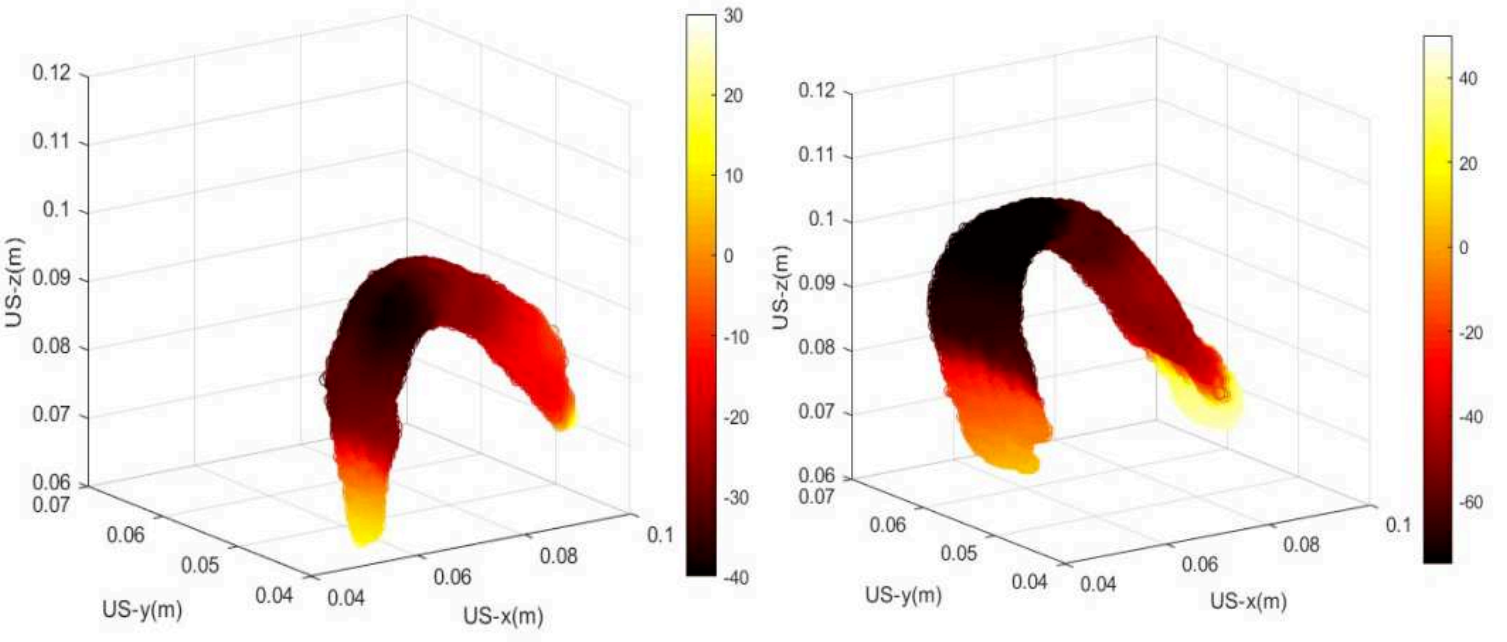

Figure S3.1: Percentage of strain at maximum contraction (shown in 3D) in two women with intact PRMs. X, Y and Z axes are in meter and the color bars show percentage of strain from negative (dark red) to positive (yellow)

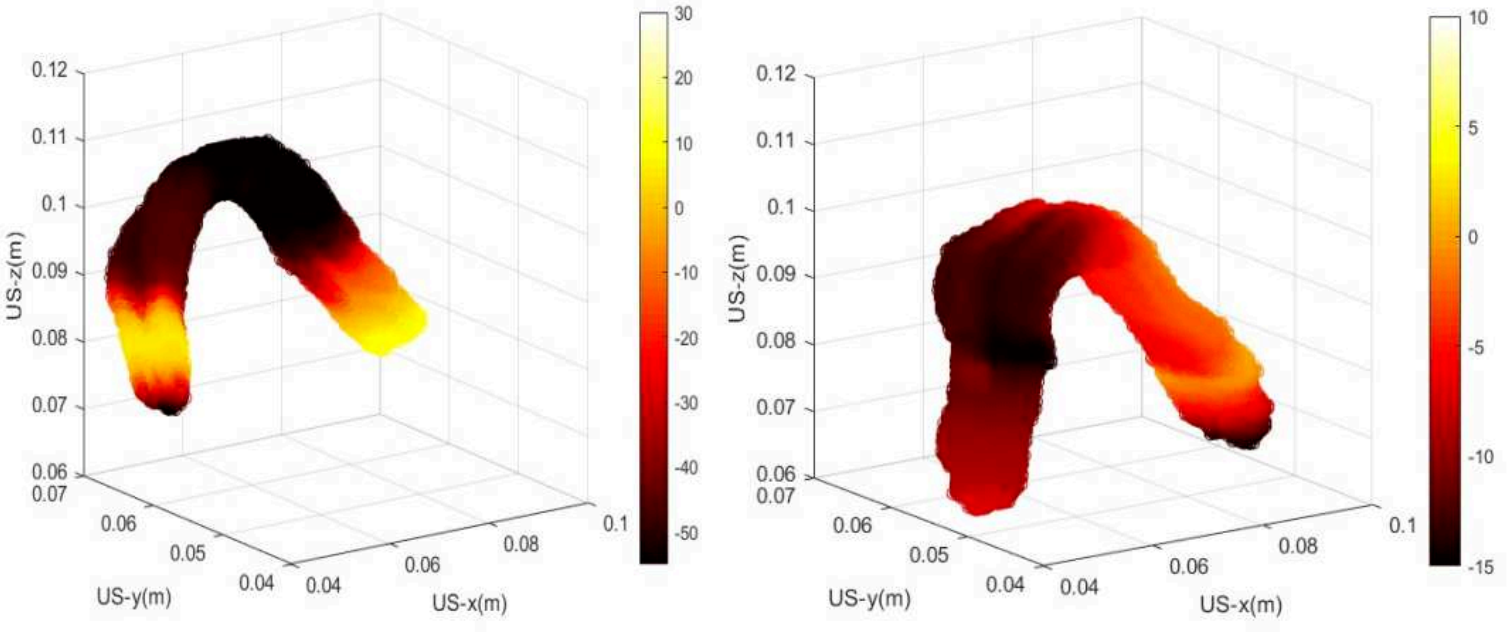

Figure S3.2: Percentage of strain at maximum contraction (shown in 3D) in two women with intact PRMs. X, Y and Z axes are in meter and the color bars show percentage of strain from negative (dark red) to positive (yellow)

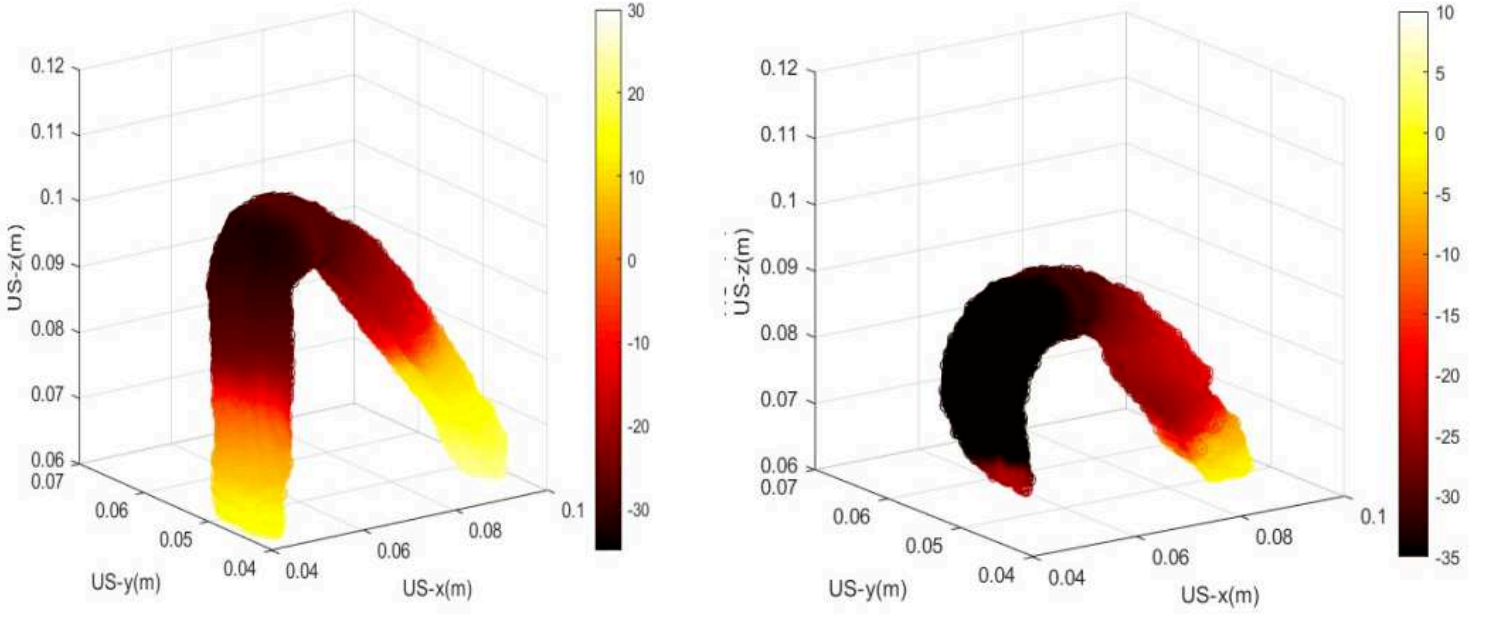

Figure S3.3: Percentage of strain at maximum contraction (shown in 3D) in two women with intact PRMs. X, Y and Z axes are in meter and the color bars show percentage of strain from negative (dark red) to positive (yellow)

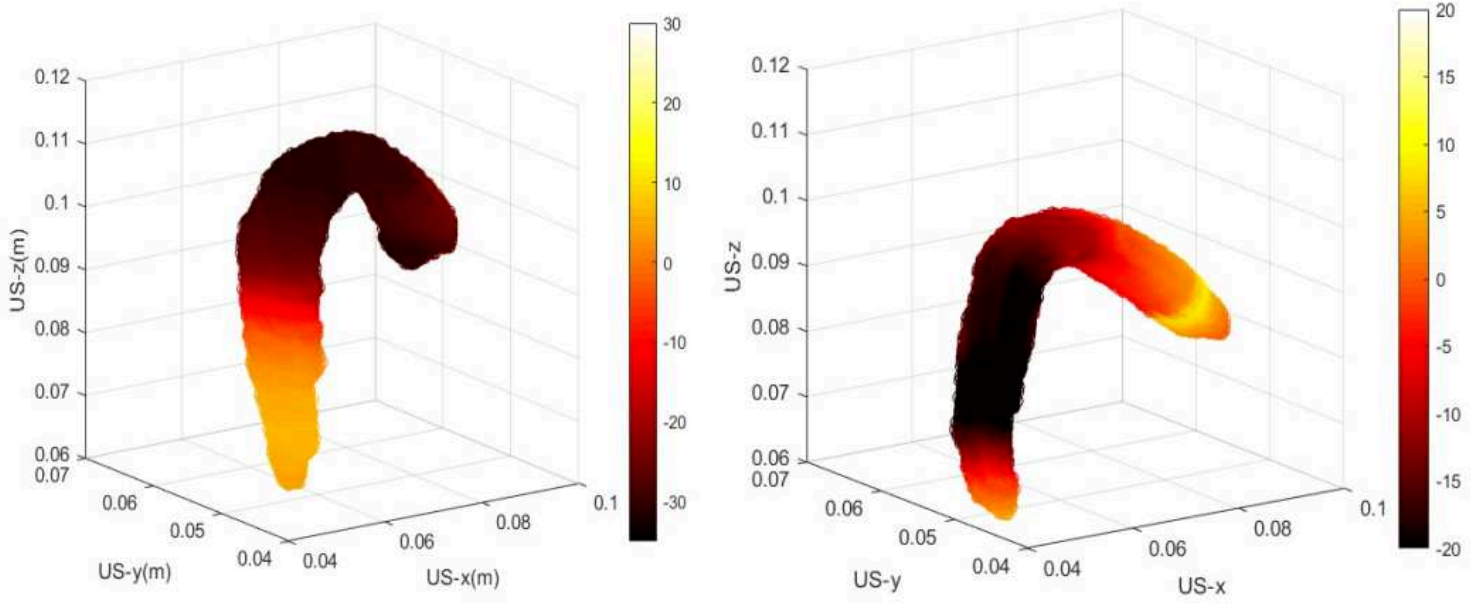

Figure S3.4: Percentage of strain at maximum contraction (shown in 3D) in two women with unilateral avulsion of PRMs. X, Y and Z axes are in meter and the color bars show percentage of strain from negative (dark red) to positive (yellow)

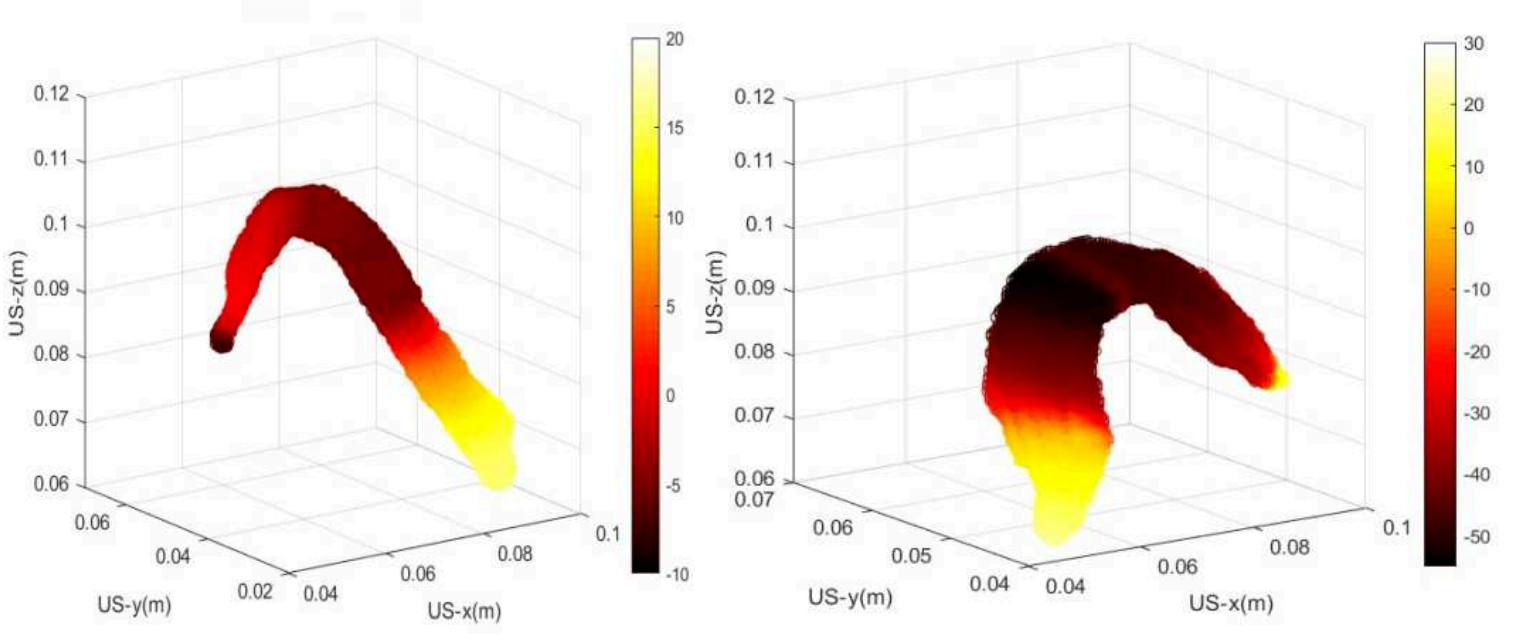

Figure S3.5: Percentage of strain at maximum contraction (shown in 3D) in two women with unilateral avulsion of PRMs. X, Y and Z axes are in meter and the color bars show percentage of strain from negative (dark red) to positive (yellow)

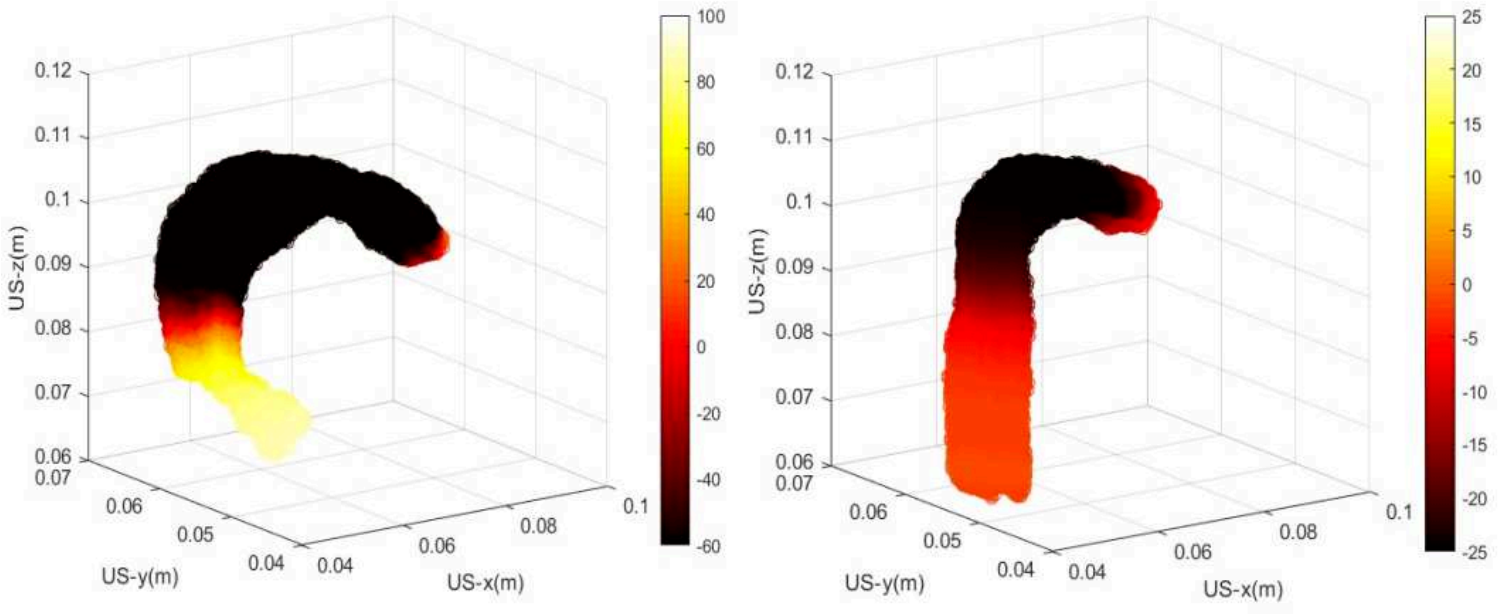

Figure S3.6: Percentage of strain at maximum contraction (shown in 3D) in two women with unilateral avulsion of PRMs. X, Y and Z axes are in meter and the color bars show percentage of strain from negative (dark red) to positive (yellow)

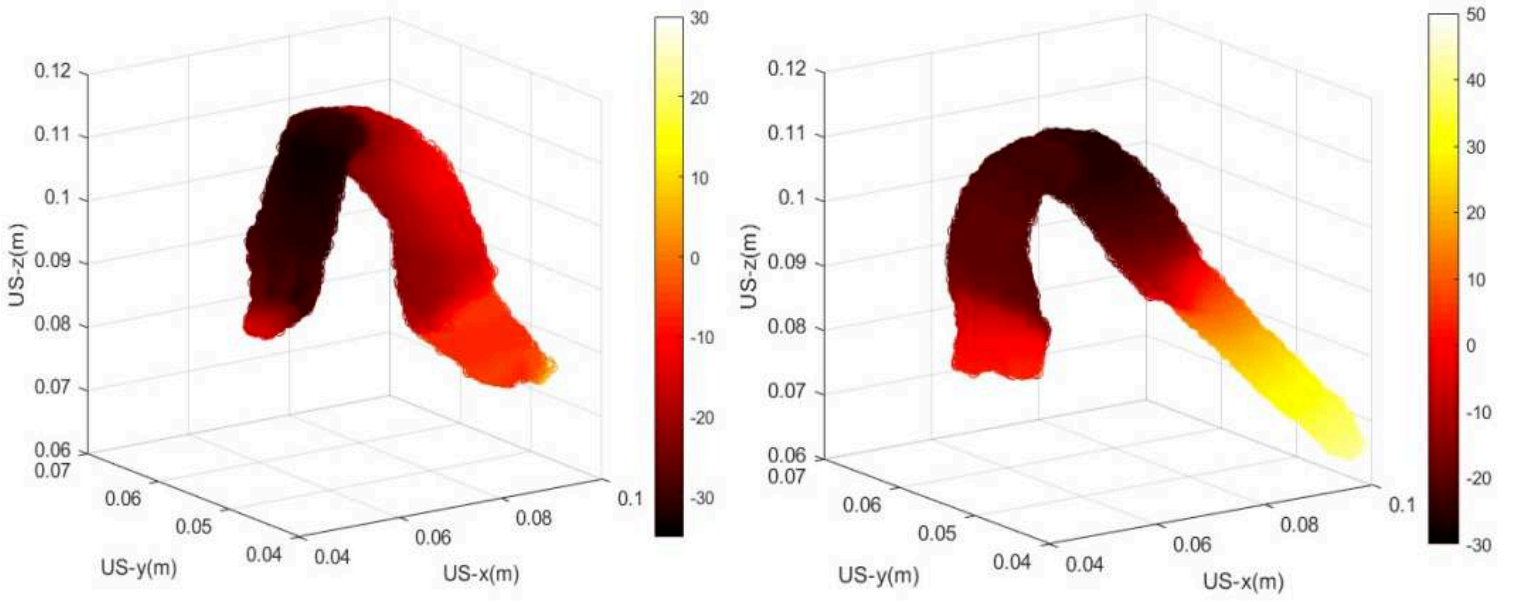

Figure S3.7: **Percentage of strain at maximum contraction (shown in 3D) in two women with unilateral avulsion of PRMs. X, Y and Z axes are in meter and the color bars show percentage of strain from negative (dark red) to positive (yellow)**

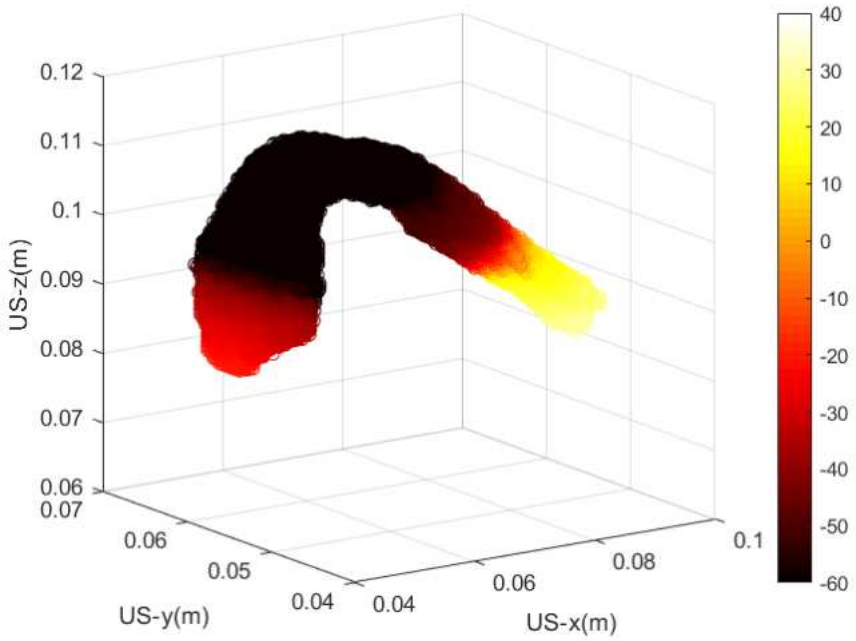

Figure S3.8: Percentage of strain at maximum contraction (shown in 3D) in one woman with unilateral avulsion of PRMs. X, Y and Z axes are in meter and the color bars show percentage of strain from negative (dark red) to positive (yellow)

Chapter 4

Functional assessment of ring pessary effect on avulsed PRM

This chapter is based on the manuscript (submitted):
S. Das, G. A. G. M. Hendriks, F. van den Noort, C. Manzini, C. H. van der Vaart & C. L. de Korte, **Effect of a ring pessary on avulsed puborectal muscle through ultrasound strain imaging.**

Abstract

Placement of a ring pessary is one of the treatment options for women with pelvic organ prolapse (POP). To determine the effect of ring pessary use in these women, usually qualitative measures like a patient experience questionnaire is used. However, quantitative functional information could provide additional information about the state of the pelvic floor muscles. In this work, we describe ultrasound (US) strain imaging of puborectal muscle (PRM) to provide functional information. We acquired US data in women with avulsion, before and after pessary fitting and subsequently, their strain patterns have been compared. Normalized strain ratios have been calculated for these women to quantitatively indicate the changes in the state of the PRM at maximum contraction, before as well as three months after pessary use . Before pessary placement, the strain ratio was elevated with respect to strain ratios found in women without an avulsion. After pessary placement, we found that the strain ratio decreased to values close to strain ratios found in women with no avulsion indicating the benefit of pessary placement.

Keywords - 3D Ultrasound, Puborectalis, Pessary, Strain imaging

4.1 Brief introduction

Pelvic organ prolapse (POP) is a common condition among women with defects in levator ani muscle (LAM). It is often observed that these women generate less vaginal closure force during a maximal contraction than controls **[1]**. One of the treatment options of symptomatic POP is pessary placement. Pessaries are an inexpensive, simple, low risk, and effective conservative treatment for POP **[2–4]**. The effectiveness of pessary fitting can be assessed by a questionnaire which is answered by the woman, post pessary fitting and usage. This questionnaire is qualitative rather than quantitative. It has been previously shown that successful pessary fitting is associated with the size of the hiatal area and that contractibility of the PRM changed after three months of pessary use **[22-24]**.

For years ultrasound (US) is a widely accepted imaging modality used for visualizing female PF muscles **[5–7]**. However, to the best of our knowledge functional information about PF muscles obtained with US imaging is limited. In our previous work, we showed that strain imaging from three-dimensional (3D) US images of PRM, can provide functional information about the muscle. The level of contraction as well as the region(s) within the PRM where this contraction occurs, can be quantified by US-based strain imaging whereas the woman voluntarily contracts the PRM **[8]**. Thus, strain imaging could be performed both prior to and post pessary fitting as a quantitative assessment of the change in PRM function. In our previous study, we have formulated a normalized strain ratio which provides a quantitative measure of the condition of the muscle. This ratio was found to be different in intact PRMs as compared to PRMs with unilateral avulsion **[20]**. The hypothesis of this study is that the normalized strain ratio after three months of pessary usage will change to levels obtained in women with intact PRMs as compared to the normalized strain ratio measured prior to pessary placement.

In this chapter, projected strains have been calculated for the puborectal muscles (PRMs) of women before and after pessary fitting. The results shown in this chapter demonstrate that strain in a PRM after pessary is affected by the pessary in women with unilateral as well as bilateral avulsion.

4.1.1 Data acquisition

Data acquisition from the women for which the results of principal strain before and after pessary fitting have been shown in **Table 4.1**.

The data were stored in the Digital Imaging and Communications in Medicine (DICOM) format. US data were obtained over time from women with unilateral (n_1 = 6) and bilateral (n_2 = 3) avulsions. In all women, US volumes were recorded from rest to maximum contraction, as the women were asked to voluntarily and actively contract their PF muscles (in supine position with empty bladder). Presence of PRM contraction in these women were ensured by a positive biofeedback while the clinician observed the muscle contraction in the US machine during data acquisition. Details of data acquisition have been explained in **Chapter 2**, **Section 2.1.1** and in **Chapter 3**, **Section 3.1.1**.

The criteria for determining avulsion had been levator–urethra gap of $\geq$25 mm on the three central slices on either right or left side as unilateral or on both sides as bilateral **[9]**. All women were fitted at intake with a ring pessary of appropriate size. The reason for choosing this type of pessary was that , it is clinically acceptable to start the pessary treatment with this type and continue usage unless deemed not fit by the woman **[10]**. Data were acquired from women both before and after three months of successful pessary use. The following appointment was scheduled two to four weeks after initial fitting to assess patients' satisfaction about the pessary. Thereafter upon success, usage continued for at least three months till the follow up acquisition. At follow-up the acquisition protocol was the same as stated earlier and the pessary was removed twenty minutes prior to data acquisition. No questionnaires were used for evaluation of user experience from the women.

4.1.2 Aim of the study

The aim of the study is to investigate if strain patterns as obtained with 3D ultrasound imaging from a contracting PRM in women with avulsion, before and after pessary fitting are different and whether the normalized strain ratio indicates this change.

4.2 Methods

4.2.1 Post-processing of US volumes

The next step, after data acquisition was to calculate strain in the PRMs using the obtained US volumes (DICOM). The method to calculate strain is explained in the Methods section of **Chapter 3** and is summarized in **Figure 3.1**. In short, inter-volume displacements were calculated between subsequent recorded volumes and used to update the segmentations of the PRMs. Those inter-volume displacements were accumulated to calculate total displacement at a time point and had been used for subsequent strain calculations at maximum muscle contraction.

Since the objective of this work is to detect whether there might be differences in the contraction pattern of the PRM, the strain in the muscle fiber direction is determined. However, since the muscle fiber direction is dependent on the location, the displacement estimates were initially determined in the x, y and z directions. From that, first the projected displacement estimates towards muscle fiber direction were estimated. Thereafter strain along the muscle fiber directions have been obtained. Therefore, we modified the original method to assess projected strain in the muscle fiber direction (gray blocks of the block diagram in Figure 1). Strain was calculated from the projected displacements using 2x2x2 cm least-squared strain estimator (LSQSE) while correcting for the change in angle or direction **[14]**. The projected strain values were obtained for the PRM at all volumes from rest to maximum contraction.

4.2.2 Normalized ratio of median of strain percentages in PRM

Anatomically, the muscle fibers in the PRM are approximately parallel to the US transducer direction in the two connected ends, when imaged in TPUS. The muscle fibers in the mid region or 'sling' of the PRM are approximately perpendicular to the US transducer direction. Similar muscle fiber directions for PRM have also been observed in fiber tractography **[12-13]**. Since we are interested in the effect of avulsion on the local contraction properties of the PRM, we have

divided the whole PRM into three parts: the two ends, that are in the undamaged condition connected to the PS and the mid-region between these two ends, containing the 'sling'. The reason for choosing three regions in the PRM is based on the observation (as shown in **Figure 2a**) that in case of intact PRMs, the two regions near the bone show similar low negative strain values as compared to the mid-region that show high negative strain values. Negative strain resembles contraction of the muscle while positive strain represents relaxation. The division of the muscle into three regions enable us to relate the strain in the ends of the PRM with that of the mid-region through normalized strain ratio.

Since the PRM for each woman has slightly different size and volume; each PRM has been individually divided into three subdivisions. The combined volume of both the subdivisions of the PRMs which includes the connection to the PS (shown in blue in **Figure 4.1**), was approximately one-third of the total volume of the PRM. These three subdivisions have been done for both intact PRMs and PRMs with avulsions. Examples of these subdivisions or regions are shown in **Figure 4.1**.

For the analysis, the strain values in the regions were used. As a first step, median values of the strain values were obtained for the three regions for the women. Since the level of contraction varies substantially among women, a wide range of strain values was obtained. To correct for this effect, the difference in strain values for both ends was normalized by relating it to average difference between the mid region and the average of both ends is according to **Equation** from **Chapter 3**. It is mentioned below again for easy reference.

$$\textit{Normalized strain ratio} = \frac{[abs(\varepsilon_{right} - \varepsilon_{left})]}{[abs(\varepsilon_{mid} – avg(\varepsilon_{right}, \varepsilon_{left}))]} \tag{4.1}$$

where,

$\varepsilon_{right} =$ median of the percentage of strain in right region of PRM,
$\varepsilon_{left} =$ median of the percentage of strain in left region of PRM,
$\varepsilon_{mid} =$ median of the percentage of strain in mid region of PRM

and *abs* and *avg* indicate *absolute* and *average* values respectively.

4.2.3 Statistical methods

The normalized strain ratio (NSR) was calculated for all women, before pessary placement and 3 months after using a pessary. Shapiro-Wilk test of normality was used to verify non-normality. Since the NSRs were not normally distributed, a Wilcoxon signed rank test was used to compare the strain ratio before and after pessary placement using the paired groups **[15-16]**. A p-value of < 0.05 was considered significant.

4.3 Results

The developed method have been applied to calculate projected strain and subsequent normalized strain ratios for women with avulsion, before and after pessary fitting. Since the aim of the study is to determine whether the strain pattern in the contracting PRM changes after fitting pessary, both unilateral (n_1 = 6) and bilateral (n_2 = 3) avulsions have been considered. Furthermore, the ratios have been calculated as an attempt to quantify the changes observed in the strain pattern.

The demographic characteristics of all these women such as median of age, median of body mass index (BMI) and parity all inclusions are shown in **Table 4.1**. These characteristics are listed as indicators of the health of their PF muscles.

Table 4.1: Demographic information about all the inclusions for effect of pessary

	Women with unilateral avulsion of PRMs (n_1 = 6)	Women with bilateral avulsion of PRMs (n_2 = 3)
Median of age (yrs)	65	67
Median of BMI (kg/m^2)	23.47	23.88
Parity	2-4	2

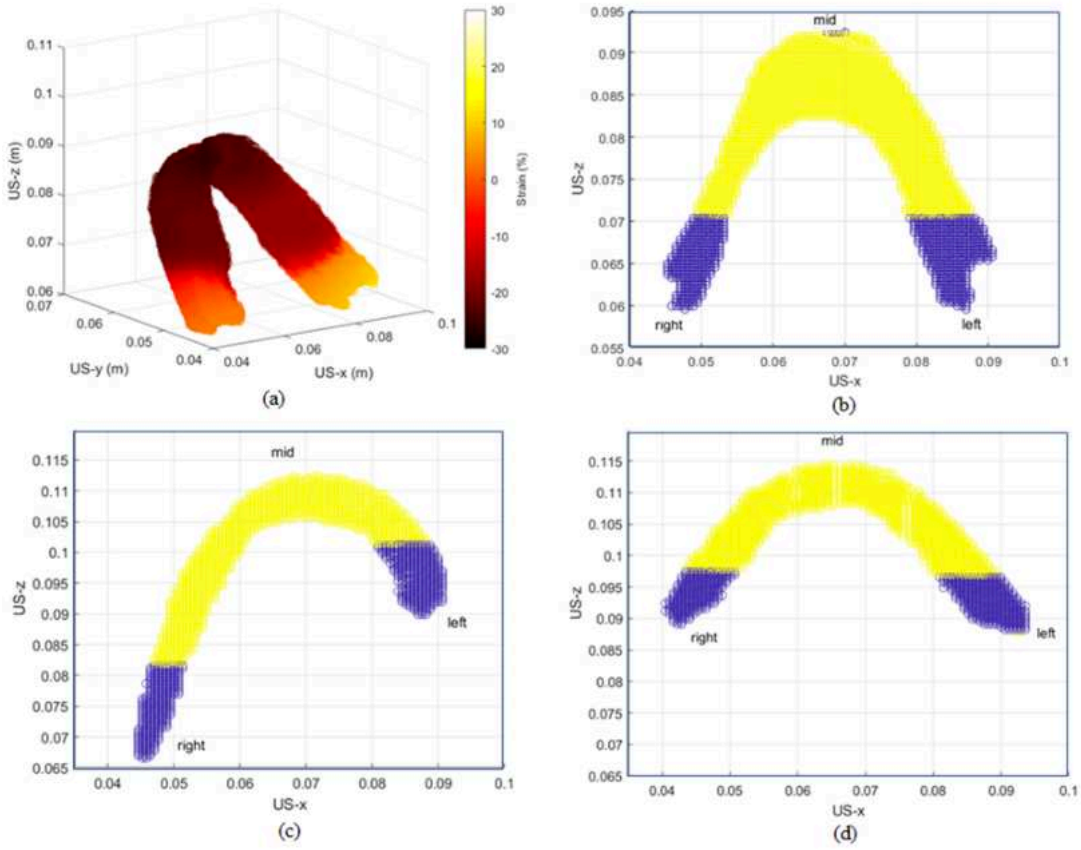

Figure 4.1: (a) Projected strain in intact PRM (b) Three regions (shown in XZ plane, axial view) within the PRM with right, left (blue) and mid (yellow) labeled, example showing intact PRM, (c) example showing unilateral avulsion, (d) example showing bilateral avulsion

4.3.1 Strain in unilateral avulsion of PRMs

In case of PRMs with unilateral avulsion, before pessary fitting, strain patterns differ from that of intact and undamaged PRM **[20]**. **Figure 4.2a** shows an example of unilateral avulsion before pessary fitting. We can observe that the muscle starts to contract from the mid region or sling of the PRM. The connected end of the PRM, shows positive strain and the mid region along with the disconnected end shows negative strain. The negative strain in the end of the muscle that is connected to the PS indicates that the tissue extends. The mid region of the PRM contracts and thus acts as normal PRM tissue. The disconnected end of the PRM also contracts along with the mid region, since this end is disconnected form the PS.

Figure 4.2b shows the same PRM as visualized in **Figure 4.2a** but after pessary fitting (**Figures S4.1** to **S4.5** in the supplementary figures show projected strains for the rest of the included women with unilateral avulsion). In this case also the mid region of the PRM is contracting. However, both ends of the PRM show a more similar contraction pattern to intact PRMs than before pessary fitting.

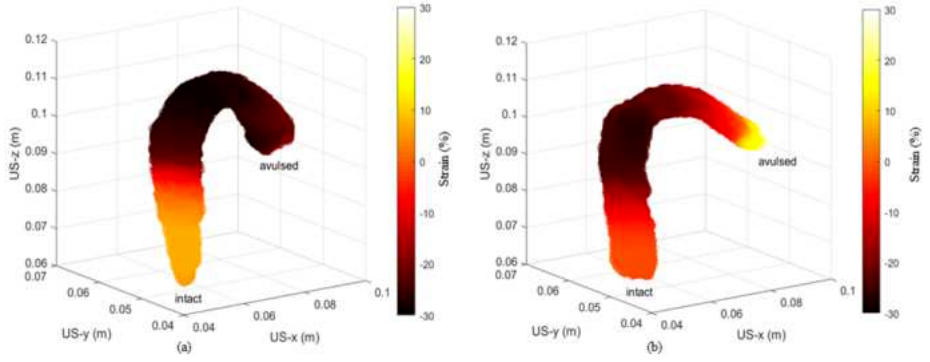

Figure 4.2: Strain in unilateral avulsion of PRM, at maximum voluntary contraction (a) Before pessary fitting (b) After pessary fitting (to be changed to 3D images)

4.3.2 Strain in bilateral avulsion of PRMs

Strain pattern in the PRMs with bilateral avulsion before pessary as shown in an example in **Figure 4.3a**, showed that, at maximum contraction, one end showed negative strain while the other end has positive strain values. However, different contraction levels can be observed in both ends. The mid part of the PRM shows negative strain values indicating contraction of this part of the muscle.

Strain pattern in these PRMs after pessary fitting, as shown in **Figure 4.3b**, showed that, both ends of the PRM showed zero to slightly positive strain to negative strain at maximum contraction (**Figures S4.6** and **S4.7** in the supplementary figures show projected strains for the rest of the included women with bilateral avulsion). But one end showed a large region of positive strain while the other showed a very small region of positive strain and the rest being negative strain as much as the mid region.

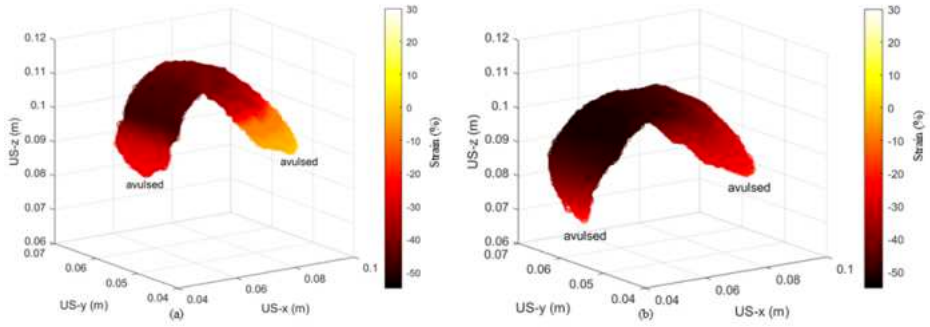

Figure 4.3: Strain in bilateral avulsion of PRM, at maximum voluntary contraction (a) Before pessary fitting (b) After pessary fitting (to be changed to 3D images)

4.3.3 Normalized strain ratio (NSR)

The NSR ratio in these women before and after pessary fitting are shown in the boxplots of **Figure 4.4a**. The median value of the NSR of all PRMs before pessary placement is 1.89 while after pessary placement a median value of 0.61 is found. Sub-analysis of unilateral and bilateral avulsions shows similar behavior before and after pessary placement: from 1.69 to 0.99 for the unilateral avulsion and from 2.54 to 0.32 for the bilateral avulsions.

We can also observe from the two boxplots, that the median of strain ratio from before pessary to after pessary reduces from 2.12 to 0.61.

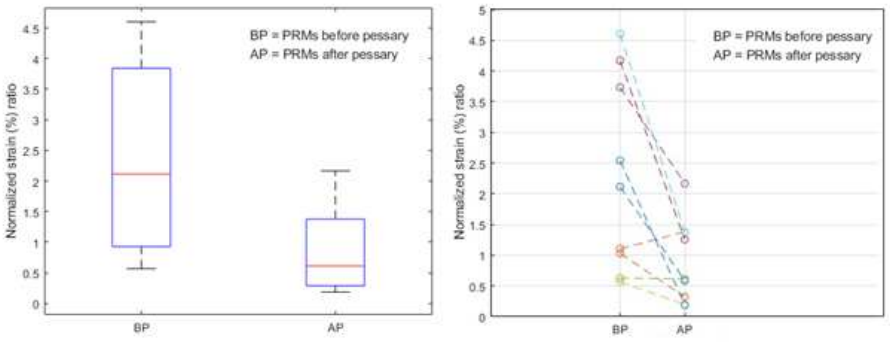

Figure 4.4: Boxplots showing normalized strain ratios for women with (a) PRMs of women with avulsion before and after pessary fitting and women with avulsion after pessary fitting (b) Change of normalized strain ratio in women with avulsion, from before pessary (BP) to after pessary (AP)

NSR in women with bilateral avulsion, similar to women with unilateral avulsion, showed a decrease in value after pessary fitting with respect to before. This is shown in **Figure 4.4b**. The only exception being one woman with unilateral avulsion who showed marginal increase from before to after pessary fitting.

Difference between strain ratio before and after pessary placement for all

women included in this study (n = 9) was significant (p = 0.004), demonstrating that women with avulsion before pessary fitting have a higher NSR than after pessary fitting . The difference of medians of the NSR between these two groups was 1.3.

4.4 Discussion

Strain imaging of the PRM is an innovative and novel technology that might be of added value to the diagnosis and follow-up of women with prolapse. In this study we have investigated if strain imaging of the PRM might be a new tool to evaluate the effect on PRM in women after pessary use. We obtained strain values in women after three months of pessary usage and compared these values with baseline before pessary fitting. The principal finding of this proof of principle study is that the strain ratio is increased with respect to normal values before pessary fitting and that these values decrease after three months pessary usage.

Prolapse occurs through the opening within the LAM, the urogenital hiatus where the urethra and the vagina pass. This hiatus is supported ventrally or anteriorly by the pubic bones and LAM and dorsally or posteriorly by the external anal sphincter muscle and perineal body. During rest, the baseline activity of an intact LAM keeps the urogenital hiatus closed by compressing the vagina, urethra and rectum against the pubic bones, the PF organs in the cephalic direction. This continuous action closes the lumen of the vagina leading to support of the overlying PF organs **[11, 17]**.

At maximum voluntary contraction of the LAM, the pubovisceral muscle and the PRM further (additional to the baseline activity) compress the mid-urethra, distal vagina and rectum against the pubic bone distally and against abdominal pressure more proximally. The part of the PRM which is supporting these three regions is the sling or mid region. Thus, as shown in **Figure 4.1a**, intact PRMs during voluntary contraction show greater strain in the mid region of the PRMs rather than the two ends connected to the pubic bone **[20]**. It is known that the PRM consists of type I slow twitch muscle fibers, which are physiologically equipped for anti-gravity and endurance activities **[1, 18, 21]**. These kind of

muscle fibers are expected to contract in the middle and not in the connected ends **[19]**.

In order to quantify, the different strains observed in the regions of the PRM, we have formulated the NSR **[20]**. This ratio, as defined in equation 1, expresses the differences between the two connected or disconnected ends of the muscle regardless of the type or sign of the contraction, positive or negative. In our previous study we have shown that increased strain ratio values are observed in women with unilateral avulsion with respect to women without avulsion. We found that the NSRs for these intact PRMs are lower than one whereas in avulsed PRM's the ratio is higher than one **[20]**.

4.4.1 Strain in avulsed PRMs prior to pessary fitting

We presented results from six women (n_1 = 6) with complete unilateral avulsion and three women (n_2 = 3) with bilateral avulsion before pessary fitting. In case of unilateral avulsion, at maximum contraction, probably the loading due to the overlying PF organs is now more on the connected end. The connected end elongates more to compensate this additional loading, whereas the disconnected end contracts along with the mid region of the PRM.

In case of bilateral avulsion, at maximum contraction, the two disconnected ends do not show same strain pattern. The mid region is still the one which starts to contract and at maximum contraction, the two ends behave in a way which might be an indication of the damage present. Since the damage in general is different both ends of the muscle, the end which is possibly more damaged is still showing higher negative strain than the other end.

In our previous study, we found that women with no avulsion showed NSR values of one or near to 1 **[20]**. Thus, this NSR showed that the high strain in the mid region were counteracted by the strains in the two connected ends. When we calculated the NSR values for the nine women in this current study, we obtained NSR values which were more than one for most of them. The high strain in the mid region in these women were not completely counteracted by the strains in the two ends. These two ends were one connected and one disconnected in case of unilateral avulsion and both disconnected in case of bilateral avulsion.

4.4.2 Strain in avulsed PRMs post pessary fitting

US acquisition from the women after pessary fitting was performed twenty minutes after pessary removal. Thus, the difference observed in the strain pattern, shows that the function of the PRM has undergone changes due to the presence of pessary for three months. These changes result in a contraction pattern of the PRM, even without pessary, that is different than that at intake. In other words, effects were observed which were more than just the mechanical effect due to the presence of pessary.

In case of unilateral avulsion, before pessary, the intact end of the PRM extends during contraction in order to pull the PRM in the direction of the pubic bone. At intake this extension might be higher to compensate for the damaged end which cannot exert this pulling function because of the damage as well as the excessive load exerted by the prolapse. As a result, the damaged end contracts along with the mid region of the PRM. The presence of pessary might counteract the additional loading of the prolapse, allowing the damaged part to (partially) recover its function, and reducing the difference in strain between the two ends.

Similarly, in case of bilateral avulsion, presence of pessary might counteract the additional loading due to prolapse. As a result the two damaged ends (partially and to different extent) recover their function, once again, reducing the difference in strain between the two ends. It can be mentioned here that the although it is bilateral avulsion, the extent of damage between the both ends might be different as shown by difference in strain, as observed in **Figure 4.4b**. Irrespective of the difference in the extent of damage in the two ends of the PRM, both ends still show difference in strain after pessary usage.

We found that, all women after pessary usage showed reduced NSR values than that before pessary as shown in figure 5b. One woman with unilateral avulsion who shows only a slight decrease in the value with respect to after pessary usage, the decrease is small (difference in NSR is 0.01) and might be in the same range as the accuracy of the method. A dedicated study investigating the reproducibility of the NSR values while scanning women at different time points is

required. The reduction in the normalized strain ratio is mainly due to the fact that the difference in the medians of strain in the two ends of the PRMs is less after pessary usage with respect to before pessary fitting. Although the strain in the mid region of the PRM is also reducing after using a pessary, the change in strain difference between the two ends is dominating.

It has been found that possibly women with POP try to relieve the additional loading due to POP by constantly contracting the PRM. The support provided by pessary would reduce the additional loading of POP and thus would also reduce this continuous contraction of the PRM. As a result, a change in PRM function during pessary treatment might influence the success of ring pessary use over time **[22]**.

4.4.3 Clinical significance

There could be at least two clinical significances or benefits of functional measurements of PRM through strain. Firstly, normalized strain ratio could be used as an indicator for the effectiveness of pessary treatment. Although the number of women included is small, a clear decrease in normalized strain ratio could be observed in women who used the pessary for three months and the difference is significant. It would be interesting to assess in future large scale studies, the correlation between normalized strain ratio and the degree of subjective satisfaction with the treatment. Additionally, if the reduction in this ratio is discovered to be an indicator of success of pessary treatment then, then this ratio could also be used to assess the best type and size of pessary for a specific woman.

Secondly, normalized strain ratio could also be used for assessing the effectiveness of PF muscle therapy (PFMT) by monitoring the PRM before and after PFMT to quantitatively score the benefit of treatment. Thereafter, the ratio could be used to tailor the PFMT to the specific problem of the patient. In this study, women with a pessary without additional PFMT were included. Normalized strain ratio could be compared in women with pessary alone and women with pessary treatment and PFMT could be done to assess the added benefit of PFMT on pessary treatment.

4.4.4 Limitations and future work

The first limitation of this study is the limited number of included women. However, since in both subgroups the NSR values decrease to normal values, the presented analysis might turn out to be a parameter. Furthermore, the decrease in NSR value is observed in both subgroups independent on the type of avulsion. Secondly, our study does not include women who have intact PRMs, yet have received pessary for some degree of prolapse. Strain imaging in these women could help in determining how support may be reduced or lost without definite avulsion.

Future extension of this work could be finite element modeling as well as strain imaging of all the female PF muscles including PRM, to have a better understanding of the bio-mechanics of the entire pelvic diaphragm.

4.5 Conclusion

The principal observation in this work is that the contraction of the PRM differs when pessary is introduced and used for three months. We observed that the normalized strain ratio of avulsed PRMs decreases after pessary use.

For women included in this study, the normalized strain ratio decreased to more normal values. Thus this normalized strain ratio could be used as an indicator for the effectiveness of pessary treatment.

References

[1] J. O. DeLancey et al., "Comparison of levator ani muscle defects and function in women with and without pelvic organ prolapse," Obstetrics and gynecology, vol. 109, no. 2 Part 1, pp. 295–302, 2007.

[2] S. D. Atnip, "Pessary use and management for pelvic organ prolapse," Obstetrics and Gynecology Clinics, vol. 36, no. 3, pp. 541–563, 2009.

[3] R. Oliver, R. Thakar, and A. H. Sultan, "The history and usage of the vaginal pessary: A review," European journal of obstetrics & gynecology and reproductive biology, vol. 156, no. 2, pp. 125–130, 2011.

[4] E. Pott-Grinstein and J. R. Newcomer, "Gynecologists' patterns of prescribing pessaries." The Journal of reproductive medicine, vol. 46, no. 3, pp. 205–208, 2001.

[5] H. P. Dietz, "Pelvic floor ultrasound: A review," American journal of obstetrics and gynecology, vol. 202, no. 4, pp. 321–334, 2010.

[6] H. Dietz, "Ultrasound imaging of the pelvic floor. Part i: Two-dimensional aspects," Ultrasound in Obstetrics and Gynecology, vol. 23, no. 1, pp. 80–92, 2004.

[7] H. Dietz, "Ultrasound imaging of the pelvic floor. Part ii: Three-dimensional or volume imaging," Ultrasound in Obstetrics and Gynecology: The Official Journal of the International Society of Ultrasound in Obstetrics and Gynecology, vol. 23, no. 6, pp. 615–625, 2004.

[8] S. Das et al., "3D ultrasound strain imaging of puborectalis muscle," Ultrasound in Medicine & Biology, vol. 47, no. 3, pp. 569–581, 2021.

[9] C. Manzini, C. H. van der Vaart, F. van den Noort, A. T. Grob, and M. I. Withagen, "Pessary fitting for pelvic organ prolapse: Parameters associated with specific reasons for failure," International urogynecology journal, vol. 33, no. 7, pp. 2037–2046, 2022.

[10] T. Manchana, "Ring pessary for all pelvic organ prolapse," Archives of gynecology and obstetrics, vol. 284, pp. 391–395, 2011.

[11] L. Hoyte and M. Damaser, Biomechanics of the female pelvic floor. Academic press, 2016.

[12] F. M. Zijta, M. Froeling, A. J. Nederveen, and J. Stoker, "Diffusion tensor imaging and fiber tractography for the visualization of the female pelvic floor," Clinical anatomy, vol. 26, no. 1, pp. 110–114, 2013.

[13] A. Zifan et al., "Connectivity of the superficial muscles of the human perineum: A diffusion tensor imaging-based global tractography study," Scientific reports, vol. 8, no. 1, p. 17867, 2018.

[14] F. Kallel and J. Ophir, "A least-squares strain estimator for elastography," Ultrasonic imaging, vol. 19, no. 3, pp. 195–208, 1997.

[15] D. G. Altman, Practical statistics for medical research. CRC press, 1990.

[16] A. Indrayan and R. K. Malhotra, Medical biostatistics. CRC Press, 2017.

[17] J. A. Ashton-Miller and J. O. DeLancey, "Functional anatomy of the female pelvic floor," Annals of the new york academy of sciences, vol. 1101, no. 1, pp. 266–296, 2007.

[18] M. Heit, J. T. Benson, B. Russell, and L. Brubaker, "Levator ani muscle in women with genitourinary prolapse: Indirect assessment by muscle histopathology," Neurourology and Urodynamics: Official Journal of the International Continence Society, vol. 15, no. 1, pp. 17–29, 1996.

[19] W. F. Boron and E. L. Boulpaep, Medical physiology e-book. Elsevier Health Sciences, 2016.

[20] S. Das et al., "3D ultrasound strain imaging of puborectal muscle with and without unilateral avulsion," International urogynecology journal, vol. 34, no. 9, pp. 2225–2233, 2023.

[21] K.-C. Lien, B. Mooney, J. O. DeLancey, and J. A. Ashton-Miller, "Levator ani muscle stretch induced by simulated vaginal birth," Obstetrics and gynecology, vol. 103, no. 1, p. 31, 2004.

[22] C. Manzini, F. van den Noort, A. T. Grob, M. I. Withagen, and C. H. van der Vaart, "The effect of pessary treatment on puborectalis muscle function," International Urogynecology Journal, vol. 32, pp. 1409–1417, 2021.

[23] C. Manzini, F. van den Noort, A. T. Grob, M. I. Withagen, C. H. Slump, and C. H. van der Vaart, "Appearance of the levator ani muscle subdivisions on 3D transperineal ultrasound," Insights into imaging, vol. 12, pp. 1–8, 2021.

[24] C. Manzini, L. M. Morsinkhof, C. H. van der Vaart, M. I. Withagen, and A. T. Grob, "Parameters associated with unsuccessful pessary fitting for pelvic organ prolapse up to three months follow-up: A systematic review and meta-analysis," International Urogynecology Journal, vol. 33, no. 7, pp. 1719–1763, 2022.

Supplementary figures

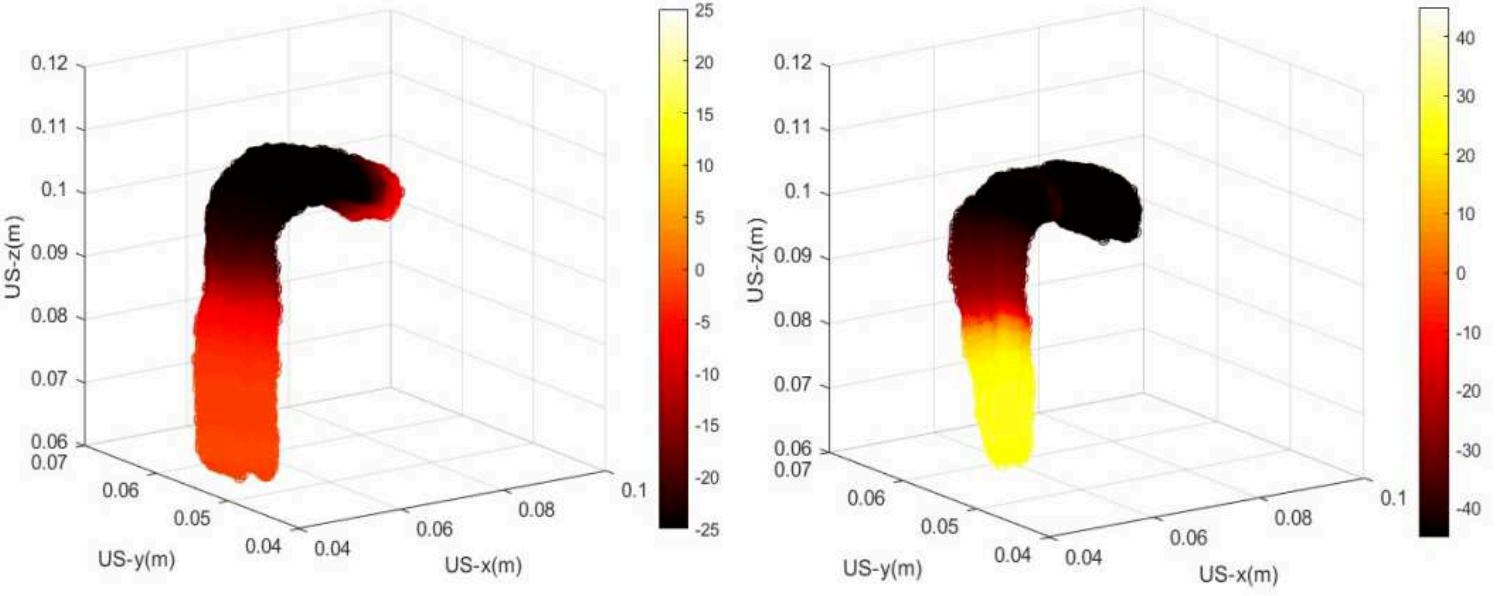

Figure S4.1: Strain in unilateral avulsion of PRMs, at maximum voluntary contraction for two women (a) Before pessary fitting (b) After pessary fitting

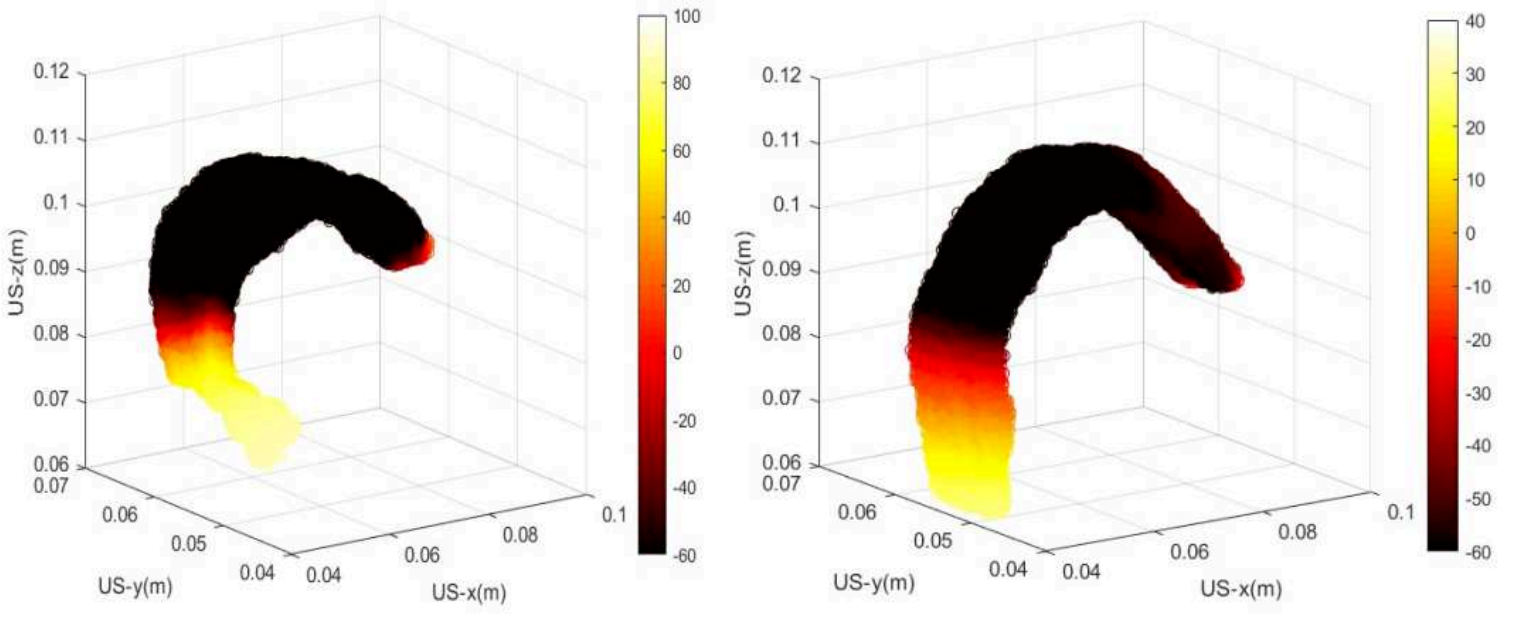

Figure S4.2: Strain in unilateral avulsion of PRMs, at maximum voluntary contraction for two women (a) Before pessary fitting (b) After pessary fitting

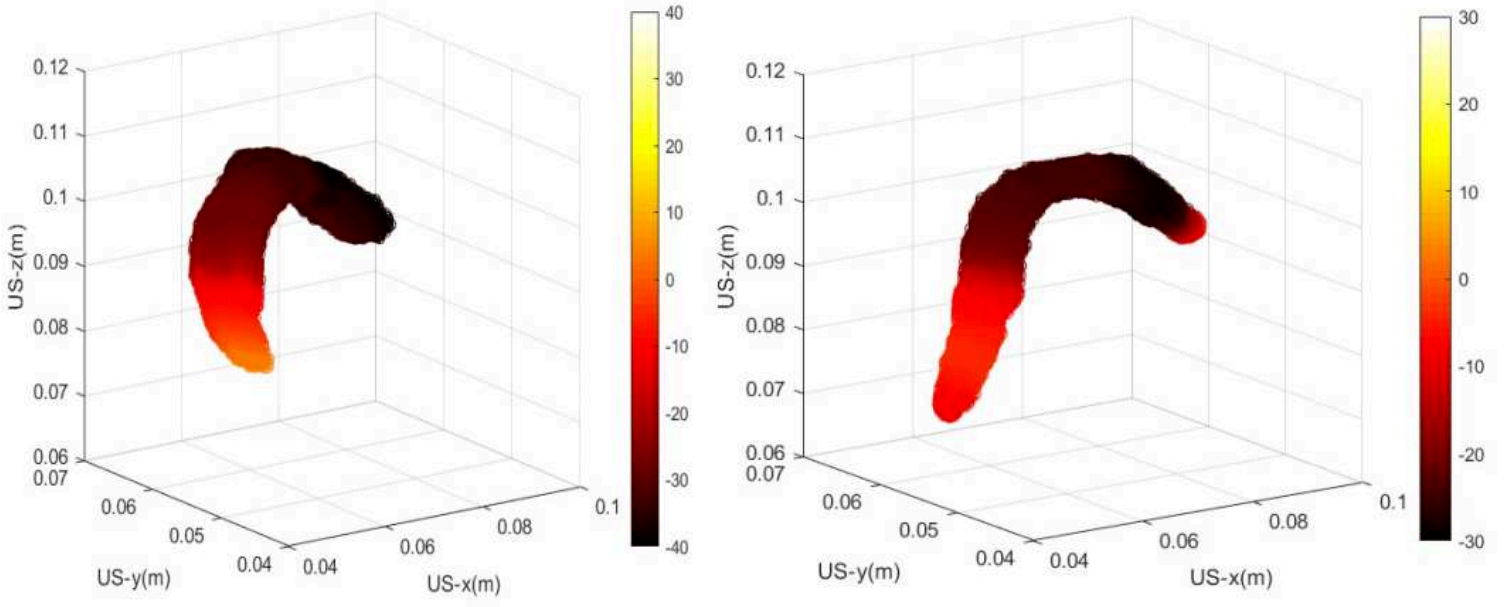

Figure S4.3: Strain in unilateral avulsion of PRMs, at maximum voluntary contraction for two women (a) Before pessary fitting (b) After pessary fitting

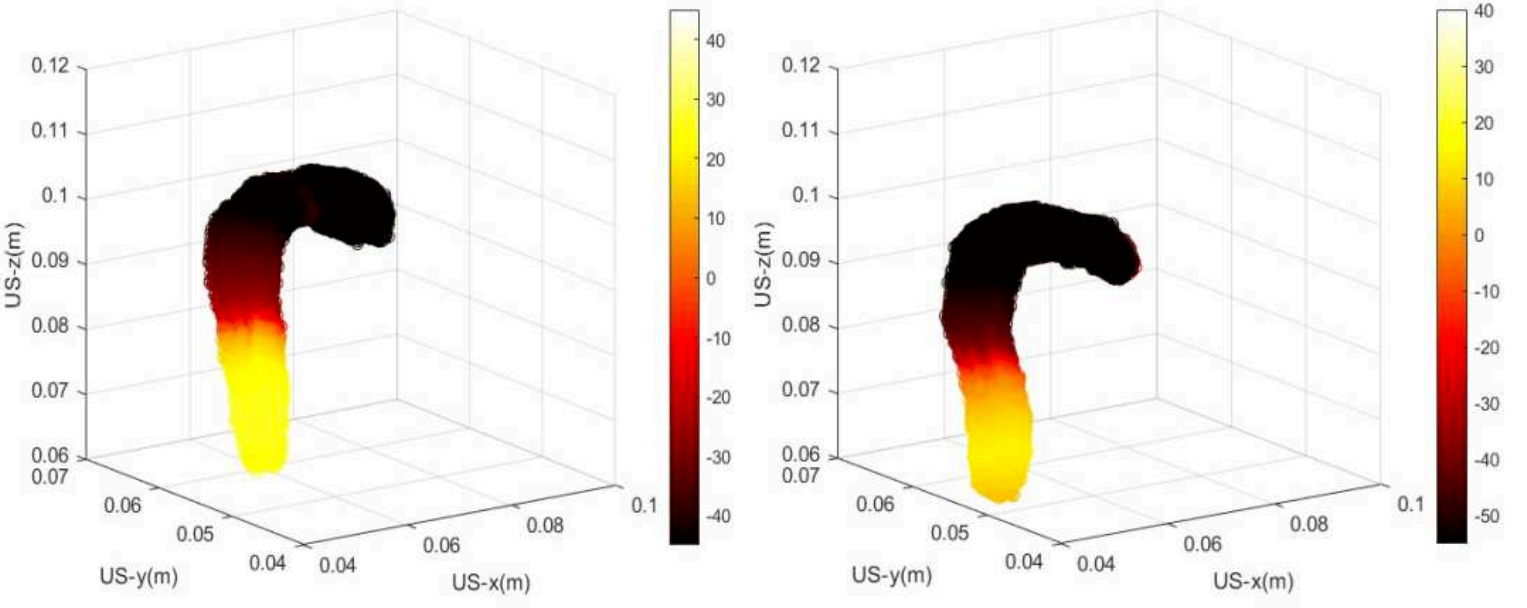

Figure S4.4: Strain in unilateral avulsion of PRMs, at maximum voluntary contraction for two women (a) Before pessary fitting (b) After pessary fitting

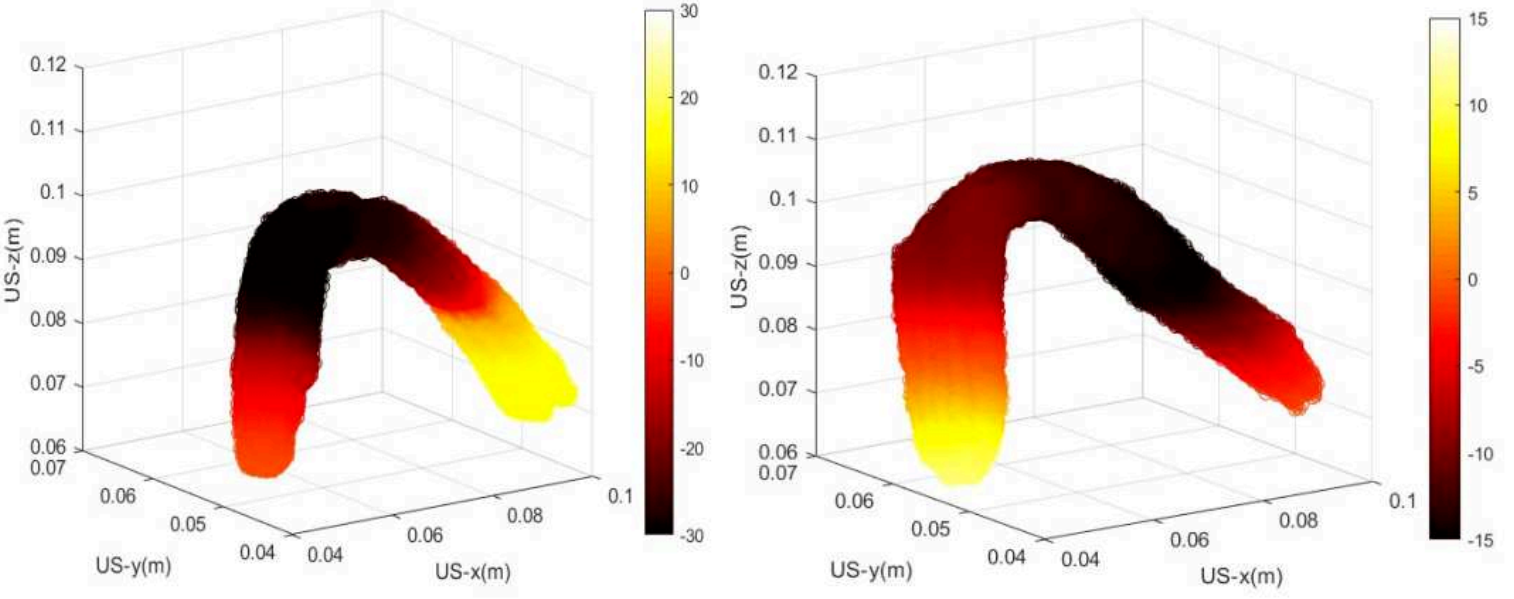

Figure S4.5: Strain in unilateral avulsion of PRMs, at maximum voluntary contraction for two women (a) Before pessary fitting (b) After pessary fitting

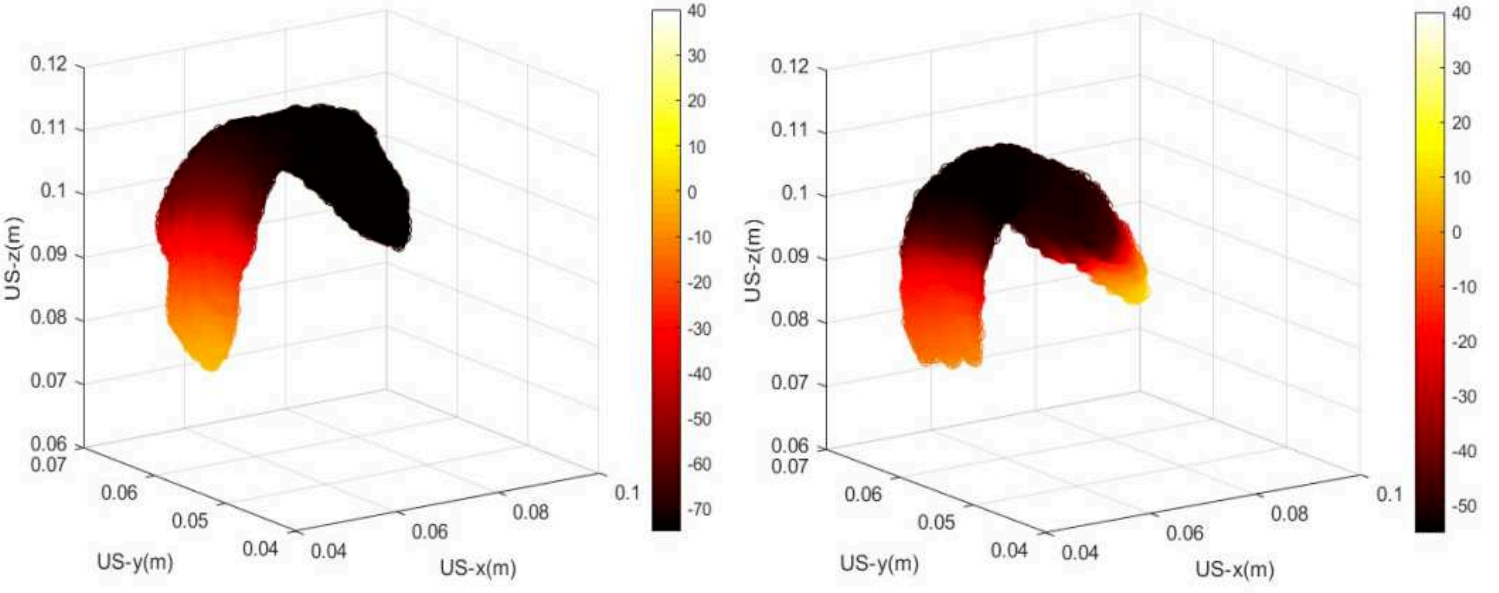

Figure S4.6: Strain in unilateral avulsion of PRMs, at maximum voluntary contraction for two women (a) Before pessary fitting (b) After pessary fitting

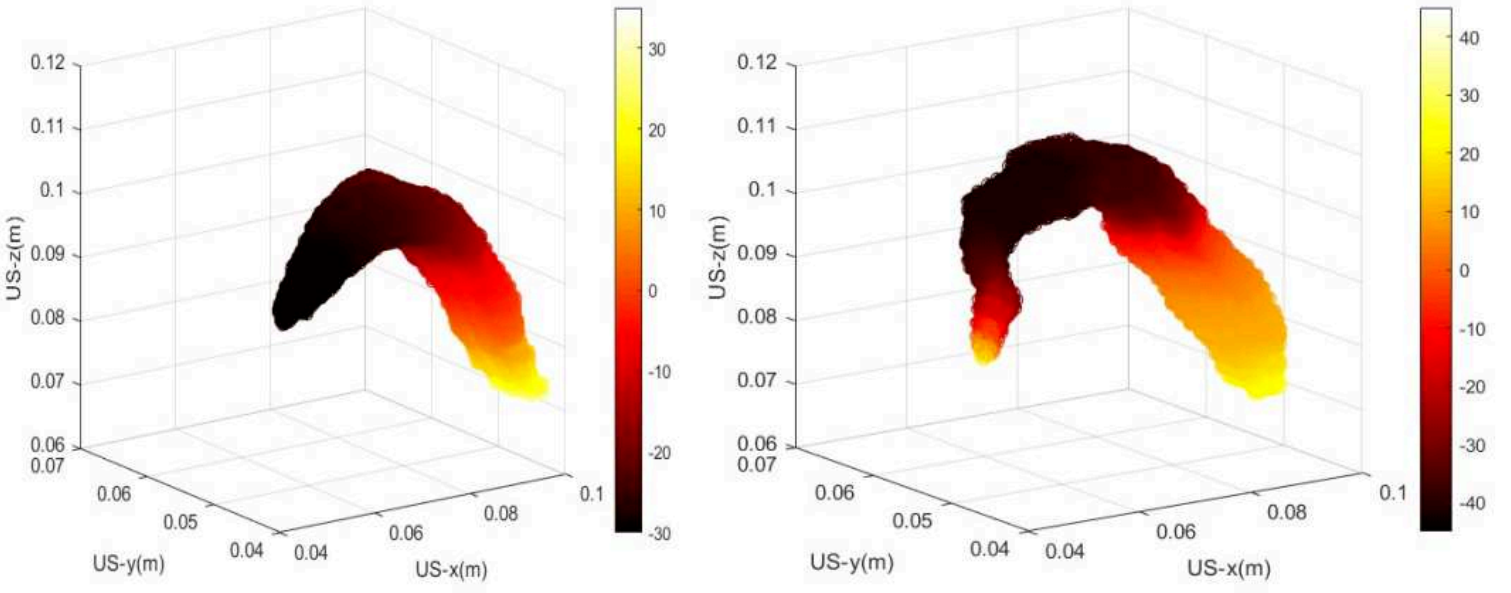

Figure S4.7: Strain in unilateral avulsion of PRMs, at maximum voluntary contraction for two women (a) Before pessary fitting (b) After pessary fitting

Chapter 5

Tissue characterization of PRM from 3D US

This chapter is based on the publication:
C. Cernat*, **S. Das***, G. A. G. M. Hendriks, F. van den Noort, C. Manzini, C. H. van der Vaart & C. L. de Korte, **Tissue characterization of puborectalis muscle from 3D ultrasound**. *Ultrasound in medicine and biology*, vol. 49, no. 2, pp. 527-538, 2022.
* The first and second authors have equal contribution.

Abstract

Pelvic floor (PF) muscles have the role to prevent pelvic organs' descent. The puborectalis muscle (PRM) which is one of the female PF muscles, can be damaged, during child delivery. This damage can potentially cause irreversible muscle trauma and even lead to an avulsion, which is disconnection of the muscle from its insertion point, the pubic bone. Ultrasound imaging allows diagnosis of such trauma based on comparison of geometric features of a damaged muscle with the geometric features of a healthy muscle. Although avulsion, which is considered a severe damage can be diagnosed, micro damages within the muscle itself leading to structural changes cannot be diagnosed by visual inspection through imaging only. Therefore, we developed a quantitative ultrasound tissue characterization method to obtain information about the state of the tissue of the PRM and the presence of micro damages in avulsed PRMs. The muscle was segmented as the region of interest (ROI) and further sub-divided into six regions of interest (sub-ROIs). Mean echogenicity, entropy, and shape parameter of the statistical distribution of gray values were analyzed on two of these sub-ROIs, nearest to the bone. The regions nearest to the bones are also the most likely regions showing damage in case of disconnection or avulsion. This analysis was performed both for the muscle at rest and at contraction. We found that, for PRMs with unilateral avulsion compared to undamaged PRMs, the mean echogenicity (p-value = 0.02) and shape parameter (p-value < 0.01) were higher, whereas the entropy was lower (p-value < 0.01). This method might be applicable on quantifying PRM damage, within the muscle.

Keywords - 3D Ultrasound, Shape Parameter, Puborectalis, Echogenicity

5.1 Brief introduction

In this chapter, from B-mode datasets, echogenicity and other statistical parameters like entropy and shape parameter have been calculated to determine whether there can be differences between undamaged puborectal muscles (PRMs) and unilaterally avulsed PRMs. The results shown in this chapter demonstrate that tissue characterization of PRMs can show difference in the state of the muscle.

5.1.1 Data acquisition

Data acquisition from all the women (intact PRMs as well as unilateral avulsion of PRMs) for which the results of this chapter have been obtained, is briefly mentioned in the **Table 5.1**.

5.1.1.1 Intact and unilateral avulsion of PRMs

US data were obtained over time from women who had intact and undamaged PRMs (n_1 = 8) and from women who had unilateral avulsion (n_2 = 6). In all women, US volumes were recorded from rest to maximum contraction. Details of data acquisition have been explained in **Chapter 2**, **Section 2.1.1** for women with intact PRMs and in **Chapter 3**, **section 3.1.1** for women with unilateral avulsion of PRMs.

5.1.2 Aim of the study

The aim of this study is to develop a Quantitative Ultrasound (QUS) tissue characterization method to obtain diagnostic information about PRMs with and without avulsion. We hypothesized that the presence of an avulsion of the PRM will result in a change in the statistical distribution of gray values in a B-mode US image of the PRM.

We performed this study to investigate if QUS parameters are different in PRMs without avulsion compared to PRMs with unilateral avulsion. Women with PRMs without damage are nulliparous women, which means that damage

due to vaginal childbirth is absent. Women with unilateral avulsion, are non-nulliparous and since avulsion is present, they have some form of damage within the PRM. Most non-nulliparous women having vaginal delivery show some form of PRM damage **[1-2]**. Furthermore, two distinct scenarios were analyzed: first, when the muscle was at rest and second when the muscle was voluntarily contracted. The accuracy of the developed QUS method is then evaluated based on its ability to distinguish between damaged and undamaged PRM using the receiver operating characteristic curve (ROC).

5.2 Materials and Methods

5.2.1 Muscle segmentation and ROIs

The PRM was segmented in the 3D volume at rest as described by Manzini et al. (2021) **[3]**. van den Noort et al. (2018) showed that automatic segmentation provides volumes similar to manual segmentation of the PRM **[4]**. For the purpose of this work, the segmented PRM at rest was used. The 3D volume of the segmented muscle can be seen in **Figure 5.1**.

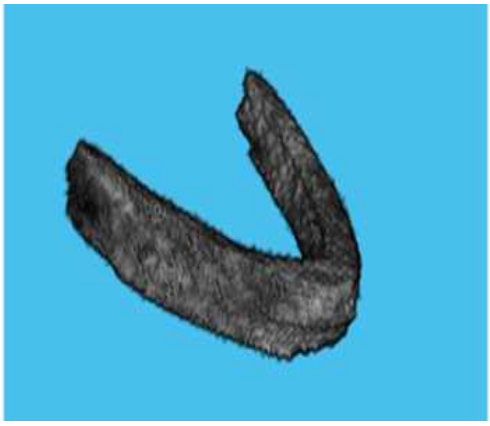

Figure 5.1: Three dimensional volume of segmented puborectalis muscle at rest

The segmented volume of the muscle at rest (**Figure 5.1**) was tracked over the contraction cycle by estimating inter-volumetric displacements. Each of the 3D US volumes contained 352 × 229 × 277 (X × Y × Z in Cartesian co-ordinate system) pixels which were uniformly sampled at distances of 0.42 mm × 0.60 mm × 0.34 mm (non-uniform intervals dx × dy × dz). For each pair of subsequent volumes using a 3D normalized cross-correlation algorithm **[5-7]**. In this algorithm, two subsequently recorded volumes were subdivided into 3D blocks called kernels and templates. The kernels were matched on the templates, and the locations of the 3D cross-correlation peaks were calculated. These locations of peaks indicated the displacements between the two blocks. To estimate subsample displacements, the cross-correlation peaks were interpolated (parabolic fit). The displacement estimates were finally filtered using a 3D median filter. For each inter-volume displacement estimates the position of the muscle was tracked by accumulating all the previous displacement estimates up to the current time point. The resulting segmentation from tracking made it possible to also analyze the PRM in the contracted state. From now on, the 3D segmentation of the PRM, both at rest and contraction, will be referred to as the 3D mask. The reference co-ordinates that we have for each volume and thus the 3D mask are rectilinear co-ordinate system (non-uniform intervals dx, dy and dz for X, Y and Z axes respectively), which is also Cartesian co-ordinate system.

The 3D mask of the PRM for both at rest and contraction volume, had been first used for dividing the muscle into two parts with approximate equal volumes. This had been done by calculating the length of the opening between two ends of the PRM (in x-axis), and dividing this length to obtain the mid-line of the muscle, from the top view. Thereafter, for each of these two parts separated by the mid-line, three equal divisions are calculated (in z-axis). Thus the total muscle is divided into approximately equal six parts. While dividing the muscle into parts, the corresponding y-axis indices are not used since y-axis represents the thickness of the muscle. In other words, each of the sub-ROIs had the complete thickness of the muscle. These 3D indices were saved as a binary mask (having 0 or 1 values), for both rest and contraction. The gray values were extracted by multiplying each sub-ROI with the US volume, in 3D. This process is illustrated in **Figure 5.2**.

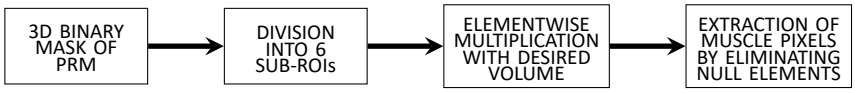

Figure 5.2: Process of division of the puborectalis muscle (PRM) into sub-regions of interest (ROI = region of interest)

Unilateral avulsion of a PRM results in a disconnection, on one end of PS whereas, a PRM without avulsion, has both ends connected to the PS. To better exploit this particularity, the muscle had been divided into six regions of interest (sub-ROI 1 to sub-ROI 6) as shown in **Figure 5.3a** and in the block diagram of **Figure 5.2**. The division of the muscle into six sub-ROIs had been done to make this method applicable to any number of woman. Since PRMs have been found to have different length and volume from woman to woman, each muscle had been subdivided after calculating its particular length (in x-axis) and depth (in z-axis). In this way, the two ends nearest to the bone has been kept as one-sixth of the total volume of the muscle, in terms of number of indices or pixels in 3D. This can be seen in the example shown in **Figure 5.3b**.

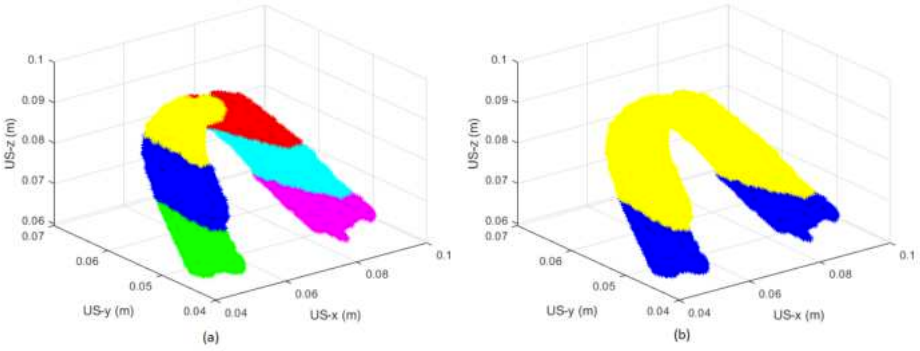

Figure 5.3: (a) Subregions of interest of puborectalis muscle after division, (b) Two subregions nearest the insertion points at the pubic bone (US = ultrasound)

The clinical reason for choosing the two end points of the PRM is that the damage to the PRM is likely to be present near the location of disconnection from the bone. Moreover, because of the complex shape of the PRM, there are parallel and perpendicular fibers with respect to the US transducer. Regions of the muscle which is connected to the PS have parallel fiber orientation whereas in the mid region, the fiber orientation is perpendicular to the US transducer as confirmed by MR tractography **[8]**. This difference in orientation would further have different backscattering from different regions of the muscle **[9]**. Since the two regions nearest to the bone have parallel muscle fibers, these are comparable.

Calculations of mean echogenicity, entropy and shape parameter for all the three sub-divisions of the muscle have been detailed in a flowchart, shown in **Appendix H**.

5.2.2 Mean echogenicity

Grob et al. (2016) showed that structural changes in the muscle can be distinguished and analyzed by measuring the mean echogenicity of the PRM (MEP), during and after pregnancy **[23]**. It was shown that six months postpartum, MEP was significantly lower ($p<0.001$) than the values during pregnancy. Therefore, it is expected that structural changes due to muscle trauma can also be analyzed using mean echogenicity. In this study, MEP was calculated by summing the gray values of the pixels in each sub-ROI and dividing the result by the number of pixels in that sub-ROI, as shown in the equation below.

$$MEP = \sum_{i=0}^{m} \sum_{j=0}^{n} I(i,j) \tag{5.1}$$

where *I(i,j)* is the gray value of the pixel at location *(i,j)* from the region of interest of size *m*x*n* pixels, where m and n are the corresponding 2D directions. In our case the gray values for each 3D indices was divided by the number of indices in that region.

5.2.3 Shannon's entropy

Shannon's entropy is a widely used QUS technique for ultrasound tissue characterization which measures the signal uncertainty or level of information. Chen et al. (2020) investigated the clinical value of Shannon's entropy in grading different stages of hepatic steatosis. The results were compared to a deep learning VGG-16 model **[10]**. It was shown that Shannon's entropy outperformed VGG-16 in identifying candidates with moderate or severe hepatic steatosis. Furthermore, the authors showed that when compared to a conventional statistical parametric method based on Nakagami distribution, Shannon's entropy outperformed it with a 10% higher area under the receiver operating characteristic (ROC) curve. For a given ROI, Shannon's entropy can be calculated as described by Chen et al. (2020) **[10]**:

$$H_c = -\sum_{i=1}^{n} \log_2 \left[w(y_i) \right] \tag{5.2}$$

where *w(y_i)* represents the probability value obtained from the normalized histogram counts, *n* is the number of bins in the histogram and y_i is the discrete random variable of the backscattered echo intensity.

In our case, since we have used gray scale values from B-mode images, *w(y_i)* denotes the probability of a gray scale value y_i which is present within the ROI. Smaller the probability of a gray scale value y_i being present, higher is the level of information of this gray scale value and vice versa. H_c is the sum of all possible gray scale values from 1 to *n*. Values of H_c range from 0 (low level of information) to infinity (high level of information). Thus, H_c measures the granularity of a region. A homogeneous region has a low level of information and thus low entropy, whereas a more granular region has a higher level of information and thus higher entropy **[11]**.

It is expected that a change in the structure of the PRM would result in a change in the entropy, leading to the change in the level of information that a region within the PRM may contain.

5.2.4 Statistical distribution of gray values

As mentioned by Girardi (2019), tissue microstructure information can be found in the envelope of the backscattered ultrasonic echo **[12]**. The envelope of the backscattered ultrasonic echo from tissues are dependent on the shape, size and density of the scatterers inside the tissue **[13]**. According to statistics of US echoes measured from biological tissues, the envelope can be classified as pre-Rayleigh, Rayleigh, and post-Rayleigh distributions. All these three types of distributions can be modeled by Nakagami distribution. The probability distribution of the Nakagami model is given by Tsui et al. (2010) **[13]**:

$$p_a(A \mid \Omega) = \frac{2m^m A^{(2m-1)}}{\Gamma(m)\Omega^m} * exp(\frac{-mA^2}{\Omega}) * U(A) \qquad (5.3)$$

where *U(A)* is the unit step function, $\Gamma(m)$ is the gamma function, *A* corresponds to possible values of the random variable of the backscattered signal envelopes, *m* is the Nakagami shape (or spread) parameter and Ω is the scaling factor.

If the envelope follows a Nakagami distribution, then the intensity follows a gamma distribution and the probability density function (PDF) is given by **[14]**:

$$P_{Gamma}(I \mid \alpha, \beta) = \frac{\beta^\alpha}{\Gamma(\alpha)} I^{(\alpha-1)} e^{-\beta I} \qquad (5.4)$$

where $\Gamma(\alpha)$ is the gamma function, *I* is the intensity of the US backscattered signal, α is the shape parameter, and β is the rate parameter.

The shape parameter of the Gamma distribution results from the pixel distribution within each ROI of the B-mode image of the PRM. It was determined using a maximum likelihood estimator.It is expected that a change in the tissue microstructure would be reflected in a change of the pixel distribution in each ROI, resulting in a change in the shape parameter as well.

5.2.5 Analysis procedure

While analyzing an undamaged PRM, both sub-ROI 1 and sub-ROI 6 were used, while for a PRM with unilateral avulsion, either sub-ROI 1 or sub-ROI 6 was used. This was based on whether the avulsion was located on the left (sub-ROI 1) or on the right (sub-ROI 6). In order to analyze the regions closest to a possible damage, the regions closest to the insertion points were considered.

The mean echogenicity, entropy and the shape parameter values of the Gamma distribution were computed for each sub-ROI at rest and at maximum contraction. Since the sample size was small, Wilcoxon Rank Sum Test was used to determine whether the computed values could be described by distributions with equal medians. Equal medians would imply that, the proposed parameters cannot be used to distinguish damaged from undamaged PRMs. Alternatively, a lower p-value, indicating that the computed values are from distributions with unequal medians, would imply that the proposed parameters can be used for distinguishing between damaged from undamaged PRMs.

Furthermore, for each parameter, the receiver operating characteristic (ROC) curve was computed and the area under the curve (AUC) was calculated to compare the diagnostic ability of a classifier using each of the three parameters described above. The ROC curve is created by plotting the true positive rate (TPR) against the false positive rate (FPR) at various threshold settings **[15]**.

5.3 Results

Table 5.1 shows the demographic characteristics of all the inclusions for this chapter.

Figure 5.4 presents the results for the mean echogenicity, entropy and shape parameter values as adjacent boxplots comparing PRMs with and without avulsion both at rest and at maximum contraction. On each boxplot, the central mark indicates the median, and the bottom and top edges of the plots indicate the 25^{th} and 75^{th} percentiles, respectively. The whiskers extend to the most extreme data points not considered outliers. The outliers are plotted individu-

Table 5.1: Demographic information about all the inclusions for tissue characterization

	Women with intact PRMs (n_1 = 8)	Women with unilateral avulsion of PRMs (n_2 = 6)
Median of age (yrs)	34	47
Median of BMI (Kg/m^2)	20.9	25.6
Parity	0-1	2-3
Additional information	7 women nulliparous, 1 woman vaginally nulliparous (with primary C-section)	4 women with 2 vaginal deliveries (1 with vacuum extraction), 2 women with 3 vaginal deliveries

ally using the + symbol (MATLAB, 2021). The statistical criteria to determine an outlier is the one used as the default in MATLAB. By default, an outlier is a value that is more than three scaled median absolute deviations (MAD) away from the median.

Figure 5.5 shows the exact ROC curves for the mean echogenicity, entropy and shape parameter values as adjacent line-plots comparing PRMs at rest and at maximum contraction.

5.3.1 Mean echogenicity

When PRMs were at rest, the mean echogenicity showed an increase (p-value < 0.01) for PRMs with unilateral avulsion compared to PRMs without avulsion. The distance between the medians of the two classes was found to be 34.69 and the AUC of 0.94. This means that it is possible to correctly distinguish damaged from undamaged PRMs with the help of mean echogenicity, with a

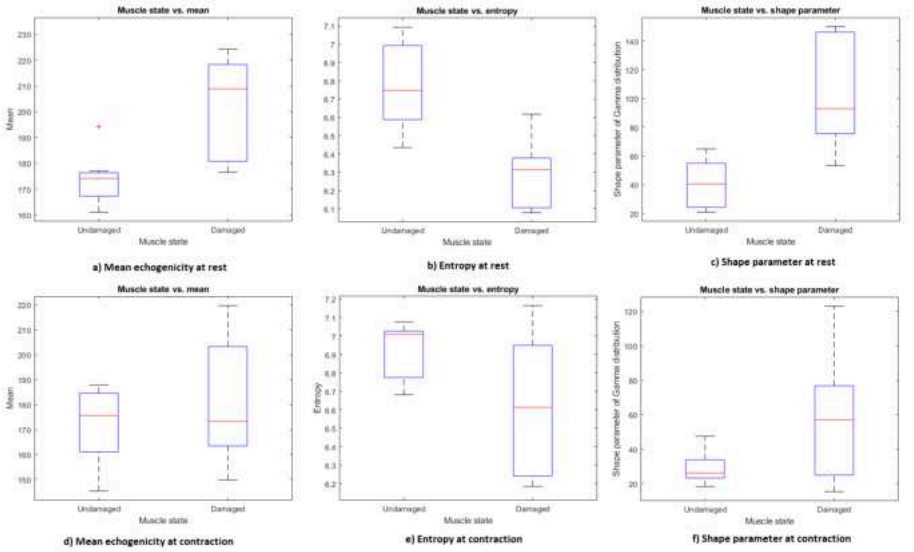

Figure 5.4: Mean echogenicity, entropy and shape parameter values for the puborectalis muscle without avulsion and with unilateral avulsion, at rest (top row) and in contraction (bottom row)

probability of 94%, when calculated at rest.

For the case when PRMs were at contraction, the mean echogenicity showed no increase (p-value = 0.75) for PRMs with unilateral avulsion compared to PRMs without avulsion. Thus, it can be said that mean echogenicity at contraction is not effective in distinguishing damaged from undamaged PRMs. The distance between the medians of the two classes was found to be 2.42. Since there is almost no difference between the two groups, the ROC analysis reveals an AUC of 0.56.

5.3.2 Entropy

When PRMs were at rest, the entropy showed a decrease (p-value < 0.01) for PRMs with unilateral avulsion compared to PRMs without avulsion. The distance between the medians of the two classes was found to be 0.43 and the

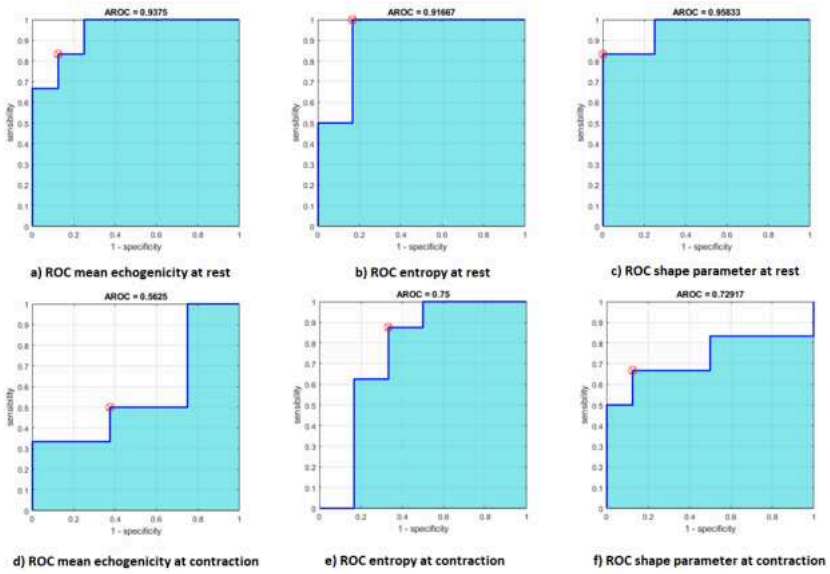

Figure 5.5: Receiver operating characteristic (ROC) curves for mean echogenicity, entropy and shape parameters when pubo-rectalis muscles were at rest (top row) and in contraction (bottom row). Here the blue area represents the area under the ROC (AROC), and the red points represent the discrete values

AUC was 0.89. The high AUC value indicates that there is a probability of 89% of correctly distinguishing a damaged PRM from an undamaged one when using entropy values calculated at rest. (p-value <0.01).

For the case when PRMs were at contraction, the entropy showed no significant decrease (p-value = 0.14) for PRMs with unilateral avulsion compared to PRMs without avulsion. The distance between the medians of the two classes was found to be 0.39 and the AUC was 0.75.

5.3.3 Shape parameter of Gamma distribution

When PRMs were at rest, the shape parameter value showed an increase

(p-value $<$ 0.01) for PRMs with unilateral avulsion compared to PRMs without avulsion. The distance between the medians of the two classes was found to be 52.19 and the AUC was 0.96.

For the case when PRMs were at contraction, the shape parameter showed no significant increase (p-value = 0.28) for PRMs with unilateral avulsion compared to PRMs without avulsion. The distance between the medians of the two classes was found to be 30.98 and the AUC was 0.73. Similar to mean echogenicity and entropy, AUC for shape parameter as well is less at contraction.

The summarized results for the distance between the medians, the statistical significance and the AUC for the fitted curve and the exact curve for each parameter can be found in **Table 5.2** for PRMs at rest and contraction.

Table 5.2: Summarized values for the three parameters at rest and contraction

	State of the puborectalis muscle					
	At rest			At contraction		
	Mean echogenicity	Entropy	Shape parameter	Mean echogenicity	Entropy	Shape parameter
Distance between medians	34.69	0.43	52.19	2.42	0.39	30.98
Statistical significance (p-value)	$<$0.01	$<$0.01	$<$0.01	0.76	0.14	0.18
AUC fitted curve	0.91	0.89	0.93	0.52	0.75	0.73
AUC exact curve	0.94	0.92	0.96	0.56	0.70	0.73

Furthermore, images with representative colors were created by assigning each ROI within the PRM the value of the shape parameter. These images can provide visual aid to the clinician in diagnosing the disconnected ends of the PRMs closest to the insertion points. This way, information regarding the locality of the damage within the PRM were visualized. Such an example can be seen in **Figures 5.6a** and **5.6b** (**Figures S5.1** to **S5.5** in the supplementary figures show shape parameter of Gamma distribution for the rest of the included women). Here blue corresponding to low values of the shape parameter which indicate regions of undamaged tissue. Whereas yellow, corresponding to high values of the shape parameter indicates regions of damaged tissue.

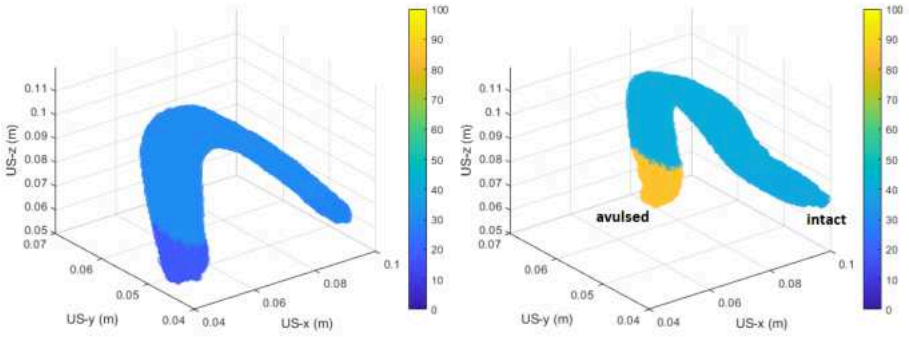

a) Undamaged PRM with all pixels replaced by the shape parameter values

b) Damaged PRM with all pixels replaced by the shape parameter value

Figure 5.6: Visual representation of the shape parameter change for (a) an undamaged, (b) a damaged puborectalis muscle (PRM) at rest (US = ultrasound)

5.4 Discussion

In this article, we described a method for QUS analysis of damaged and undamaged PRM to distinguish between avulsion and non-avulsion. The principal finding of the study is that the echogenicity, entropy and shape parameters investigated for the avulsion group are different from the non-avulsion group when the PRM is at rest. In women without avulsion, the echogenicity-based

parameters of the two sides of the PRM are similar, at rest.

At contraction, all parameters performed worse in classifying the damaged PRMs from the undamaged ones. During contraction, while the tissue composition is not changed, the muscle fibers are contracted, which will result in a different backscattering of the US waves with respect to the rest situation **[9, 16]**.

5.4.1 Physical interpretation

Van de Waarsenburg et al. (2019) investigated the structural composition of PRM before and after delivery. It was shown that MEP significantly increased from one day to twenty-four weeks after delivery. The authors studied this using 2D images of the levator hiatus in an axial position and minimal hiatal area **[17]**. This is in line with our finding that MEP increases for the damaged PRM, at rest. Furthermore, instead of one slice from the volumetric data, we used the entire PRM, automatically segmented. The increase in MEP means that the brightness of the region has increased which might be the result of connective tissue formation in damaged PRMs. MEP is less for undamaged PRM, which indicates absence of connective tissues.

Our finding that at contraction the echogenicity of the avulsed regions is decreased is in line with fundamental studies performed at the myocardial wall. Integrated backscatter, a normalized parameter representing echogenicity is decreased in the myocardium during systole compared to diastole **[16]**. In systole the cardiac muscle is thickened with respect to diastole which is perfectly in line with our finding that at contraction the echogenicity of the avulsed part is decreased.

Since information content of a region in an image is known as entropy, a homogeneous region would have low entropy and inhomogeneous or granular region of would lead to more entropy. From our results, entropy showed a decrease for PRMs with unilateral avulsion compared to PRMs without avulsion, at rest. This could indicate that the entire region has a homogeneous formation of scar tissue throughout the muscle, which has replaced the muscle fibers. Thus the presence of normal muscle tissue with echogenicity determined by the

orientation of the fibers would still have more entropy or granularity than PRM with unilateral avulsion, especially since we have always considered the end of the muscle which is disconnected and likely to contain scar or connective tissue.

Lastly, our results showed that, there was a change in the tissue microstructure depicted through the shape parameter. The shape parameter was lower for the undamaged PRMs and higher for the damaged ones, at rest. Shape parameter follows a Rayleigh distribution according to different scatterer concentrations in the tissue. It moves from a pre-Rayleigh to a Rayleigh distribution if the tissue distribution becomes more homogenous (and vice versa) **[18]**. Thus, if the scar or connective tissue formation in the disconnected region of the damaged PRMs are homogeneous formations, this would lead to an increase of the shape parameter in damaged PRMs as compared to undamaged ones. This is also consistent the results obtained for the damaged PRMs with lower entropy and higher echogenicity as compared to undamaged.

Our finding that microstructural damage of the PRM might be made visible using the method described in this research has the potential to become of clinical relevance as an early indicator of possible avulsion/later life disorders. Such a use case could be when a woman would like to have a second childbirth and the US image of the PRM is analyzed using the shape parameter. If the muscle shows microstructural damage, then the clinician could estimate whether it is going to become avulsed after the childbirth or not. However, thorough validation of this method on a bigger dataset containing women with or without known damage of the PRM, is required to evaluate if the algorithm can reliably aid the clinician in the diagnosis of microstructural damage.

5.4.2 Limitation and shortcomings

One main limitation and two shortcomings of the method have been identified. The limitation is that the number of the datasets (n = 14) was small which resulted in the use of a non-parametric test for evaluation. This limits the techniques that could be used to rather conventional ones as opposed to more modern, machine learning/deep-learning oriented ones. However, even while having a low number of patients and while using a non-parametric test, a significant

difference between undamaged and avulsion was found for the three parameters investigated. Furthermore, the age of the women was unknown and therefore, if age has any influence on the structure of the muscle, it could not have been accounted for.

A shortcoming is that different US machines and transducers provide unique B-mode images. It makes the application of this method machine dependent since different machines utilize different transmitted frequencies, transducer sensitivities, beam profiles, signal-to-noise ratios etc. resulting in different echograms. This limits direct translation of our findings to other machines and centers. To overcome this shortcoming, a comparison of the echogenicity using phantoms can be done using matrix transducers for different commercially available US machines. Thereafter, factors by which the echogenicity might change can be calculated and applied to have comparable measurements **[19-21]**.

The second shortcoming is that although the methods proposed can distinguish between PRMs with and without avulsion relative to each other, no conclusion can be drawn regarding the type of damage/trauma each muscle had suffered. The increase in the mean echogenicity of the PRMs with unilateral avulsion, at rest, might indicate scar tissue formation, although this conclusion cannot be drawn from this measurement alone. This shortcoming can be overcome by calculating functional parameters like strain to determine differences in contractility between undamaged and damaged muscles **[7]**.

Furthermore, although Dieter et al. (2015) indicates that high-frequency linear array probes, $>$ 7MHz and preferably $>$ 10MHz, are required to adequately image muscle, a 1-6MHz matrix probe has been used **[1]**. This is because increased spatial resolution (achieved through higher US frequencies) comes at the cost of decreased penetration depth limiting the ability to image deeper located structures **[22]**. Therefore, it was crucial that depth penetration was ensured such that the PRM could be imaged completely. Furthermore, the number of elements has to be increased to obtain similar field of view when applying to high frequency.

5.4.3 Future directions

The results obtained in this article show the potential of quantitative echography to identify PRM avulsion. The different parameters could serve as input (a so called feature) for more specialized machine learning algorithms such as neural networks. However, it is crucial for such applications that the dataset is enlarged to a level which allows training and testing of such algorithms.

On the other hand, a deep learning approach could be used for both feature detection and classification. An entire segmented PRM could be fed to a deep neural network (DNN) or convolutional neural network (CNN) which could potentially classify both the state of the muscle (damaged and undamaged) as well as the type of trauma that the muscle could have suffered. For this scenario, only the database of segmented PRMs has to be increased.

5.5 Conclusion

In this study, we used mean echogenicity, Shannon's entropy, and shape parameter value based on log-compressed B-mode images for assessing the state of the PRM in two scenarios: at rest and at maximum contraction. The results demonstrate that the shape parameter of the first order statistics of the speckle (gray value distribution) is the strongest parameter to distinguish intact and damaged PRMs. This has been demonstrated by analyzing the AUC. The entropy has slightly less performance. Also, analysis of the muscle at contraction has decreased performance with respect to analysis at rest. This supports the hypothesis that a change in the state of the tissue will result in a change in the statistical distribution of gray values in a B-mode image of the PRM.

References

[1] A. A. Dieter, M. F. Wilkins, and J. M. Wu, "Epidemiological trends and future care needs for pelvic floor disorders," Current opinion in obstetrics & gynecology, vol. 27, no. 5, p. 380, 2015.

[2] C. C. de Araujo, S. A. Coelho, P. Stahlschmidt, and C. R. Juliato, "Does vaginal delivery cause more damage to the pelvic floor than cesarean section as determined by 3D ultrasound evaluation? A systematic review," International urogynecology journal, vol. 29, pp. 639–645, 2018.

[3] C. Manzini, F. van den Noort, A. T. Grob, M. I. Withagen, C. H. Slump, and C. H. van der Vaart, "Appearance of the levator ani muscle subdivisions on 3D transperineal ultrasound," Insights into imaging, vol. 12, pp. 1–8, 2021.

[4] F. van den Noort, A. T. Grob, C. H. Slump, C. H. van der Vaart, and M. van Stralen, "Automatic segmentation of puborectalis muscle on three-dimensional transperineal ultrasound," Ultrasound in obstetrics & gynecology, vol. 52, no. 1, pp. 97–102, 2018.

[5] K. Gijsbertse et al., "Three-dimensional ultrasound strain imaging of skeletal muscles," Physics in Medicine & Biology, vol. 62, no. 2, p. 596, 2016.

[6] G. A. Hendriks, B. Holländer, J. Menssen, A. Milkowski, H. H. Hansen, and C. L. de Korte, "Automated 3D ultrasound elastography of the breast: A phantom validation study," Physics in Medicine & Biology, vol. 61, no. 7, p. 2665, 2016.

[7] S. Das et al., "3D ultrasound strain imaging of puborectalis muscle," Ultrasound in Medicine & Biology, vol. 47, no. 3, pp. 569–581, 2021.

[8] F. M. Zijta, M. Froeling, A. J. Nederveen, and J. Stoker, "Diffusion tensor imaging and fiber tractography for the visualization of the female pelvic floor," Clinical anatomy, vol. 26, no. 1, pp. 110–114, 2013.

[9] M. R. Holland et al., "Effects of tissue anisotropy on the spectral characteristics of ultrasonic backscatter measured with a clinical imaging system," Ultrasonic imaging, vol. 20, no. 3, pp. 178–190, 1998.

[10] J.-R. Chen et al., "Clinical value of information entropy compared with deep learning for ultrasound grading of hepatic steatosis," Entropy, vol. 22, no. 9, p. 1006, 2020.

[11] H.-J. Gdynia, H.-P. Müller, A. C. Ludolph, H. Köninger, and R. Huber, "Quantitative muscle ultrasound in neuromuscular disorders using the parameters 'intensity,''entropy,' and 'fractal dimension'," European journal of neurology, vol. 16, no. 10, pp. 1151–1158, 2009.

[12] A. Girardi, "Assessment of ultrasonic tissue characterization," Master's thesis, University of Twente, 2019.

[13] P.-H. Tsui et al., "Three-dimensional ultrasonic nakagami imaging for tissue characterization," Physics in Medicine & Biology, vol. 55, no. 19, p. 5849, 2010.

[14] S. Sikdar et al., "Quantification of muscle tissue properties by modeling the statistics of ultrasound image intensities using a mixture of gamma distributions in children with and without cerebral palsy," Journal of Ultrasound in Medicine, vol. 37, no. 9, pp. 2157–2169, 2018.

[15] Cardillo G. ROC curve: Compute a receiver operating characteristics curve. 2021. Available at: https://github.com/dnafinder/roc. Accessed June 2021.

[16] H. Rijsterborgh et al., "Ultrasonic myocardial integrated backscatter and myocardial wall thickness in animal experiments," Ultrasound in medicine & biology, vol. 16, no. 1, pp. 29–36, 1990.

[17] M. Van de Waarsenburg, C. Van der Vaart, and M. Withagen, "Structural changes in puborectalis muscle after vaginal delivery," Ultrasound in Obstetrics & Gynecology, vol. 53, no. 2, pp. 256–261, 2019.

[18] W.-C. Weng et al., "Evaluation of muscular changes by ultrasound nakagami imaging in duchenne muscular dystrophy," Scientific reports, vol. 7, no. 1, p. 4429, 2017.

[19] G. Weijers, G. Wanten, J. M. Thijssen, M. van der Graaf, and C. L. de Korte, "Quantitative ultrasound for staging of hepatic steatosis in patients on home parenteral nutrition validated with magnetic resonance spectroscopy: A feasibility study," Ultrasound in Medicine & Biology, vol. 42, no. 3, pp. 637–644, 2016.

[20] G. Weijers et al., "Transcutaneous vs. Intraoperative quantitative ultrasound for staging bovine hepatic steatosis," Ultrasound in medicine & biology, vol. 38, no. 8, pp. 1404–1413, 2012.

[21] J. M. Thijssen et al., "Computer-aided b-mode ultrasound diagnosis of hepatic steatosis: A feasibility study," ieee transactions on ultrasonics, ferroelectrics, and frequency control, vol. 55, no. 6, pp. 1343–1354, 2008.

[22] M. Van Holsbeeck and J. Introcaso, "Artifacts in musculoskeletal ultrasound," Muskuloskeletal ultrasound, 2nd ed, St. Louis, Missouri, Mosby, pp. 9–21, 2001.

[23] A. T. Grob, "Structural and functional ultrasound imaging of the pelvic floor during pregnancy and postpartum," PhD thesis, Utrecht University, 2016.

Supplementary figures

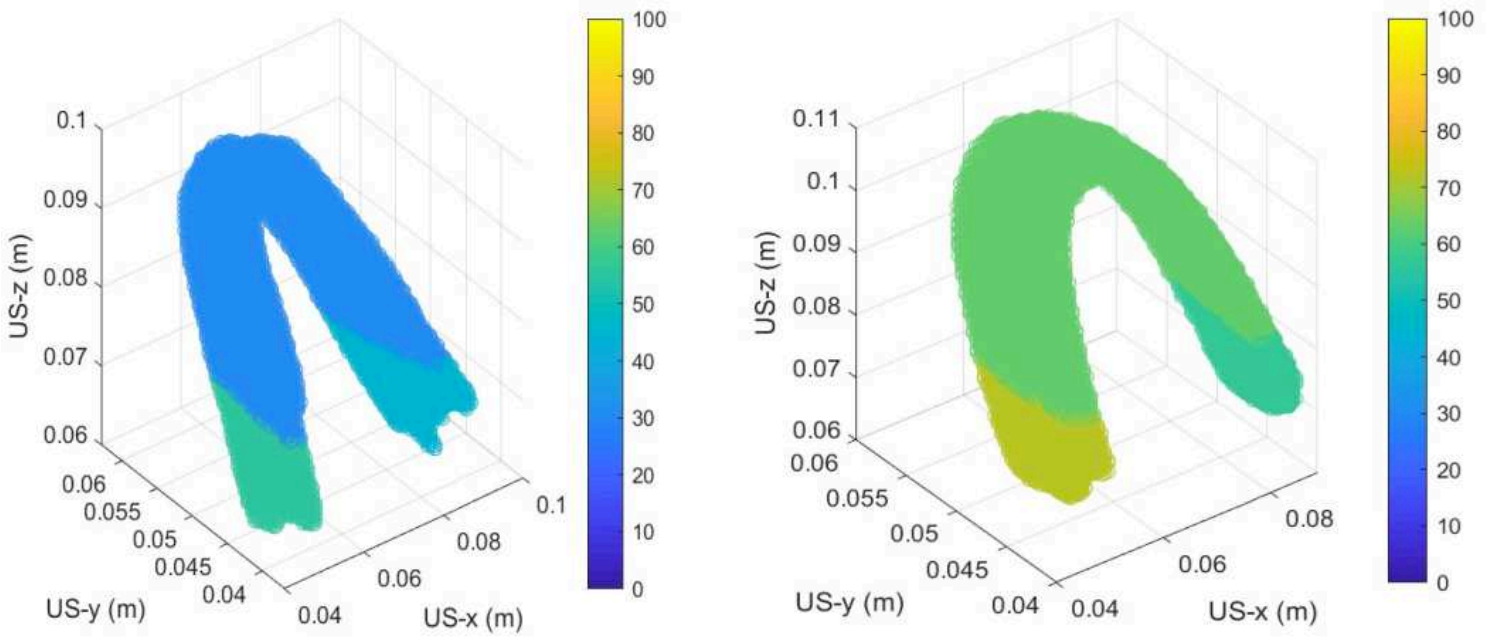

Figure S5.1: Visual representation of the shape parameter change for two undamaged puborectalis muscles (PRMs) at rest (US = ultrasound)

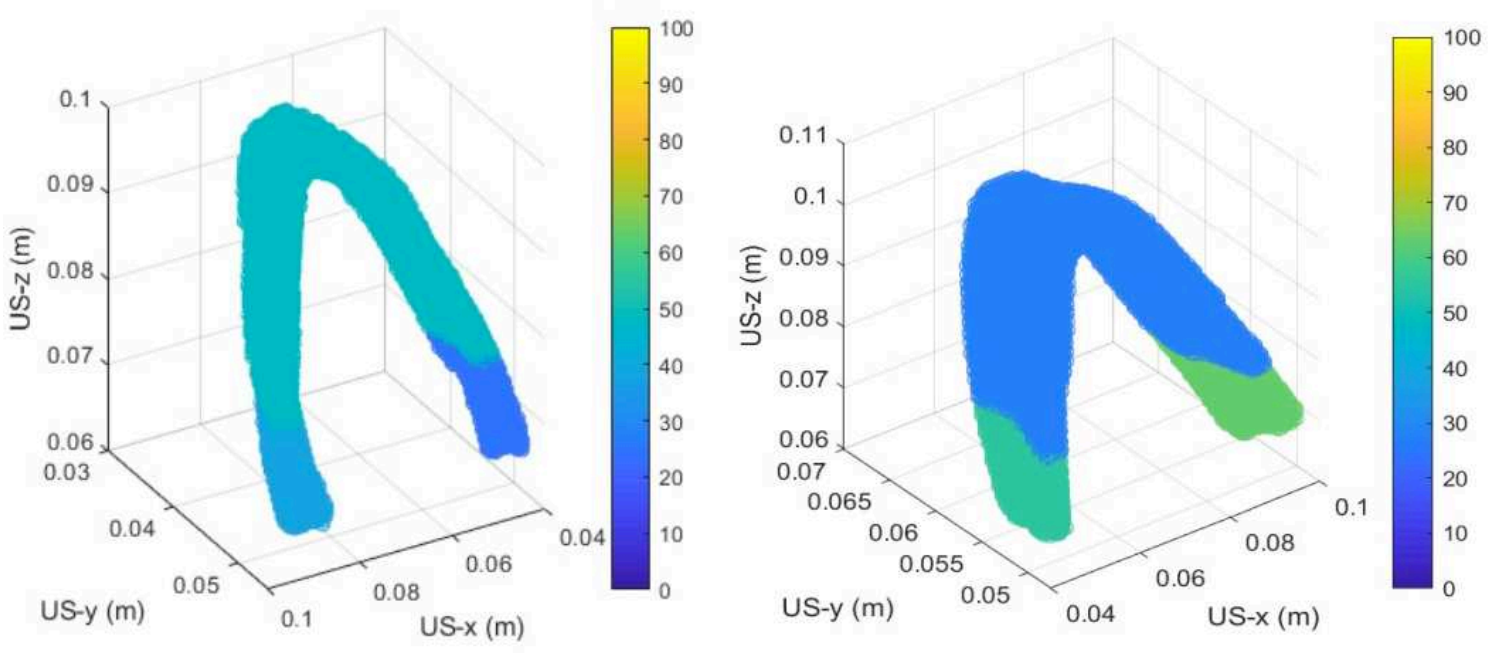

Figure S5.2: Visual representation of the shape parameter change for two undamaged puborectalis muscles (PRMs) at rest (US = ultrasound)

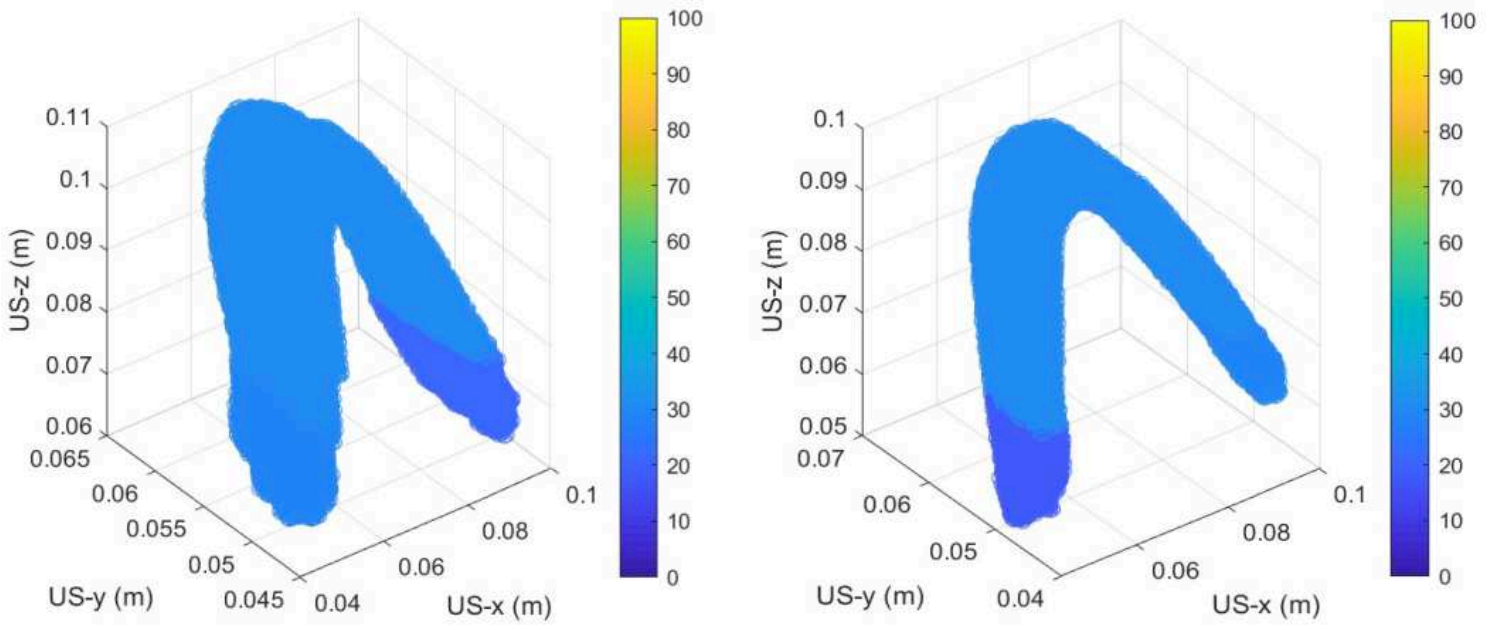

Figure S5.3: Visual representation of the shape parameter change for two undamaged puborectalis muscles (PRMs) at rest (US = ultrasound)

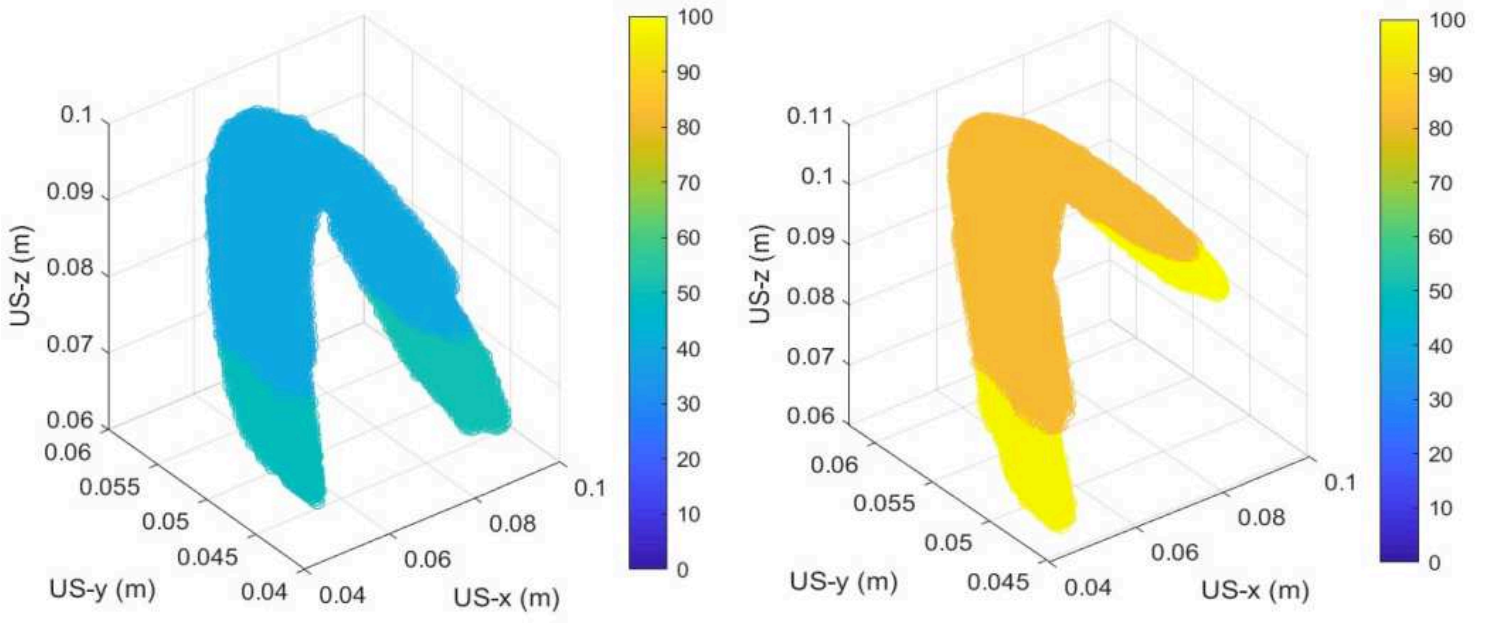

Figure S5.4: Visual representation of the shape parameter change for (a) an undamaged, (b) a damaged puborectalis muscle (PRM) at rest (US = ultrasound)

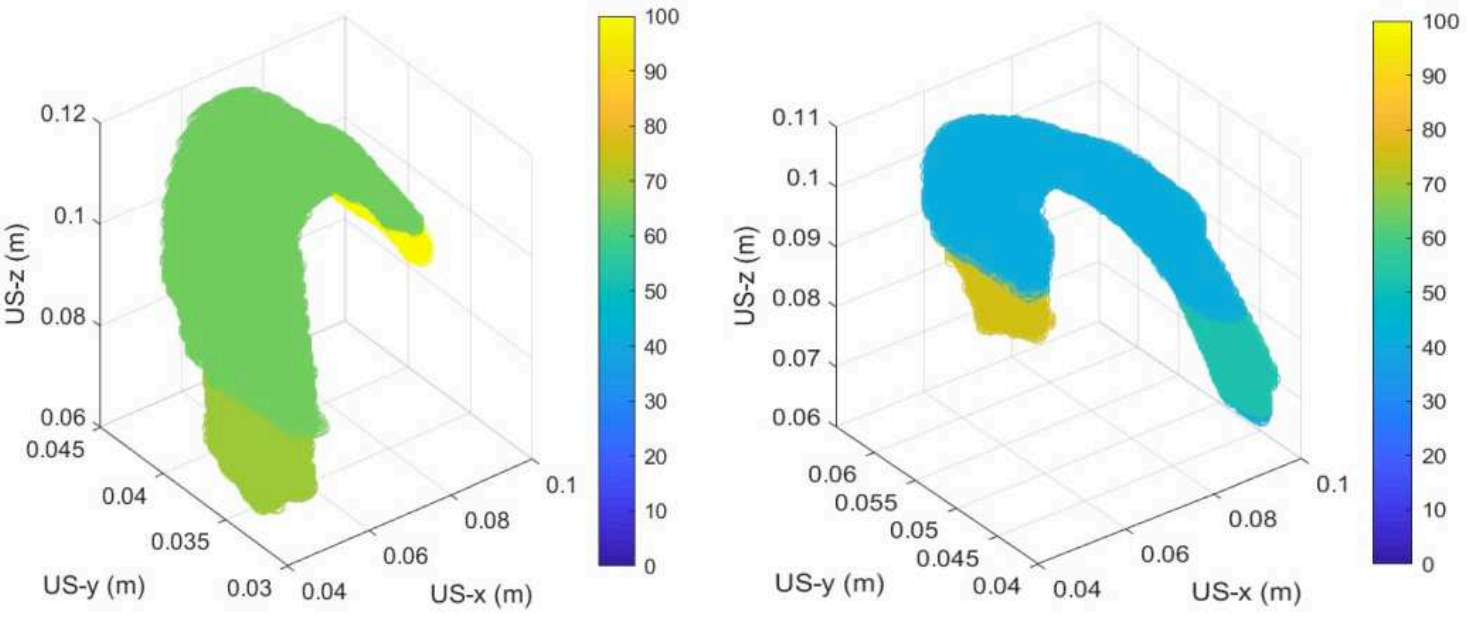

Figure S5.5: Visual representation of the shape parameter change for (a) an undamaged, (b) a damaged puborectalis muscle (PRM) at rest (US = ultrasound)

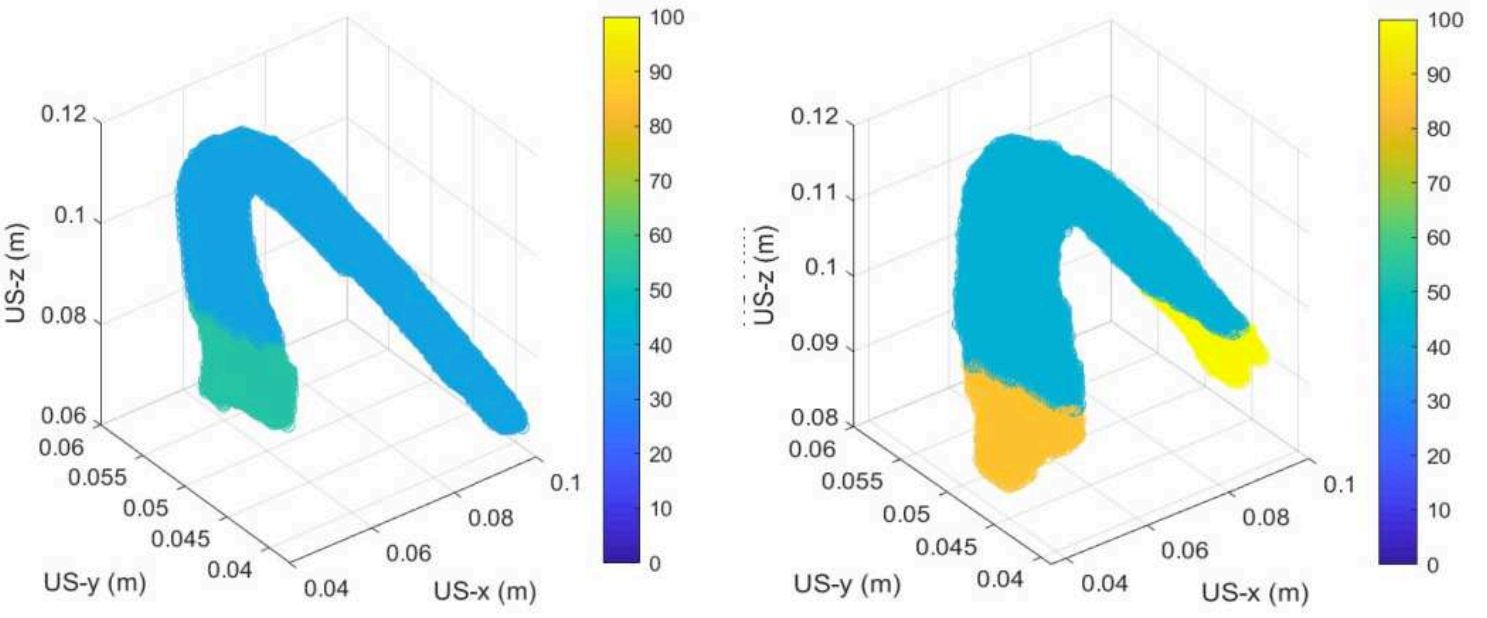

Figure S5.6: Visual representation of the shape parameter change for (a) an undamaged, (b) a damaged puborectalis muscle (PRM) at rest (US = ultrasound)

Chapter 6

General discussion

In this chapter, the work which have been presented in the preceding four chapters will be discussed. After a brief mention of the research objectives, the existing clinical and research workflows will be discussed, followed by the background and contribution of the work and further clinical significance. Following those sections, limitations of the developed methods are also discussed. And lastly, prospective future extensions for the work are outlined followed by conclusion.

6.1 Research objectives

The female pelvic floor (PF) consists of the PF organs and the pelvic diaphragm. This pelvic diaphragm is located around the inlet of the lower birth canal and consists of the muscle group called levator ani muscle (LAM). The LAM includes the puborectal muscle (PRM), which has been primarily investigated in the current work. This muscle gets frequently damaged during childbirth which may lead to prolapse in later life. In this work, three-dimensional (3D) strain imaging of the PRM had been investigated.

US analysis of the PRM, using real-time 3D volumetric datasets over time were analyzed to quantify the global and regional strain of the LAM. A US image is characterized by its noisy appearance which are called speckles. As is well known, this speckle is not noise but the result of coherent summation of the echo signals received by the individual elements of the US transducer. If the tissue motion/deformation which is being imaged is small, the speckle pattern moves but remains almost unchanged. Tracking the speckle pattern over time allows to quantify tissue displacement. In 3D volumetric datasets, the displacement of the tissue in three orthogonal directions can be quantified. These displacement datasets can be used to determine the strain of the tissue in 3D.

Thus, functional measurements and tissue characterization of the LAM, including the PRM were the two research objectives of this thesis, as mentioned below:

- Dedicated speckle tracking algorithms tailored to the LAM were to be developed. Based on 3D strain estimation strategies available at the research

group Medical UltraSound Imaging Center (MUSIC). Thus, combination of segmentation, speckle tracking and quantitative echography methods were to be developed, tailored for LAM. The resulting technique were to provide functional as well as echographic information over the contraction and relaxation cycle of the LAM.

- For US based tissue characterization, the currently used 2D methods expanded to 3D and sophisticated echographic parameters were to be investigated **[1]**. Instead of only echogenicity that has been utilized for characterization of the LAM, based on the research group's experience in liver and muscles, other statistical parameters would be investigated for distinguishing between undamaged and damaged muscle **[2-3]**.

These two research objectives were met for PRM through pilot studies carried on small number of women as proofs of concepts. These studies and the obtained results are described in **Chapters 2, 3, 4** and **5**. Calculation of strain was developed from principal strain to obtain the strain in the muscle fiber directions. Thereafter, a comparison between strain in PRM before and after pessary use was obtained. Lastly, tissue characterization of PRM were shown to differentiate between avulsed and intact PRMs.

6.2 Clinical and research workflows

The clinical workflow started with the woman experiencing symptoms of PF disorders and deciding to visit the clinic. In general, all the women who were included in the studies experienced overactive PF. These women were subjected to US imaging to examine the state of their PF muscles. In addition to this imaging, one more acquisition was made using a preset in the US machine. This preset was used to eliminate any additional filtering in the US machine for improved viewing on the screen of the machine. It also ensured that there would not be any settings change in data acquisition from patient to patient, such as brightness, contrast or time gain compensation (TGC).

The research workflow started after data was acquired through the US machine at the clinic by the clinician. These DICOM (Digital Imaging and Communications in Medicine) volumes were thereafter, converted from machine DICOM

to files to files containing the individual volumes with grey values. These files were used for manually segmenting the PRMs at the volumes when the muscles were at rest. Thereafter, these volume files were further converted to be used as inputs for the upgraded 'strainMUSIC' algorithm in MATLAB, for calculations of displacement estimates and thereafter strain.

These two workflows are required for future implementation of the developed methods in clinic as explained later in **Section 6.4.1**.

6.3 Brief background and contribution

The normalized cross-correlation algorithm developed in MUSIC research group have been utilized, upgraded and tailored to be used for strain analysis of PRM. This algorithm was originally developed to be used with radio frequency (RF) data for carotid arteries as well as for breast imaging. RF data contains the raw, unprocessed US signal information before it is converted into the B-mode image. As is well known, using RF data in US research offers several benefits over simple amplitude detection and provides additional information that can be leveraged in various ways. Since, calculation of strain requires accurate displacement estimates, RF-based displacement (or strain) estimation is better than envelope based methods. It has been demonstrated that there is significant reduction in the variability of strain estimated as well as improvements in the spatial resolution and signal-to-noise ratios obtained using RF signals as compared to envelope data **[12]**. Traditional and clinical US imaging generates B-mode images by detecting the amplitude of the beam-formed RF data. This is also known as the envelope data.

However, instead of RF, in this work, B-mode images consisting of gray values or envelope data have been used. The reason for using gray values are two-fold.

- Firstly, the deformation in the PRM is too large to be tracked using RF-based techniques. If the deformation is high, deformation of the rf-signal will be so high that it cannot be correlated to the signal obtained before deformation. This typically is the case for strains in the order of 5% or higher **[4]**. Due to 3D imaging, the volume rate that was available was

limited resulting in high strain of the tissue between two subsequently acquired volumes and thus the need for envelope based strain estimation. Moreover, Philips EPIQ US system, which is a commercially available US machine, was provided for data acquisition in this project. This system did not provide access to the RF or raw data.

- Secondly, clinical data acquisition involved acquisition through commercially available US machine. From the point of view of the clinician, who is already busy, no major extra steps were needed during data acquisition. As mentioned earlier, a simple preset was saved for the acquisitions. Strain analysis using B-mode gray values would enable data acquisition from any commercially available US machines, without any need for extra apparatus or proprietary additions to the machine. This would enable data acquisition from any clinic, for future extensions.

Segmentation of the muscles of the LAM and particularly of the PRM was not one of the research objectives of the current work since it was performed by another PhD student, who was also part of the GYNIUS project. Segmentation of the PRM at rest was needed for developing the methods for the current work, namely, tracking the PRM over the contraction cycle. An initial region of interest (ROI) was required as initial input using 'strainMUSIC' algorithm. This manual step could be fully automated by future research involving artificial intelligence (AI). The developed AI network could be trained on different datasets to have automated segmentations. Furthermore, AI-based segmentation and tissue tracking can be utilised as complimentary to each other in order to improve the segmentation over the contraction cycle and make it more robust. The clinical reason, for segmentation was that LAM being a group of muscles, the ROI representing only the PRM needed to be singled out for analysis of the obtained strain measurements. Also, the muscle fiber orientation of PRM is different from the surrounding muscles of the LAM, thus, would also result in different strain.

Transperineal US (TPUS) is frequently used for imaging PF muscles because of its versatility and real-time capabilities **[5]**. To obtain information about the state of the PF muscles, US acquisition from these muscles is from rest to contraction. Although information is obtained over the contraction cycle, only global geometrical changes can be determined from the static 2D images forming the

3D volumes. Thus only indirect information on the contractile properties can be deduced and local functional information cannot be deduced at all **[6-7]**. Whereas, measuring strain from this same TPUS images could provide insight about the functional information, thus was selected for the current work.

6.3.1 Contribution of the current work

The current work was a first attempt towards explaining the behavior of the PRM through 3D US strain imaging, which has not previously been investigated or published. Through 3D strain, certain patterns have been observed in the intact PRM while different patterns were found in avulsed PRM's. In all PRMs, strain towards muscle fiber direction showed that the sling or mid region of PRM show negative strain representing contraction. And the intact ends of the PRMs show positive strain or extension. This indicates that the contractile properties of these parts of the PRM are limited and more or less behave passively. The positive strain represents extension that is induced by the contracting mid-part of the PRM. The PRM consists of both skeletal and smooth muscle fibers and this is in line with the characteristic of the complex functionality of the combination of these two muscle fibers **[8]**. The LAM, and thus also PRM have resting myoelectric activity, to support the overlying pelvic organs. This activity has been suggested to be related to the presence of smooth muscle fiber bundles in the LAM, whereas, the skeletal muscle fibers are responsible for voluntary contraction of the muscle **[8]**. The strain results of the current work show different strain values for different regions of the PRM during contraction. This difference in local strain might also indicate the difference in distribution of smooth and skeletal muscle fibers in the PRM. Further large scale histological studies could specifically link the type of strain to the type of muscle fibers, namely the pattern of elongation in the ends and contraction in the mid region. This pattern was complimentary for the avulsed ends of PRMs, which did not show positive strain. Thus the primary observation has been that 3D strain is capable of showing changes in the deformation of the muscle. Also, the strain results obtained from PRMs after pessary use indicated the changes in the muscle already after a short time of three months, when compared with strain from PRM before use of pessary. These short term changes in the muscle, could be related to the

fact that the smooth muscle fibers do not have to remain constantly severely contracted to support the load of the pelvic organs since the presence of the pessary provides support to the PRM. This release could have led to morphological changes in the PRM, which results in less strain even when pessary was removed during data acquisition. Thus, strain showed marked difference from before to after pessary use.

It is to be mentioned here that in the current work, all the reported studies have been performed as pilot studies on small number of women. Although the included number of women is small, already significant differences were found, strengthening the opinion that 3D strain analysis could be a very promising technology with high sensitivity and specificity. Thus future large scale and diverse studies would be required for further confirmation of the conclusions of the current study. Of course, unintended bias might have been present in the inclusions of the current studies, leading to biased results which could be addressed by performing large scale studies with balanced inclusions representing the diversity of population.

6.4 Clinical significance of functional information

The current work shows that it is possible to obtain functional information representing the state of the PRM. This functional information could be used to detect local defects like avulsion. Furthermore, it might bear quantitative information by comparing the avulsed end with the connected end. This quantitative information was also shown to be able to distinguish changes in the avulsed PRMs from before to after pessary usage. Adding quantitative functional information might provide an improved figure of merit of the effect of pessary on the PRM since currently analysis is limited to the experience of the woman without providing a quantitative measure.

The clinician can already determine from the symptoms as well as from the US images of the PF, if there is an avulsion in the PRM. In other words, it is not necessary to know strain in the muscle to determine avulsion. However, when this additional information is available to the clinician, it would enable him/her to know whether the avulsed muscle is still functional to some extent and to

what extent. It would also ideally, aid in identifying the reason whether the muscle has lost functionality due to damage in it or there might be other cause like damage to the nerve as well [9]. Ideally, if a muscle is not disconnected and yet does not show normal functionality, it could also be a consequence of nerve damage. Thus, if loss of functionality is a result of nerve damage instead of muscle damage, then PF muscle therapy (PFMT) might be less beneficial.

Deriving functional information is emphasized in the current study, not only for the current conclusions but also for further insights through large scale studies with diverse inclusions. Since, the PRM is of crucial importance in female PF functioning, this functional information would be able to lead to insights such as:

- predict which pregnant women are at high risk for obstructive labor. In that case, strain imaging would be needed to be performed for PRMs during different stages of pregnancy as well as before pregnancy
- develop and test early regenerative therapies that enhance functional recovery of the PRM after delivery trauma. In this case, the strain information before delivery would provide a means for comparison to the extent of damage in the PRM after delivery
- predict which women having pelvic organ prolapse (POP) would benefit from PF muscle therapy (PFMT). In this case, functional information through strain before PFMT would provide a means for comparison for the extent of damage. Strain imaging after PFMT would show if there have been any improvement in the function of the PRM
- visualization of the recovery or the lack thereof of PRM, from before to after pessary usage for women with avulsion treated with pessary
- allow the development of specialized and patient-centered treatment protocols for urinary incontinence (UI) and POP

6.4.1 Implementation in clinic

Implementation of any new technology in the clinic can be complicated, especially when new equipment or apparatus is required. However, since no addi-

tional apparatus/protocol is needed for data acquisition by the US machine and since a clinically standardized acquisition such as TPUS is utilized, implementation of the developed method in the clinic could be comparatively straightforward. Implementation would involve only two prior steps, as mentioned in the clinical and research workflows **(Section 6.2)**. These two steps are data acquisition with a specified preset and segmentation of the PRM at rest. After these two steps, calculation of the 3D strain over the full contraction cycle is automated, thus free of intra or inter-observer variabilities. These calculations can be simply added as an additional tool/feature either in the US machine itself or through another computer. For the current calculations, results would be available in approximately one day after the aforementioned steps, for analysis by the clinician. It has to be noted that only minor effort has been put in speeding up the 3D strain calculations since first the potential and benefit of the method needed to be provided. However, since real-time 3D strain calculation is already commercially available for cardiac applications, it can be expected that this long calculation times can also be reduced to become semi real-time. Strain analysis could be performed for all women, who could benefit from functional information (as mentioned in the previous section), who are already visiting the clinic for US imaging.

Usually, when a woman with symptoms visits a clinic, TPUS is performed to assess the condition of the PF. In the US volumes, the whole PF is imaged and details about the PRM can be qualitatively observed. These same US volumes can now be used for further functional and quantitative information of the specific muscle PRM, through strain and echogenicity analysis. This new information would then aid the clinician to know which parts of the muscle is functional and also to which extent, rather than just the fact as to whether the muscle is avulsed or not. In other words, the new information is showing the functionality of the whole muscle in 3D, including the connected or disconnected ends. The normalized strain ratio (NSR) as presented in Chapter 3 and 4 already provides an indication of the effect of an avulsion. Thus, NSR provides a threshold number which could be used to distinguish between functional PRM from non-functional one, irrespective of whether avulsion can be observed in US volumes.

The NSR for women with no damage to the PRM will have values close to one, indicating that both ends of the PRM as well as the mid region or sling of the PRM are functioning properly. In case of women with avulsions, the disconnected end of the PRM can be directly observed through strain, even without making any additional measurements. In case of unilateral avulsion, a difference would be present between the connected and disconnected end. Especially, when the connected end would show positive strain and the disconnected end would show negative strain, the difference will be large leading to a high NSR. In case of bilateral avulsion, the strain in both ends would be more similar but very different from the mid region also resulting in a large NSR.

Usually, the success of pessary use is determined by the absence of POP symptoms and a positive response of the woman. If the woman still continues to use the same pessary in follow up studies after the first trial, then it is accepted that treatment is successful. However, the success of pessary treatment on certain parameters measured through TPUS have also been used to assess the effect of pessary treatment on PRM function **[10-11]**. But these parameters have been calculated from 2D slices from 3D volumes introducing observer variability. However, the PRM is a 3D structure and 3D strain and subsequently NSR provides a direct measure of functionality of the PRM. If there is no change in NSR from before to after pessary usage, it might indicate that there has been no functional improvement due to the pessary. Similarly, a normalization of NSR even after a short period of three months of pessary use, as shown in **Chapter 4**, indicate success of pessary treatment. Thus NSR provides an objective and quantitative measure. It is to be emphasized here that a large scale study to validate NSR is required to demonstrate the effectiveness of NSR as quantitative method to determine pessary placement success.

Tissue characterization of the PRMs of women with avulsion would show that there has been changes in the tissue in the disconnected end, apart from the fact that there has been also a functional change. The results showing a comparison of the tissue characterization between PRMs of women with and without unilateral avulsion have been shown and discussed in **Chapter 5**. Here as well, tissue characterization of the 3D muscle is provided in this work, unlike the current availability of measures like echogenicity only from 2D images of the

muscle.

Combination of strain and tissue characterization could be complimentary to each other, the former showing functional information while the later showing composition and condition of the muscle fibers. Especially, for women who cannot contract their PRMs due to nerve damage or any other pathological condition, strain cannot be measured. But tissue characterization from US volumes can still be done. And local changes in the tissue of PRM, such as scar tissue formation could be discovered by the increased echogenicity with respect to normal tissue. Thus, in absence of histological studies, tissue characterization could be used to provide information on the composition of the local parts of the muscle.

6.5 Limitations

There are certain limitations for the current work as mentioned below.

- Firstly, there was no ground truth yet available for strain in PRM. Potentially, this limitation could be overcome by using MRI tagging as ground truth. However this requires a very extensive study. A large scale study with inclusions comprising of different age, ethnicity, body mass index (BMI) etc. could also be performed. If the reported strain patterns are found in most of the women for the different situations (avulsion, pre and post pessary placement), then that could be established as the ground truth.

- Secondly, in the current work TPUS data acquisition was performed by only one clinician. This eliminated the presence of any inter-operator or inter-machine variabilities in the included datasets. This is a limitation because this might also allow for some kind of unintentional bias. Since US imaging is operator dependent, even for standardized acquisition like TPUS, further investigation might be required for eliminating variabilities or biases when multiple operators would be acquire data in future.

- Thirdly, the complete dataset has been acquired using only one US machine and one matrix transducer. Changes in US machine parameters like (TGC, gain, brightness) and/or changes in transducer frequency might re-

sult in difference in strain calculations. This limitation could be overcome by performing comparison studies among US machines provided by different vendors, using phantoms. Thereafter, the existing dataset could be extended with TPUS acquisitions using multiple US machines.

- Fourth limitation would be about the computational barriers. Ideally, if computational barriers could be overcome, both segmentation and strain measurement could be implemented even real-time. So, the clinician would be able to observe the changes in strain directly on screen of the US machine (during data acquisition) as the woman is contracting or performing Valsalva maneuver. This would require both the automatic segmentation and the complete strain algorithm to run on real-time. But in reality, only near real-time would be possible to be achieved. Near real-time is mentioned because complete data acquisition step has to be prior to segmentation and strain calculations steps. However, the reduction in the time difference between acquisition and strain measurements to sub-minute would still be overcoming of this limitation for all practical purposes.

- Lastly, since RF data was not available, tissue characterization could only be done from B-mode gray values. It is known that strain estimation using the RF-signal has a ten times better performance than based on the envelope **[9]**. However, this only counts for strain estimation in the direction of the ultrasound image lines. Since we quantified the strain in 3D with the probe at the perineum, this will preclude RF-based 3D strain estimation. Furthermore, the strain values are relatively large limiting the beneficial effect of RF-based strain estimation, as is also mentioned in **Section 6.3**.

6.6 Future extensions

The goal of future extensions of this work would be to establish strain analysis as an additional aid for the clinician to be able to determine the state of the PRM as well as the entire LAM. Future studies of this work can have both clinical extensions as well as extensions involving improvement of the developed algorithm. The clinical extensions could be carried out with the current version of the algorithm already, with certain minor changes. More inclusions would then

allow parametrical statistical analysis.

6.6.1 Clinical extensions

The developed algorithm in its current version could be used for application in the following types of studies for extensive clinical analysis. As extensions of this work, it is suggested to have three directions. These are briefly explained below.

- 3D strain analysis of more inclusions is required to investigate further how the normal and undamaged PRM deforms. It would be even more useful if the strain analysis could be validated with the clinicians' diagnosis for a large number of women with and without any damage in their LAMs and/or PFs as well as with magnetic resonance imaging (MRI) preferably using MRI tagging to validate the US strain measurements. Thus, the first extension would be to include more data for nulliparous women with intact and undamaged PRMs. These inclusions should be for both contraction and Valsalva maneuver.

- The second extension would be to also perform the strain analysis for all the remaining muscles of the LAM and investigate how the muscles behave in relation to each other. This should include both damaged and undamaged muscles. For this, manual or automatic segmentation of the individual muscles of the LAM would be required. Furthermore, certain tailoring of the algorithm would be required to include the muscle fiber orientation of a specific muscle.

- The third direction would be to do strain analysis of different data consisting of patients with different pathological conditions regarding the PF, apart from avulsions of PRMs. These pathological conditions could be such as rectocele (affecting support of posterior compartment of PF) or cystocele (affecting support of anterior compartment of PF). Through 3D strain, the functionality of the affected muscles of the PF in these pathological conditions compared to normal functionality could be investigated.

6.6.2 Algorithm improvement

Improvement for the current version of algorithm can be achieved through speeding up the calculation time and addition of features. The extensions for improvement could be as faster calculations and modelling.

- The current version of the algorithm requires long time to compute. This computation time needs to be reduced in order to achieve near/semi real-time results. Thus computational optimizations of the whole calculation including cross-correlation, interpolation and filtering is required. One way of doing these optimizations is to use dedicated GPU for these calculations.
- Future extension of this work could include, finite element modeling apart from strain imaging of the PRM and all the female PF muscles, to have a better understanding of the bio-mechanics of the entire pelvic diaphragm. Modelling would provide a comparison to strain.

6.7 Conclusion

This thesis describes a new 3D strain and quantitative echo analysis method to assess the function and composition of the PRM. It has been demonstrated that the difference in functionality of intact PRM as compared to avulsed PRM could be determined through strain. Furthermore, strain could also demonstrate the changes in PRM from before to after pessary usage.

References

[1] A. T. Grob, M. I. Withagen, M. K. van de Waarsenburg, K. J. Schweitzer, and C. H. van der Vaart, "Changes in the mean echogenicity and area of the puborectalis muscle during pregnancy and postpartum," International urogynecology journal, vol. 27, pp. 895–901, 2016.

[2] G. Weijers, G. Wanten, J. M. Thijssen, M. van der Graaf, and C. L. de Korte, "Quantitative ultrasound for staging of hepatic steatosis in patients on home parenteral nutrition validated with magnetic resonance spectroscopy: A feasibility study," Ultrasound in Medicine & Biology, vol. 42, no. 3, pp. 637–644, 2016.

[3] S. Pillen, A. Verrips, N. van Alfen, I. Arts, L. Sie, and M. Zwarts, "Quantitative skeletal muscle ultrasound: Diagnostic value in childhood neuromuscular disease," Neuromuscular disorders, vol. 17, no. 7, pp. 509–516, 2007.

[4] E. I. Céspedes, C. L. de Korte, and A. F. van der Steen, "Echo decorrelation from displacement gradients," Ultrasonics, vol. 36, nos. 1-5, pp. 661–666, 1998.

[5] H. P. Dietz, "Pelvic floor ultrasound: A review," American journal of obstetrics and gynecology, vol. 202, no. 4, pp. 321–334, 2010.

[6] H. Dietz, "Clinical consequences of levator trauma," Ultrasound in obstetrics & gynecology, vol. 39. Wiley Online Library, pp. 367–371, 2012.

[7] M. van de Waarsenburg, C. Van der Vaart, and M. Withagen, "Structural changes in puborectalis muscle after vaginal delivery," Ultrasound in Obstetrics & Gynecology, vol. 53, no. 2, pp. 256–261, 2019.

[8] A. Shafik, S. Asaad, and S. Doss, "The histomorphologic structure of the levator ani muscle and its functional significance," International urogynecology journal, vol. 13, pp. 116–124, 2002.

[9] J. A. Ashton-Miller and J. O. DeLancey, "Functional anatomy of the female pelvic floor," Annals of the New York Academy of Sciences, vol. 1101, no. 1, pp. 266–296, 2007.

[10] C. Manzini, F. van den Noort, A. T. Grob, M. I. Withagen, and C. H. van der Vaart, "The effect of pessary treatment on puborectalis muscle function," International Urogynecology Journal, vol. 32, pp. 1409–1417, 2021.

[11] C. Manzini, L. M. Morsinkhof, C. H. van der Vaart, M. I. Withagen, and A. T. Grob, "Parameters associated with unsuccessful pessary fitting for pelvic organ prolapse up to three months follow-up: A systematic review and meta-analysis," International Urogynecology Journal, vol. 33, no. 7, pp. 1719–1763, 2022.

[12] C. Ma and T. Varghese, "Comparison of cardiac displacement and strain imaging using ultrasound radiofrequency and envelope signals," Ultrasonics, vol. 53, no. 3, pp. 782–792, 2013.

Chapter 7

Summary

7.1 Summary in English

Functional information about the female pelvic floor (PF) muscles were deemed necessary for investigating damage frequently inflicted on these muscles by vaginal delivery. Ultrasound (US) imaging is already used for investigating the state of PF muscles to diagnose damage in it such as avulsion. Since cardiac strain imaging has been beneficial to know functional information of cardiac muscles, it was hypothesized that strain imaging of the PF muscles would also be feasable.

One of the PF muscles is the puborectal muscle (PRM). PRM has been investigated for deformation and strain, since disconnection from the bone or avulsion frequently occurs for this muscle, causing loss of support. The PRM was segmented in the initial 3D volume when the muscle was at rest. Thereafter the deforming muscle was tracked in each volume for two types of muscle movements; rest to contraction and rest to Valsalva maneuver (VM). Displacement estimates were estimated using an in-house developed cross-correlation based algorithm, using the acquired 3D US volumes and the segmented or tracked PRM. Principal strain were calculated from the displacement estimates for both of the movements. These two movements, namely, contraction and VM showed complimentary strains. While maximum contraction showed negative strain, maximum VM showed positive strain. These results demonstrated that the developed algorithm, could distinguish between the two different muscle movements.

Since the PRM being a striated muscle, it is expected that the strain in it would also be directed towards the orientation or direction of the muscle fibers. Whereas, the directions of the previously calculated principal strain did not align with the muscle fiber direction or orientation. Thus, the algorithm was further updated to calculate displacement estimates and strain in muscle fiber direction. This so-called projected strain was acquired from US volumes recorded of PRMs from rest to contraction from intact and undamaged PRMs as well as PRMs with unilateral avulsion or disconnection. The algorithm could show differences in strain in different parts of the muscle, whether connected to the bone or disconnected. Thus the avulsed end could be distinguished from the connected end through strain. Thereafter, normalized strain ratio had been calculated to

indicate the difference in regions of the muscle showing contraction and elongation. This ratio could be used to differentiate between disconnected or avulsed PRMs and intact PRMs. Statistical analysis showed that this difference was statistically significant.

One of the objectives of investigating PRM through strain was to get functional information from it. So that, the state of the muscle could be determined from before to after PF muscle therapy or pessary use. Strain could also be used to show difference in the state of the avulsed PRMs from before to after pessary use. In this case, data consisted of PRMs with both unilateral as well as bilateral avulsions. Data were acquired before pessary fitting and after pessary fitting with subsequent use for three months. Acquisitions were from the same women while they voluntarily contracted their PRMs from rest. Projected strain and the earlier formulated normalized strain ratio were calculated for both before and after pessary use for all these women. This ratio showed a decrease in all the women from before to after pessary use except one that had already a normal ratio that only slightly increased. This indicated that difference between the two ends of the PRMs had reduced after three months of pessary use. Statistical analysis showed that this difference was significant.

The other objective of the work was to develop a 3D Quantitative US (QUS) tissue characterization method to obtain diagnostic information about PRMs with and without avulsion. It was hypothesized that the presence of an avulsion of the PRM would result in a change in the statistical distribution of gray values in a B-mode US volume of the PRM. Echogenicity and other statistical parameters like entropy and shape parameter have been calculated to determine whether there can be differences between undamaged PRMs and unilaterally avulsed PRMs. The obtained results demonstrated that tissue characterization of PRMs could show difference in the state of the muscle.

The four studies form a continuum from idea to proofs of concepts. Thus all the studies have been carried out on small number of datasets. The positive outcome was that the results were already significant in spite of small datasets. In order for strain analysis of PRM being utilized in clinic, it would be necessary to perform the developed methods on a large number of datasets, which would allow for inclusion of more diverse populations and prevention of possible in-

clusion bias. Furthermore, it would also allow for parametric statistical analyses instead of non-parametric ones. These datasets should include both intact and avulsed PRMs. Moreover, it would be beneficial to do strain analysis of all the neighboring muscles of PRM in the PF and investigate how the muscles behave in relation to each other.

7.2 Samenvatting in Nederlands

Functionele informatie over de vrouwelijke bekkenbodemspieren (BB) wordt noodzakelijk geacht voor het onderzoeken van schade die vaak aan deze spieren wordt toegebracht door vaginale bevalling. Echografie (US) beeldvorming wordt gebruikt voor het onderzoeken van de toestand van BB spieren om schade daarin te diagnosticeren, zoals avulsie. Aangezien beeldvorming van de 'strain' van het hart nuttig is geweest om de functie van de hartspier te onderzoeken, werd verondersteld dat beeldvorming van de 'strain' van de bekkenbodemspieren ook haalbaar zou zijn.

Eén van de BB spieren is de puborectalis spier (PRS). De PRS is onderzocht op vervorming en rek, aangezien losraken van het bot of avulsie vaak optreedt voor deze spier, waardoor wat leidt tit verlies van wat houdt dit in. De PRS werd gesegmenteerd in het oorspronkelijke 3D-volume wanneer de spier in rust was. Daarna werd de vervorming van de spier in elk volume gevolgd voor twee soorten spierbewegingen; rust tot contractie en rust tot Valsalva-manoeuvre (VM). Schattingen van de verplaatsing werden geschat met behulp van een in huis ontwikkeld algoritme op basis van kruiscorrelatie, met behulp van de verkregen 3D-volumes uit de US en de gesegmenteerde of gevolgde PRS. De hoofd 'strain' werd berekend op basis van schattingen van de verplaatsing voor beide bewegingen. Deze twee bewegingen, namelijk contractie en VM, vertoonden complementaire spanningen. Terwijl de maximale contractie een negatieve spanning vertoonde, vertoonde de maximale VM een positieve spanning. Deze resultaten toonden aan dat het ontwikkelde algoritme onderscheid kon maken tussen de twee verschillende spierbewegingen.

Aangezien de PRM een dwarsgestreepte spier is, wordt verwacht dat de spanning erin ook gelijk zou zijn aan de richting of oriëntatie van de spiervezels. Terwijl de richtingen van de eerder berekende hoofd 'strain' niet overeenkwamen met de richting of oriëntatie van de spiervezels. Zo werd het algoritme verder geüpdatet om verplaatsingsschattingen en 'strain' in de richting van spiervezels te berekenen. Deze zogenaamde geprojecteerde 'strain' werd verkregen uit US volumes geregistreerd van PRS's van rust tot samentrekking van intacte en onbeschadigde PRS's, evenals PRS's met eenzijdige avulsie of ontkoppeling.

Het algoritme kan verschillen in spanning laten zien tussen verschillende delen van de spier, of ze nu verbonden zijn met het bot of zijn afgescheurd. Zo kon 'strain' onderscheid maken tussen een geavulseerd of verbonden uiteinde. Daarna werd de genormaliseerde 'strain' verhouding berekend om het verschil aan te geven tussen verschillende delen van de spier, welke contractie en rek vertoondenn. Deze genormaliseerde 'strain' verhouding kan worden gebruikt om onderscheid te maken tussen niet-verbonden of geavulseerde PRS's en intacte PRS's. Statistische analyse toonde aan dat dit verschil statistisch significant was.

Eén van de doelstellingen van het onderzoek van PRM door middel van belasting was om er functionele informatie uit te halen. Zodat de toestand van de spier kan worden bepaald van voor tot na PF-spiertherapie of pessariumgebruik. Stam kan ook worden gebruikt om een verschil aan te tonen in de toestand van de geavulseerde PRM's van voor tot na het gebruik van het pessarium. In dit geval bestonden de gegevens uit PBM's met zowel unilaterale als bilaterale avulsies. De gegevens werden verkregen vóór het passen van het pessarium en na het plaatsen van het pessarium met daaropvolgend gebruik gedurende drie maanden. Acquisities waren van dezelfde vrouwen, terwijl ze vrijwillig hun PRM's uit rust opliepen. De geprojecteerde stam en de eerder geformuleerde genormaliseerde stamverhouding werden berekend voor zowel voor als na het gebruik van het pessarium voor al deze vrouwen.Deze verhouding nam bij alle vrouwen af na het gebruik van het pessarium, behalve bij één vrouw die al een normale 'strain' verhouding had, in dit geval nam de verhoudinglicht toe. Dit gaf aan dat het verschil in 'strain' tussen de twee uiteinden van de PRS's was afgenomen na drie maanden pessariumgebruik. Statistische analyse toonde aan dat dit verschil significant was.

Het andere doel van het werk was het ontwikkelen van een 3D kwantitatieve ultrageluid (QUS) weefselkarakteriseringsmethode om diagnostische informatie te verkrijgen over PRS's met en zonder avulsie. Er werd verondersteld dat de aanwezigheid van een avulsie van de PRS zou resulteren in een verandering in de statistische verdeling van grijswaarden in een B-mode US volume afbeelding van de PRS. Echogeniciteit en andere statistische parameters zoals entropie en vormparameter zijn berekend om te bepalen of er verschillen kunnen zijn tussen

onbeschadigde PRS's en eenzijdig geavulseerde PRS's. De verkregen resultaten toonden aan dat weefselkarakterisering van PRS's een verschil in de toestand van de spier kon aantonen.

De vier studies beschreven in die dit proefschrift vormen een continuüm van idee tot proofs of concepts. Alle studies zijn dus uitgevoerd op een klein aantal datasets. Desondanks, waren de resultaten statistisch significant. Om 'strain' analyse van de PRS in het kliniek te kunnen gebruiken. Het is nodig om de ontwikkelde methoden uit te voeren op een groot aantal datasets, waardoor meer diverse populaties kunnen worden meegenomen en mogelijke inclusie bias kan worden voorkomen. Bovendien zou dit parametrische statistische analyses mogelijk maken in plaats van niet-parametrische. Deze datasets moeten zowel intacte als geavulseerde PRS's bevatten. Bovendien zou het nuttig zijn om een spanningsanalyse uit te voeren van alle aangrenzende spieren van PRM in de bekkenbodem en te onderzoeken hoe al deze spieren zich ten opzichte van elkaar gedragen.

Appendices of flowcharts

Appendix A

Volumetric data preparation

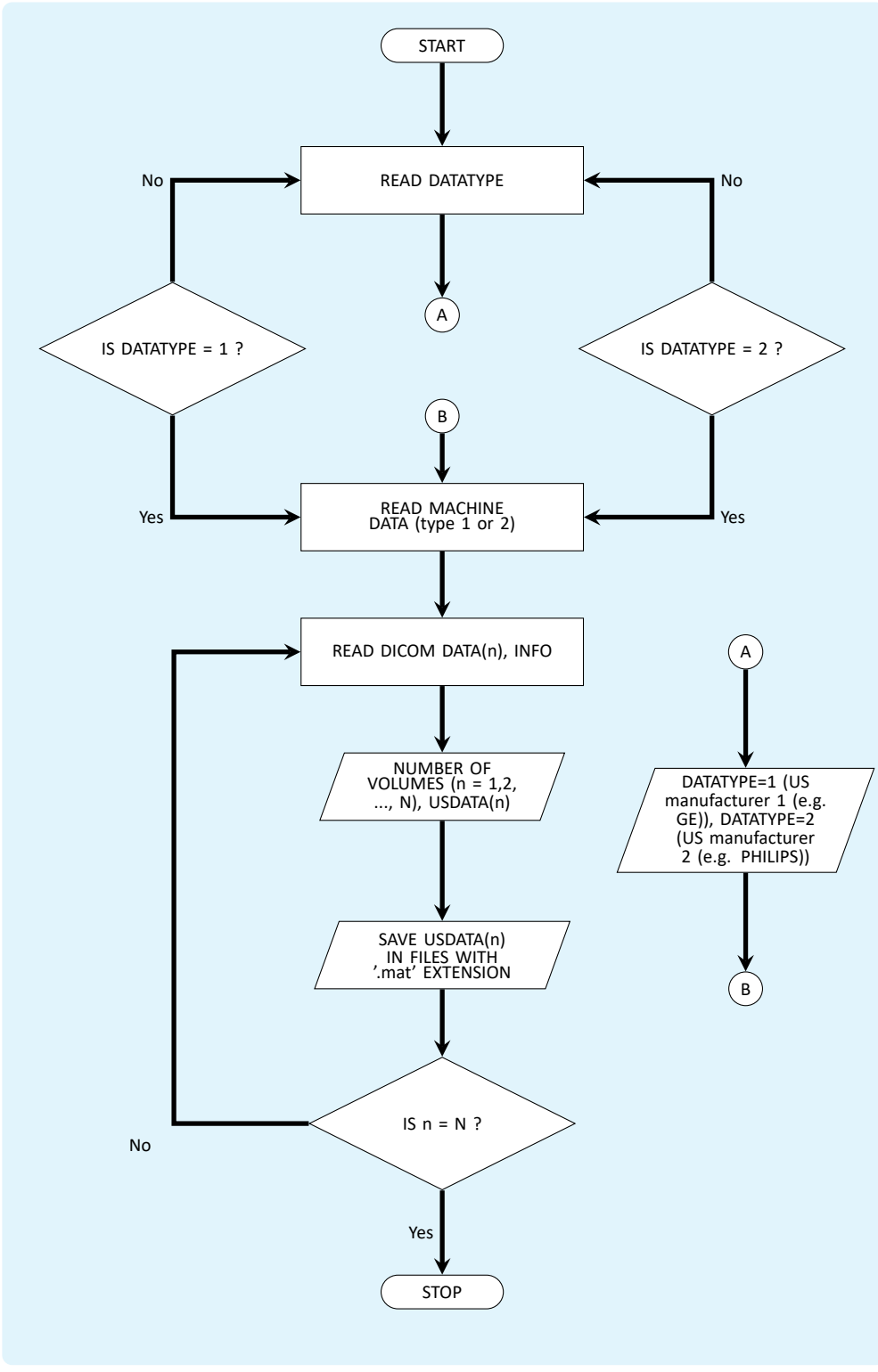
START
READ DATATYPE
No
No
A
IS DATATYPE = 1 ?
IS DATATYPE = 2 ?
B
Yes
READ MACHINE DATA (type 1 or 2)
Yes
READ DICOM DATA(n), INFO
A
NUMBER OF VOLUMES (n = 1,2, ..., N), USDATA(n)
DATATYPE=1 (US manufacturer 1 (e.g. GE)), DATATYPE=2 (US manufacturer 2 (e.g. PHILIPS))
SAVE USDATA(n) IN FILES WITH '.mat' EXTENSION
B
IS n = N ?
No
Yes
STOP

Appendix B

’strainMUSIC’ algorithm

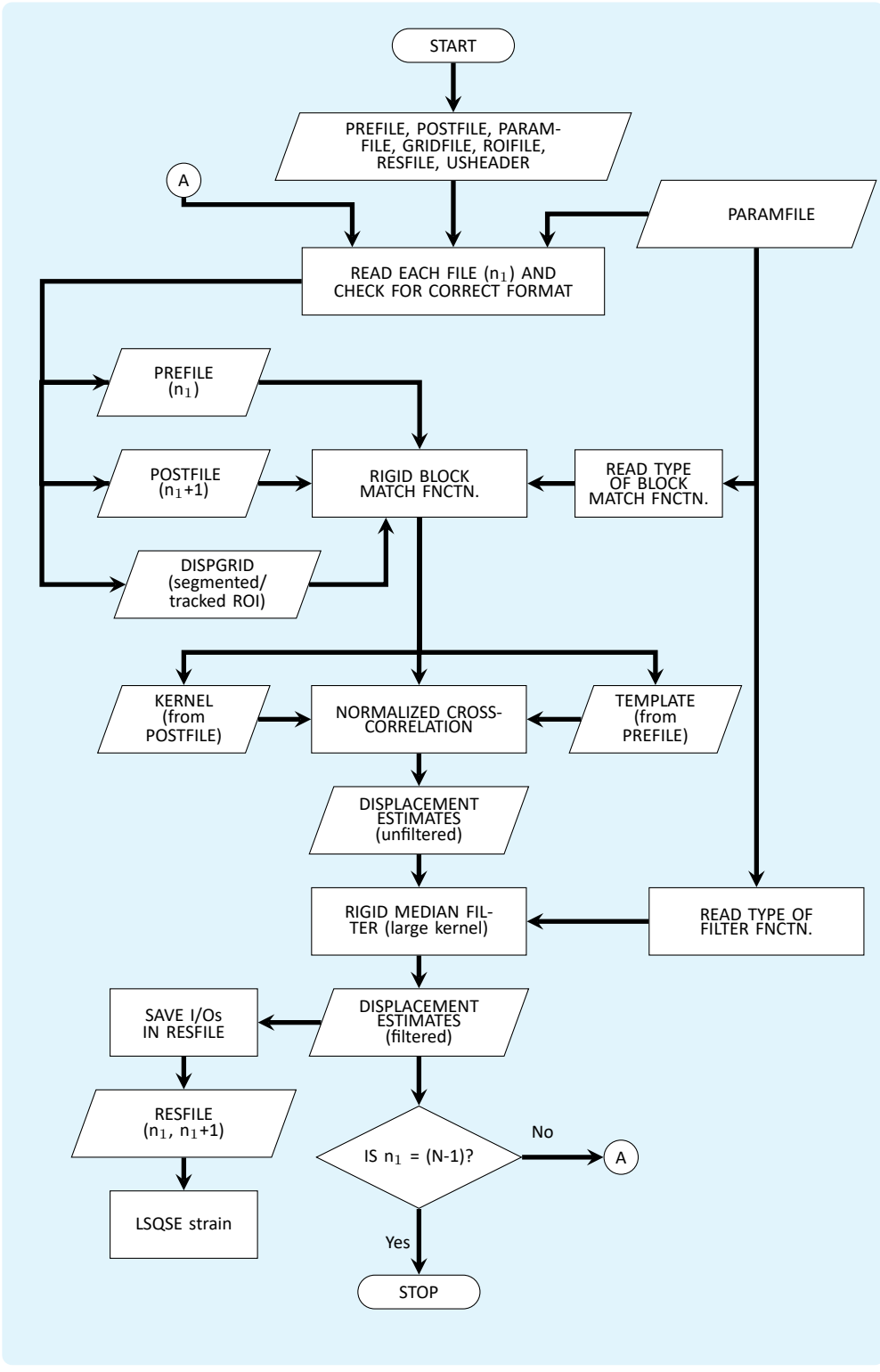
START
PREFILE, POSTFILE, PARAM-FILE, GRIDFILE, ROIFILE, RESFILE, USHEADER
A
PARAMFILE
READ EACH FILE (n_1) AND CHECK FOR CORRECT FORMAT
PREFILE (n_1)
POSTFILE (n_1+1)
RIGID BLOCK MATCH FNCTN.
READ TYPE OF BLOCK MATCH FNCTN.
DISPGRID (segmented/ tracked ROI)
KERNEL (from POSTFILE)
NORMALIZED CROSS-CORRELATION
TEMPLATE (from PREFILE)
DISPLACEMENT ESTIMATES (unfiltered)
RIGID MEDIAN FIL-TER (large kernel)
READ TYPE OF FILTER FNCTN.
SAVE I/Os IN RESFILE
DISPLACEMENT ESTIMATES (filtered)
RESFILE (n_1, n_1+1)
IS n_1 = (N-1)?
No
A
LSQSE strain
Yes
STOP

Appendix C

Least Squared Strain Estimator (LSQSE)

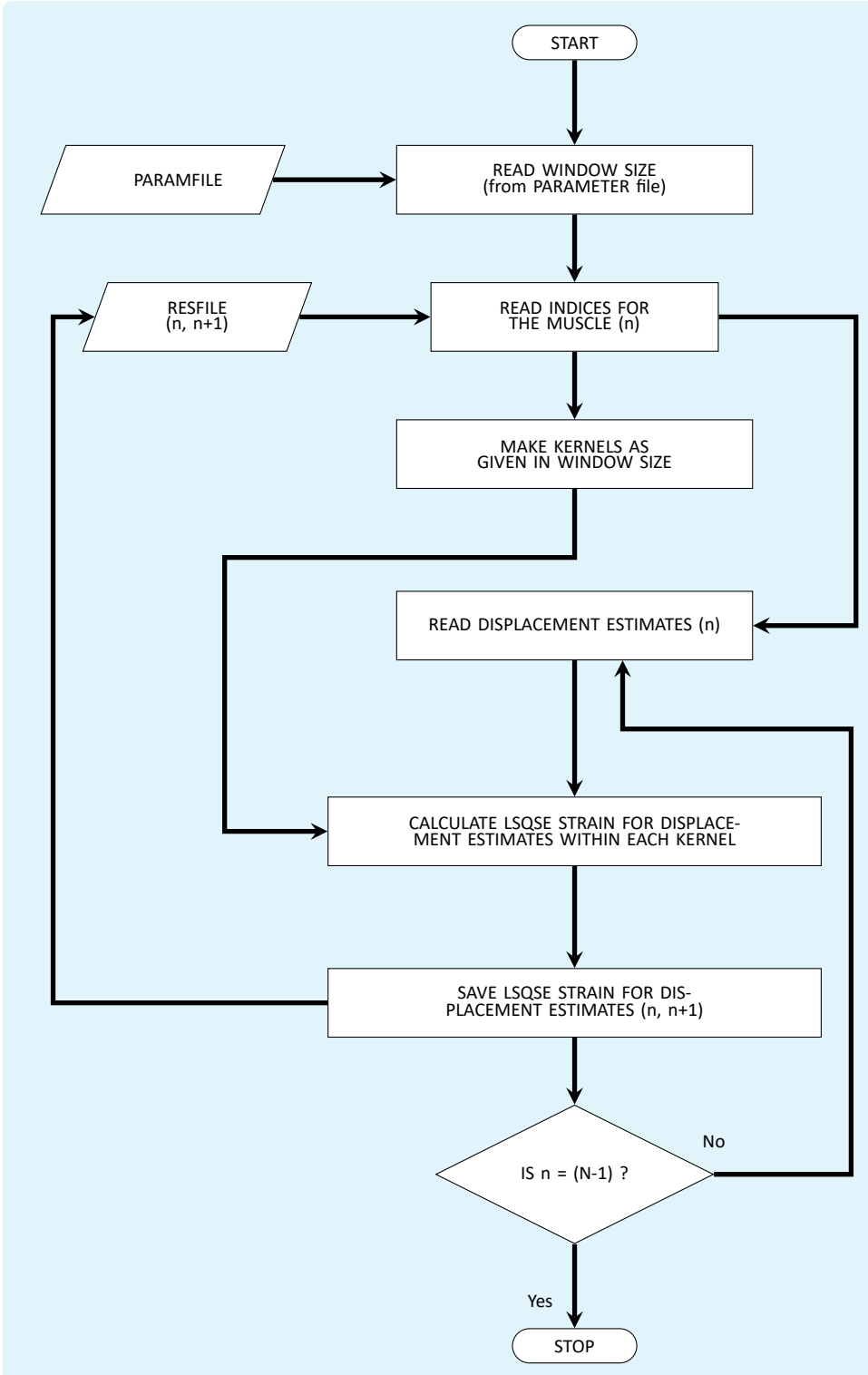
START
PARAMFILE
READ WINDOW SIZE
(from PARAMETER file)
RESFILE
(n, n+1)
READ INDICES FOR
THE MUSCLE (n)
MAKE KERNELS AS
GIVEN IN WINDOW SIZE
READ DISPLACEMENT ESTIMATES (n)
CALCULATE LSQSE STRAIN FOR DISPLACE-
MENT ESTIMATES WITHIN EACH KERNEL
SAVE LSQSE STRAIN FOR DIS-
PLACEMENT ESTIMATES (n, n+1)
IS n = (N-1) ?
No
Yes
STOP

Appendix D

Tracking
(upgrade to the ’strainMUSIC’ algorithm)

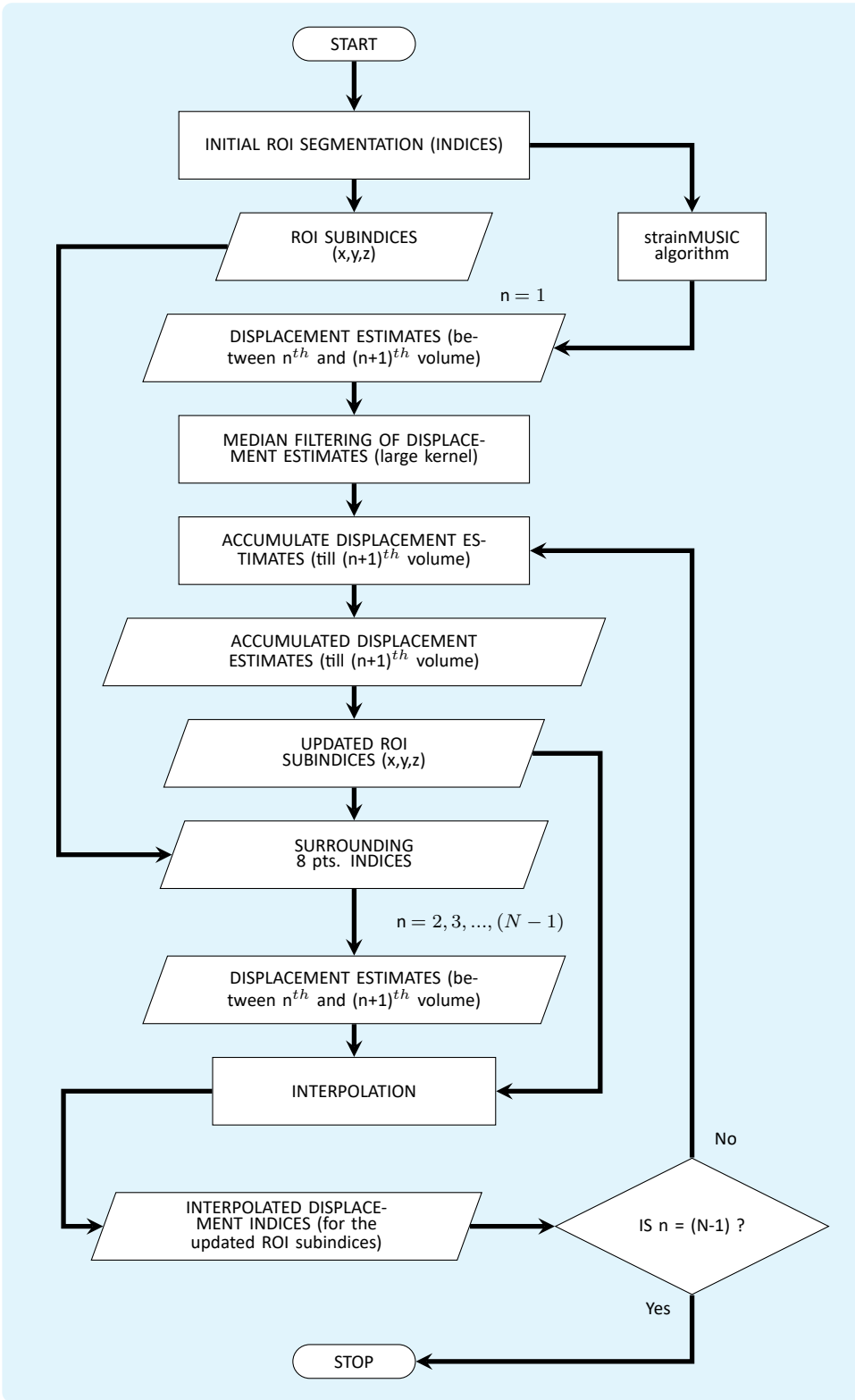
START
INITIAL ROI SEGMENTATION (INDICES)
ROI SUBINDICES (x,y,z)
strainMUSIC algorithm
n = 1
DISPLACEMENT ESTIMATES (between nth and (n+1)th volume)
MEDIAN FILTERING OF DISPLACEMENT ESTIMATES (large kernel)
ACCUMULATE DISPLACEMENT ESTIMATES (till (n+1)th volume)
ACCUMULATED DISPLACEMENT ESTIMATES (till (n+1)th volume)
UPDATED ROI SUBINDICES (x,y,z)
SURROUNDING 8 pts. INDICES
n = 2, 3, ..., (N − 1)
DISPLACEMENT ESTIMATES (between nth and (n+1)th volume)
INTERPOLATION
INTERPOLATED DISPLACEMENT INDICES (for the updated ROI subindices)
IS n = (N-1) ?
No
Yes
STOP

Appendix E

Filtering and principal strain

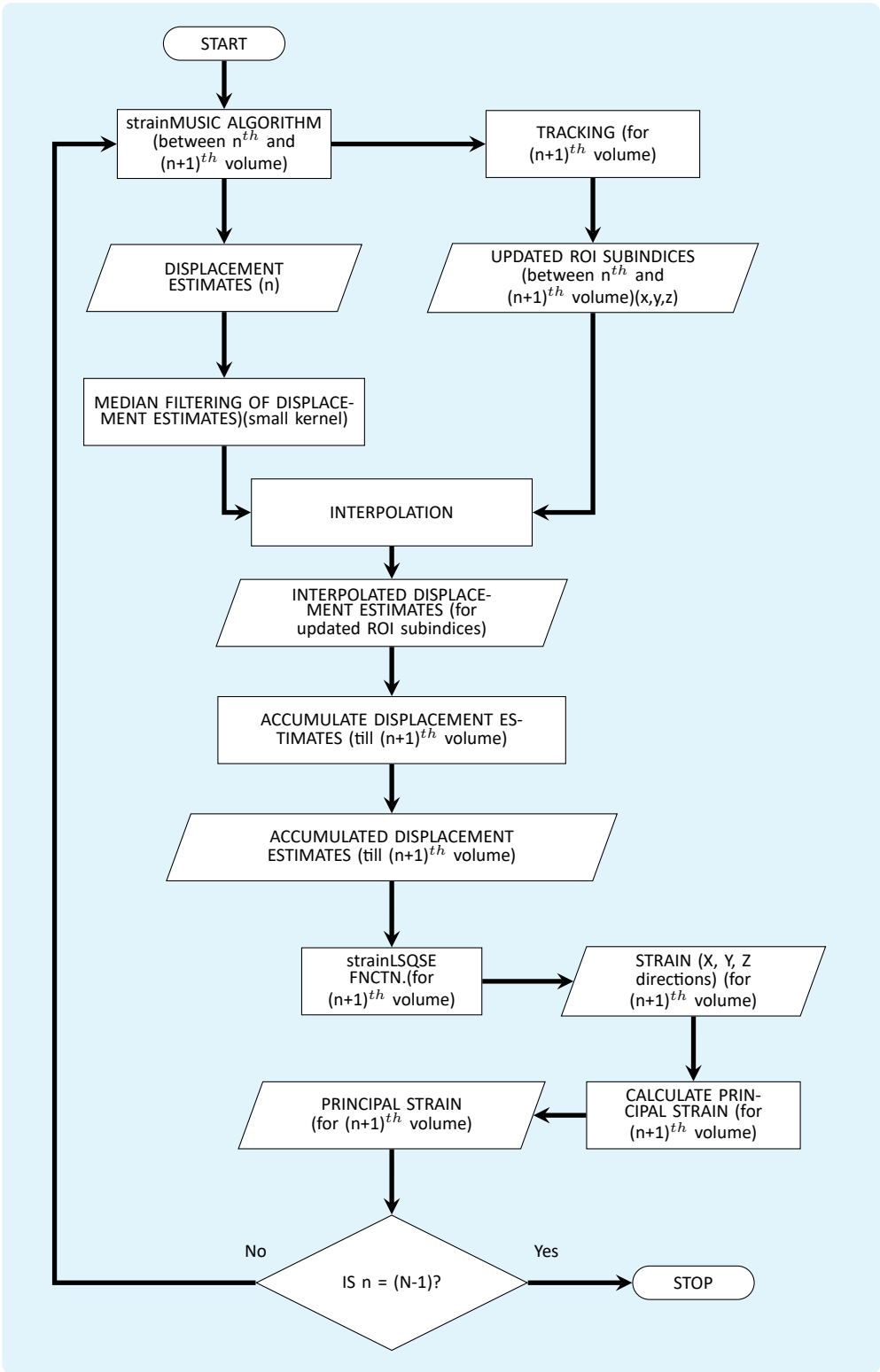
START
strainMUSIC ALGORITHM (between nth and (n+1)th volume)
TRACKING (for (n+1)th volume)
DISPLACEMENT ESTIMATES (n)
UPDATED ROI SUBINDICES (between nth and (n+1)th volume)(x,y,z)
MEDIAN FILTERING OF DISPLACEMENT ESTIMATES)(small kernel)
INTERPOLATION
INTERPOLATED DISPLACEMENT ESTIMATES (for updated ROI subindices)
ACCUMULATE DISPLACEMENT ESTIMATES (till (n+1)th volume)
ACCUMULATED DISPLACEMENT ESTIMATES (till (n+1)th volume)
strainLSQSE FNCTN.(for (n+1)th volume)
STRAIN (X, Y, Z directions) (for (n+1)th volume)
CALCULATE PRINCIPAL STRAIN (for (n+1)th volume)
PRINCIPAL STRAIN (for (n+1)th volume)
No
IS n = (N-1)?
Yes
STOP

Appendix F

Displacement estimation (along muscle fibre direction)

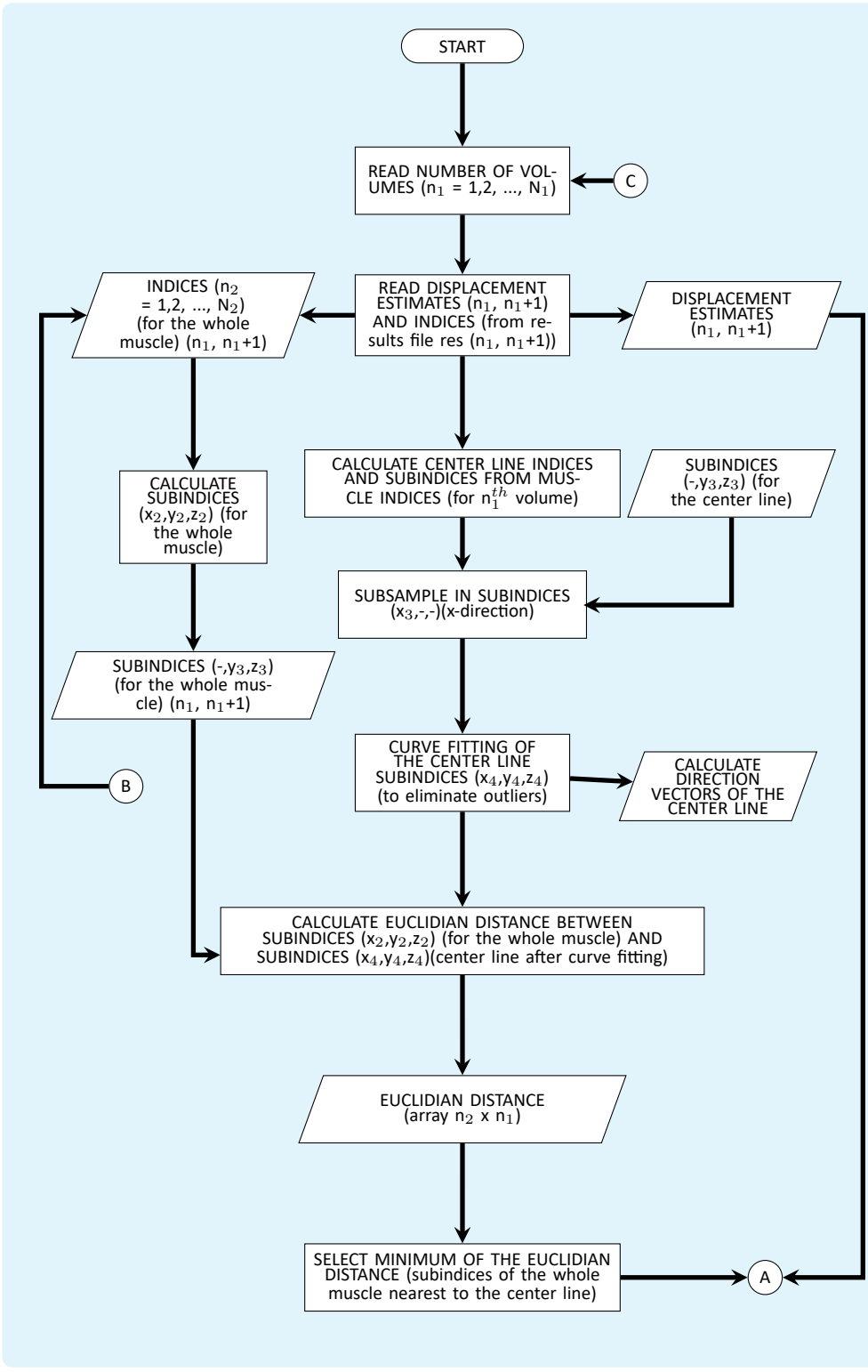
START
READ NUMBER OF VOLUMES (n_1 = 1,2, ..., N_1)
C
READ DISPLACEMENT ESTIMATES (n_1, n_1+1) AND INDICES (from results file res (n_1, n_1+1))
INDICES (n_2 = 1,2, ..., N_2) (for the whole muscle) (n_1, n_1+1)
DISPLACEMENT ESTIMATES (n_1, n_1+1)
CALCULATE SUBINDICES (x_2,y_2,z_2) (for the whole muscle)
CALCULATE CENTER LINE INDICES AND SUBINDICES FROM MUSCLE INDICES (for n_1^{th} volume)
SUBINDICES (-,y_3,z_3) (for the center line)
SUBSAMPLE IN SUBINDICES (x_3,-,-)(x-direction)
SUBINDICES (-,y_3,z_3) (for the whole muscle) (n_1, n_1+1)
CURVE FITTING OF THE CENTER LINE SUBINDICES (x_4,y_4,z_4) (to eliminate outliers)
CALCULATE DIRECTION VECTORS OF THE CENTER LINE
B
CALCULATE EUCLIDIAN DISTANCE BETWEEN SUBINDICES (x_2,y_2,z_2) (for the whole muscle) AND SUBINDICES (x_4,y_4,z_4)(center line after curve fitting)
EUCLIDIAN DISTANCE (array n_2 x n_1)
SELECT MINIMUM OF THE EUCLIDIAN DISTANCE (subindices of the whole muscle nearest to the center line)
A

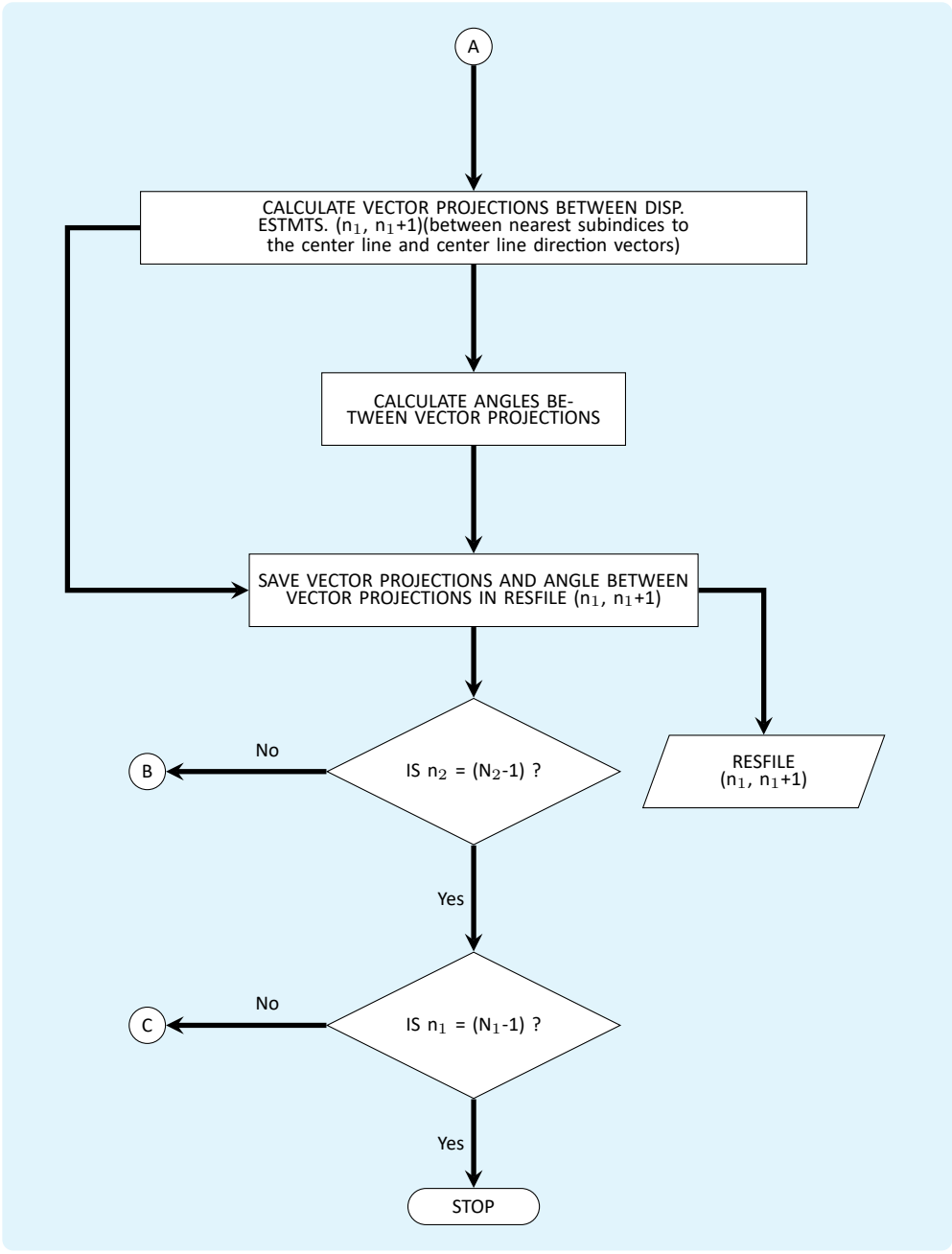
A
CALCULATE VECTOR PROJECTIONS BETWEEN DISP. ESTMTS. (n_1, n_1+1)(between nearest subindices to the center line and center line direction vectors)
CALCULATE ANGLES BE-TWEEN VECTOR PROJECTIONS
SAVE VECTOR PROJECTIONS AND ANGLE BETWEEN VECTOR PROJECTIONS IN RESFILE (n_1, n_1+1)
RESFILE (n_1, n_1+1)
IS n_2 = (N_2-1) ?
No
B
Yes
IS n_1 = (N_1-1) ?
No
C
Yes
STOP

Appendix G

Strain calculations (along muscle fibre direction)

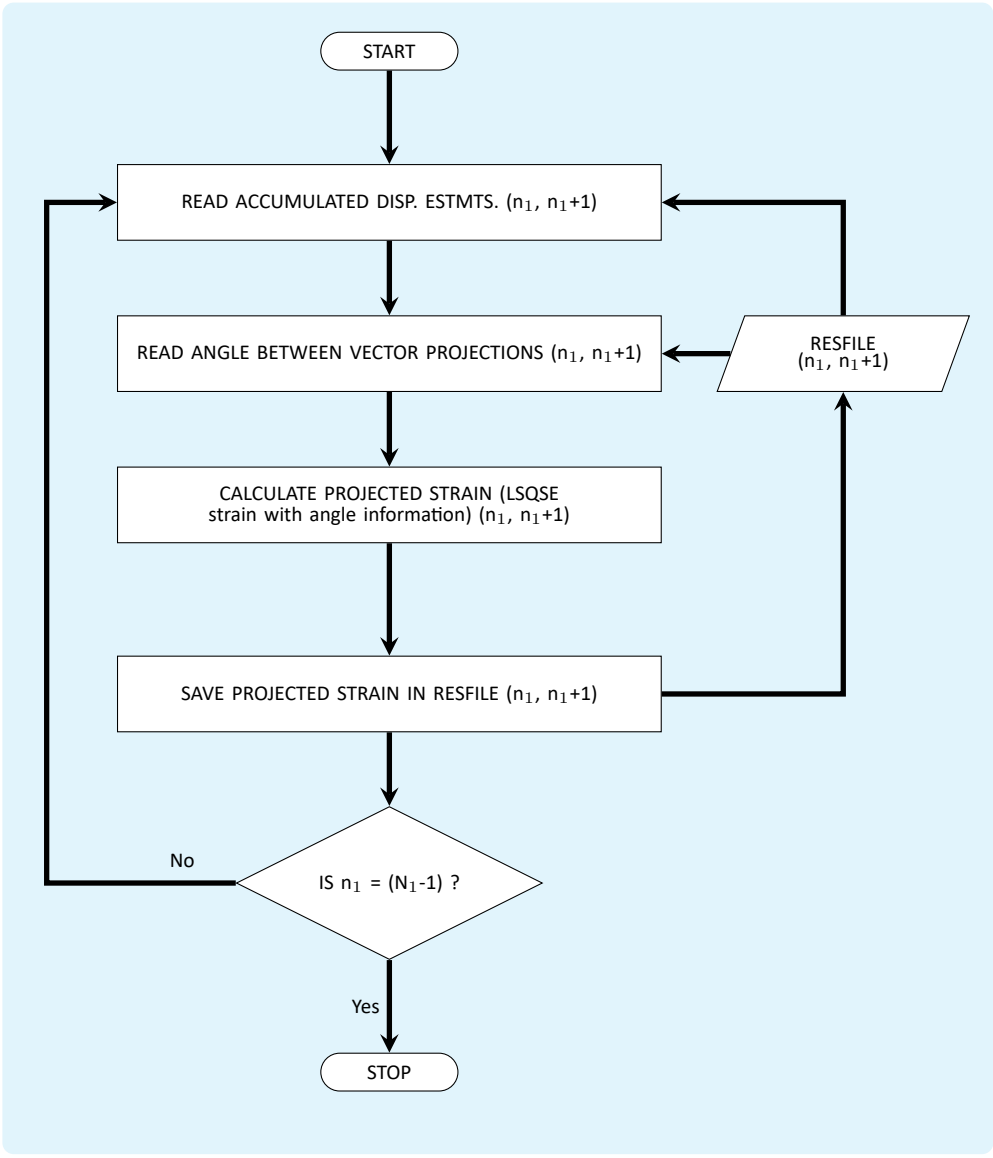
START
READ ACCUMULATED DISP. ESTMTS. (n_1, n_1+1)
READ ANGLE BETWEEN VECTOR PROJECTIONS (n_1, n_1+1)
RESFILE (n_1, n_1+1)
CALCULATE PROJECTED STRAIN (LSQSE strain with angle information) (n_1, n_1+1)
SAVE PROJECTED STRAIN IN RESFILE (n_1, n_1+1)
No
IS n_1 = (N_1-1) ?
Yes
STOP

Appendix H

Calculations for tissue characterization

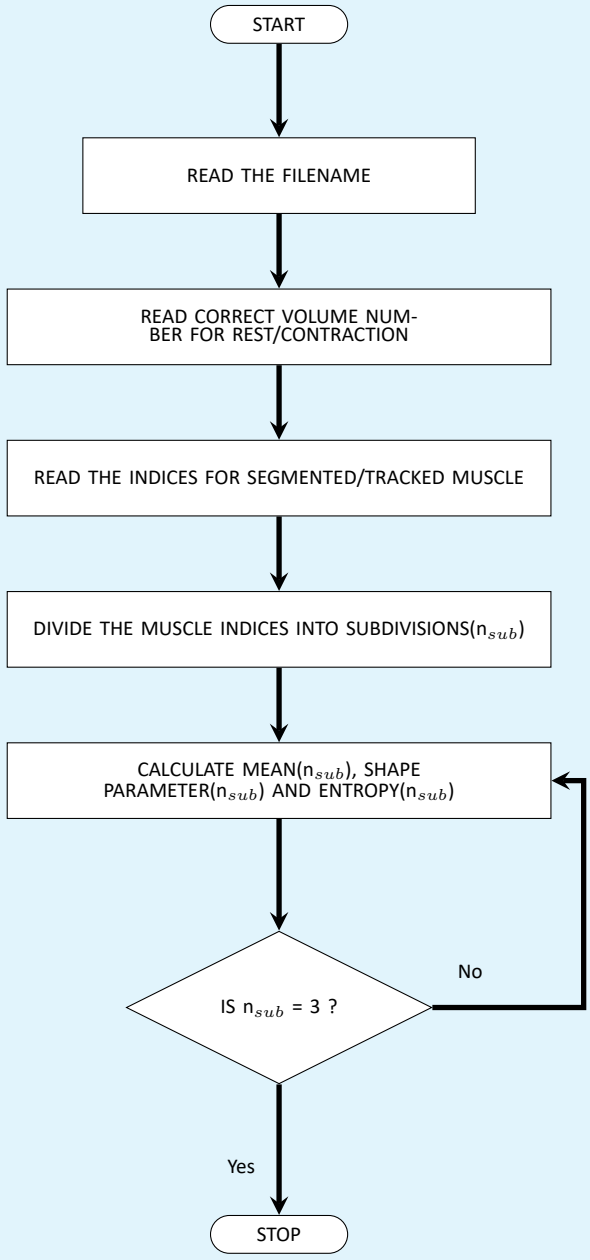
START
READ THE FILENAME
READ CORRECT VOLUME NUM-
BER FOR REST/CONTRACTION
READ THE INDICES FOR SEGMENTED/TRACKED MUSCLE
DIVIDE THE MUSCLE INDICES INTO SUBDIVISIONS(n_{sub})
CALCULATE MEAN(n_{sub}), SHAPE
PARAMETER(n_{sub}) AND ENTROPY(n_{sub})
IS n_{sub} = 3 ?
No
Yes
STOP

List of Figures

Figure 1.1 Sagittal view of the pelvic organs after removal of the bladder and rectum showing the anterior and posterior compartments separated by the uterus and vagina (deLancey book) **[6]** 15

Figure 1.2 A schematic view of the levator ani muscles (LAM) from below after the vulvar structures and perineal membrane have been removed showing the urethra (U), vagina (V), external anal sphincter (EAS), puboanal muscle (PAM), perineal body (PB) uniting the two ends of the puboperineal muscle (PPM), iliococcygeal muscle (ICM) and puborectal muscle (PRM) **[6]** 16

Figure 1.3 Female pelvic floor (PF) anatomy showing the surrounding pelvic bones and the levator ani muscle (LAM) forming the pelvic diaphragm. The puborectalis muscle (PRM) is highlighted in green **[**Kenhub (www.kenhub.com), illustrator: L. Znotina] 17

Figure 1.4 Pelvic floor (PF) anatomy and puborectalis muscle (PRM) as observed in transperineal ultrasound (US) data in sagittal view (z-y plane in US grid) (a) B-mode US image, (b) B-mode US image with labeling of the important PF organs, (c) Outline of the B-mode US in sagittal view with labeling of the PF organs **[10, 57]** 23

Figure 1.5 Transperineal ultrasound (US) data of the pelvic floor (puborectalis muscle in yellow) in; (a) axial view (z-x plane in US grid), (b) coronal view (y-x plane in US grid) **[57]** 24

Figure 1.6 Rectus femoris showing partial tears (arrowheads) and a small hematoma (arrows). Permission has been granted by the publisher to use this image **[69]** 28

Figure 2.1 Block diagram of the processing steps involved to obtain 3D strain output from the 3D ultrasound data sequence (PRM = puborectalis muscle; ROI = region of interest) 42

Figure 2.2 Visual explanation of the temporary surrounding eight-point grid; (a) Part of the ultrasound grid, where the circled corners represent the positions or indices forming part of the region of interest (black circles), (b) Changes in positions of the indexes when updated by accumulated z, x and y displacement estimates to positions that are out of grid (gray circles), (c) One example of surrounding eight points in the ultrasound grid (blue circles) to follow a certain updated out of grid position or index (gray circle) 44

Figure 2.3 Puborectalis muscle (PRM) as observed in transperineal ultrasound (US) data in sagittal view (z-y plane in US grid) (a) B-mode US image, showing PRM at rest in yellow (b) B-mode US image, showing PRM at max. contraction in yellow and the position at rest in dark gray (c) B-mode US image, showing PRM at Valsalva maneuver in yellow and the position at rest in dark gray . . . 45

Figure 2.4 Accumulated displacement estimates at three time points during the rest-contraction-rest sequence of volunteer 1; (a-c) Accumulated z-direction displacement estimates, (d-f) Accumulated x-direction displacement estimates, (g-i) Accumulated y-direction displacement estimates) 49

Figure 2.5 Accumulated displacement estimates at two time points during the rest-Valsalva maneuver sequence of volunteer 4; (a-c) Accumulated z-direction displacement estimates, (d-f) Accumulated x-direction displacement estimates, (g-i) Accumulated y-direction displacement estimates 50

Figure 2.6 Accumulated principal strain (%) magnitudes (first row) and their respective directions (second row) for volunteer 1 (US = ultrasound) 51

Figure 2.7 Accumulated principal strain (%) magnitudes (first row) and their respective directions (second row) for volunteer 4 (US = ultrasound; Val. Man. = Valsalva maneuver) 52

Figure 2.8 Deformation of the puborectalis muscle (PRM) at contracted state (red) when compared with the rest state (blue) for volunteer 1; (a) The undeformed PRM at rest state in the ultrasound grid, (b) Deformation of the PRM in z-y plane, (c) Deformation of PRM in y-x plane, (d) Deformation of PRM in z-x plane (US = ultrasound) . . 55

Figure 2.9 Deformation of the puborectalis muscle (PRM) at Valsalva maneuver state (green) compared with the rest state (blue) for volunteer 4; (a) The undeformed PRM in rest state in the ultrasound (US) grid, (b) Deformation of PRM in z-y plane, (c) Deformation of PRM in y-x plane, (d) Deformation of PRM in z-x plane 56

Figure S2.1 Accumulated displacement estimates at three time points during the rest-contraction-rest sequence of volunteer 2; (a-c) Accumulated z-direction displacement estimates, (d-f) Accumulated x-direction displacement estimates, (g-i) Accumulated y-direction displacement estimates) 61

Figure S2.2 Accumulated principal strain (%) magnitudes (first row) and their respective directions (second row) for volunteer 2 (US = ultrasound) 62

Figure S2.3 Accumulated displacement estimates at three time points during the rest-contraction-rest sequence of volunteer 3; (a-c) Accumulated z-direction displacement estimates, (d-f) Accumulated x-direction displacement estimates, (g-i) Accumulated y-direction displacement estimates) 63

Figure S2.4 Accumulated principal strain (%) magnitudes (first row) and their respective directions (second row) for volunteer 3 (US = ultrasound) 64

Figure S2.5 Accumulated displacement estimates at three time points during the rest-contraction-rest sequence of volunteer 4; (a-c) Accumulated z-direction displacement estimates, (d-f) Accumulated x-direction displacement estimates, (g-i) Accumulated y-direction displacement estimates) 65

Figure S2.6 Accumulated principal strain (%) magnitudes (first row) and their respective directions (second row) for volunteer 4 (US = ultrasound) 66

Figure 3.1 Block diagram 1; the blocks in white have been explained in our previous publication **[1]** (The blocks in grey with bold letters have been explained in the current section) 70

Figure 3.2 (a) Pelvic floor anatomy showing PRM **[2]** (Permission granted by the publisher to use this image), (b) MR tractography showing the muscle fiber orientation of the PRM and the puborectal sling **[3]** (Permission granted by the publisher to use this image) 71

Figure 3.3 An example of a segmented PRM (in 3D), showing the center line through it and center line after curve fitting and scaling (Steps 1-3). The last figure shows the displacement estimates projected on the center line . . . 72

Figure 3.4 Three regions (shown in XZ plane, axial view) within the PRM with the right, left (blue) and mid regions (yellow) labeled; (a) example showing intact PRM, (b) example showing PRM with unilateral avulsion 73

Figure 3.5 Percentage of strain at maximum contraction (shown in 3D) in two women with; (a) intact PRM, (b) unilateral avulsion of PRM (The avulsed and intact ends of the avulsed PRM are labeled. X, Y and Z axes are in meter and the color bars show percentage of strain from negative (dark red) to positive (yellow)) 77

Figure 3.6 Boxplots showing normalized strain ratio for women with intact PRMs and women with unilateral avulsion . 78

Figure S3.1 Percentage of strain at maximum contraction (shown in 3D) in two women with intact PRMs. X, Y and Z axes are in meter and the color bars show percentage of strain from negative (dark red) to positive (yellow) 84

Figure S3.2 Percentage of strain at maximum contraction (shown in 3D) in two women with intact PRMs. X, Y and Z axes are in meter and the color bars show percentage of strain from negative (dark red) to positive (yellow) 85

Figure S3.3 Percentage of strain at maximum contraction (shown in 3D) in two women with intact PRMs. X, Y and Z axes are in meter and the color bars show percentage of strain from negative (dark red) to positive (yellow) 86

Figure S3.4 Percentage of strain at maximum contraction (shown in 3D) in two women with unilateral avulsion of PRMs. X, Y and Z axes are in meter and the color bars show percentage of strain from negative (dark red) to positive (yellow) 87

Figure S3.5 Percentage of strain at maximum contraction (shown in 3D) in two women with unilateral avulsion of PRMs. X, Y and Z axes are in meter and the color bars show percentage of strain from negative (dark red) to positive (yellow) 88

Figure S3.6 Percentage of strain at maximum contraction (shown in 3D) in two women with unilateral avulsion of PRMs. X, Y and Z axes are in meter and the color bars show percentage of strain from negative (dark red) to positive (yellow) 89

Figure S3.7 Percentage of strain at maximum contraction (shown in 3D) in two women with unilateral avulsion of PRMs. X, Y and Z axes are in meter and the color bars show percentage of strain from negative (dark red) to positive (yellow) 90

Figure S3.8 Percentage of strain at maximum contraction (shown in 3D) in one woman with unilateral avulsion of PRMs. X, Y and Z axes are in meter and the color bars show percentage of strain from negative (dark red) to positive (yellow) 91

Figure 4.1 (a) Projected strain in intact PRM (b) Three regions (shown in XZ plane, axial view) within the PRM with right, left (blue) and mid (yellow) labeled, example showing intact PRM, (c) example showing unilateral avulsion, (d) example showing bilateral avulsion 100

Figure 4.2 Strain in unilateral avulsion of PRM, at maximum voluntary contraction (a) Before pessary fitting (b) After pessary fitting (to be changed to 3D images) 101

Figure 4.3 Strain in bilateral avulsion of PRM, at maximum voluntary contraction (a) Before pessary fitting (b) After pessary fitting (to be changed to 3D images) 102

Figure 4.4 Boxplots showing normalized strain ratios for women with (a) PRMs of women with avulsion before and after pessary fitting and women with avulsion after pessary fitting (b) Change of normalized strain ratio in women with avulsion, from before pessary (BP) to after pessary (AP) 103

Figure S4.1 Strain in unilateral avulsion of PRMs, at maximum voluntary contraction for two women (a) Before pessary fitting (b) After pessary fitting 112

Figure S4.2 Strain in unilateral avulsion of PRMs, at maximum voluntary contraction for two women (a) Before pessary fitting (b) After pessary fitting 113

Figure S4.3 Strain in unilateral avulsion of PRMs, at maximum voluntary contraction for two women (a) Before pessary fitting (b) After pessary fitting 114

Figure S4.4 Strain in unilateral avulsion of PRMs, at maximum voluntary contraction for two women (a) Before pessary fitting (b) After pessary fitting 115

Figure S4.5 Strain in unilateral avulsion of PRMs, at maximum voluntary contraction for two women (a) Before pessary fitting (b) After pessary fitting 116

Figure S4.6 Strain in unilateral avulsion of PRMs, at maximum voluntary contraction for two women (a) Before pessary fitting (b) After pessary fitting 117

Figure S4.7 Strain in unilateral avulsion of PRMs, at maximum voluntary contraction for two women (a) Before pessary fitting (b) After pessary fitting 118

Figure 5.1 Three dimensional volume of segmented puborectalis muscle at rest 122

Figure 5.2 Process of division of the puborectalis muscle (PRM) into sub-regions of interest (ROI = region of interest) . 124

Figure 5.3 (a) Subregions of interest of puborectalis muscle after division, (b) Two subregions nearest the insertion points at the pubic bone (US = ultrasound) 124

Figure 5.4 Mean echogenicity, entropy and shape parameter values for the puborectalis muscle without avulsion and with unilateral avulsion, at rest (top row) and in contraction (bottom row) 130

Figure 5.5 Receiver operating characteristic (ROC) curves for mean echogenicity, entropy and shape parameters when puborectalis muscles were at rest (top row) and in contraction (bottom row). Here the blue area represents the area under the ROC (AROC), and the red points represent the discrete values 131

Figure 5.6 Visual representation of the shape parameter change for (a) an undamaged, (b) a damaged puborectalis muscle (PRM) at rest (US = ultrasound) 133

Figure S5.1 Visual representation of the shape parameter change for two undamaged puborectalis muscles (PRMs) at rest (US = ultrasound) 141

Figure S5.2 Visual representation of the shape parameter change for two undamaged puborectalis muscles (PRMs) at rest (US = ultrasound) 142

Figure S5.3 Visual representation of the shape parameter change for two undamaged puborectalis muscles (PRMs) at rest (US = ultrasound) 143

Figure S5.4 Visual representation of the shape parameter change for (a) an undamaged, (b) a damaged puborectalis muscle (PRM) at rest (US = ultrasound) 144

Figure S5.5 Visual representation of the shape parameter change for (a) an undamaged, (b) a damaged puborectalis muscle (PRM) at rest (US = ultrasound) 145

Figure S5.6 Visual representation of the shape parameter change for (a) an undamaged, (b) a damaged puborectalis muscle (PRM) at rest (US = ultrasound) 146

List of Tables

Table 2.1 Demographic information about all the inclusions . . . 47

Table 2.2 Mean principal strain values of the four volunteers included in the study 53

Table 3.1 Demographic information about all the inclusions . . . 76

Table 4.1 Demographic information about all the inclusions for effect of pessary 99

Table 5.1 Demographic information about all the inclusions for tissue characterization 129

Table 5.2 Summarized values for the three parameters at rest and contraction 132

List of Publications

Peer-reviewed journal articles

[1] **S. Das**, G. A. G. M. Hendriks, F. van den Noort, C. Manzini, C. H. van der Vaart & C. L. de Korte, **3D ultrasound strain imaging of puborectal muscle with and without unilateral avulsion**. *International urogynecology journal*, vol. 34, no. 9, pp. 2225-2233, 2023.
DOI: https://doi.org/10.1007/s00192-023-05498-1

[2] C. Cernat*, **S. Das***, G. A. G. M. Hendriks, F. van den Noort, C. Manzini, C. H. van der Vaart & C. L. de Korte, **Tissue characterization of puborectalis muscle from 3D ultrasound**. *Ultrasound in medicine and biology*, vol. 49, no. 2, pp. 527-538, 2022.
DOI: https://doi.org/10.1016/j.ultrasmedbio.2022.10.003

* The first and second authors have equal contribution.

[3] **S. Das**, H. H. G. Hansen, G. A. G. M. Hendriks, F. van den Noort, C. Manzini, C. H. van der Vaart & C. L. de Korte, **3D ultrasound strain imaging of puborectalis muscle**. *Ultrasound in medicine and biology*, vol. 47, no. 3, pp. 569-581, 2021.
DOI: https://doi.org/10.1016/j.ultrasmedbio.2020.11.016

Article submitted for publication

[1] **S. Das**, G. A. G. M. Hendriks, F. van den Noort, C. Manzini, C. H. van der Vaart & C. L. de Korte, **Effect of a ring pessary on avulsed puborectal muscle through ultrasound strain imaging**

Conference publications

[1] Dutch Biomedical Engineering **(BME)** conference - January 2023
Poster acceptance
(https://www.bme2023.nl)

[2] IEEE International Ultrasound **(IEEE IUS)** conference - September 2021
Poster presentation
(https://2021.ieee-ius.org)

[3] International Uro-Gynecological Annual Meeting **(IUGA)** - August 2020
Poster acceptance
(https://www.iuga.org/events/annual-meetings/2020-iuga-45th-annual-meeting)

[4] IEEE International Ultrasound **(IEEE IUS)** conference - September 2020
Poster presentation
(https://2020.ieee-ius.org)

[5] Dutch Biomedical Engineering **(BME)** conference - January 2019
Oral presentation
(https://www.bme2019.nl)

[6] International Tissue Elasticity Conference **(ITEC)** - September 2018
Oral presentation

Data management

The data obtained during my PhD at the Radboud university medical center have been captured and stored on a local server. The most relevant data was additionally backed up on university servers belonging to the department. All data archives are accessible by the associated staff members from the group. Published data generated or analyzed in this thesis are part of published articles and its additional files are available from the associated corresponding authors on request. To ensure interpretability of the data, all filenames, primary and secondary data, metadata, descriptive files and program code and scripts used to provide the final results are documented along with the data.

PhD portfolio

PhD portfolio of Shreya Das

Department: **Department of Medical Imaging**
PhD period: **01/01/2018 – 31/12/2022**
PhD Supervisor(s): **Prof. C.L. de Korte, Prof. C.H. van der Vaart**
PhD Co-supervisor(s): **Dr. G.A.G.M. Hendriks**

Training activities	Hours
Courses	
- RU - Digital Tools (2018)	4.00
- IMM - The Art of Presenting Science (2018)	33.00
- RIHS - Introduction course for PhD candidates (2018)	15.00
- Radboudumc - Scientific integrity (2019)	20.00
- RU - Scientific Writing for PhD candidates (2019)	84.00
Conferences	
- International Tissue Elasticity Conference (ITEC) (2018) - oral presentation	33.00
- 7th Dutch conference on Biomedical Engineering (2019) - oral presentation	33.00
- IUGA - International Urogynecological Association 45th annual meeting (2020) - e-poster	4.00
- IEEE International Ultrasonics Symposium (2020) - e-poster presentation	33.00
- IEEE International Ultrasonics Symposium (2021) - e-poster presentation	33.00
Other	
- Meet the PhD program (2020)	33.00
- Meet the PhD program (2021)	33.00
- Weekly MUSIC research meetings (2022)	84.00
- Bi-annual GYNIUS user committee meetings (2022)	84.00
- Weekly Radiology meetings (2023)	84.00
Teaching activities	
Supervision of internships / other	
- Supervision of Master student for Master thesis (2021)	84.00
- Supervision of Master student for internship (2022)	84.00
Total	**778.00**

Acknowledgements

There are so many people that I need to thank that I believe it is difficult not to write another twenty pages or so, just for this chapter. Nonetheless, I will try to make it not too long.

First and foremost, I would like to thank my parents for their lifelong support that they have provided me without asking for anything in return. My mother have taught me to be resilient and focus on my work irrespective of anything else going on otherwise. She taught me this by being a great example herself. My father taught me to be stoic and that no achievements or failures are to be dwelt upon. He showed me that achievements are only moments for humility and failures are moments for learning lessons. Nothing less and nothing more. And needless to mention, my father has been the greatest stoic that I have ever seen. It would be always a regret for me, that I could not show this thesis to him as he passed away before I could finish writing.

Guido, my beloved and partner to be, has been incredibly patient with me throughout these six years. I have complained to him a lot about stress, being not productive, long hours and what not. He has been like a rock of support, who has always led me gently to being functional again. I would like to thank him deeply for lending a helping hand whenever I needed. And of course, he took care of our little daughter Siya on countless times when I needed to work late.

I would also like to thank Gerda and Hans, Guido's parents who have helped me numerous times when I needed a friendly advice or a day out to clear my mind. They have helped me sometimes even before I had asked for help.

My oldest and closest friend Pooja deserves special thanks. We have been friends since we were four years old. We grew up together in Kolkata. During these six years, she made me believe in myself when sometimes I could not myself. Even though she lives far away in America, distance did not come in between us.

I had met Renate and Hans-Jörg Märtens during my years as a student in Halle (Saale), Germany. I would like to thank them for being like my parents while my own parents were on a different continent altogether. It has been in-

credibly fortunate of me to have been under their care when I needed to rest and recover before I came to the Netherlands. Also I could not have practiced my German without their constant supervision, help and friendly advice. Not only that, during these five years they have always lifted my spirits up with wonderful letters and postcards. Thanks to them, I did not miss out on the 'old-world' charm of receiving beautifully handwritten letters.

My colleagues, Joosje and Judith deserve special mention. They have been more friends than colleagues to me, with always a friendly smile or a patient hearing when I just needed to talk to a friend. Anne, has been another friend and colleague who has reassured me whenever I had doubts. I have known Sofia only for about a year since she has joined the group. But she has already been a good friend. We could share our feelings about being in a foreign land and trying to make it our homes. Janna and Brigitte have been colleagues with whom I have enjoyed conversations about Dutch culture among other things.

Rik and Gijs have been my supervisors. But I would like to thank them for being more than supervisors with many useful discussions about the work as well as our personal lives.

I have to also mention my former colleagues, Chuan and Anton. Both of them have been good friends to me with their useful suggestions for my work. Especially, Anton and I even worked together at his place during Covid times when the hospital was closed for researchers. I would like to thank them both for being with me, during the long hours when we worked together.

I would like to specially thank Remy, for the valuable discussions we had about statistics among numerous other matters.

Stein, Kai, Roel, Leon and Thomas have been former colleagues. We have had great fun during MUSIC group events as well as conferences. I appreciate having got to know them and work with them.

The GYNIUS project, which this PhD is a part of, started with Prof. Huub van der Vaart, Chris and their colleagues writing the project proposal. I would not have this opportunity at all, without him and his work. I would like to thank him for starting the project and also for answering numerous clinical questions that

I had asked him. Claudia and Frieda have been the two other PhD students who were also part of GYNIUS project. Both of them deserve thanks from me, for always helping me with useful feedbacks about our research articles.

Lastly, and definitely not the least, I would like to give my heartfelt thanks and gratitude to Chris for his incredible amount of motivation and help in every step of the work. Before being in his research group, I could have never imagined how much a mentor he is both professionally as well as personally. He has shown his care with many friendly and frank discussions, suggestions about my work as well as about my personal life. I remember that he was even concerned about my well-being when I visited my parents in Kolkata, India. This was before my daughter Siya was born. And I had mentioned to him of me being unsure how my parents would take the news of Siya.

Speaking of Siya, although she is too young to understand this yet, but in her own sweet way she has motivated me to complete my work. She is only four years old, but I am very proud of her already. It is my hope and wish that when she is old enough to read and understand this work, it would be something to inspire her.

I believe I could in effect compress my thoughts in these few words about all the people that I wanted to thank.

About the author

Shreya Das was born on July 14^{th}, 1986 in Kolkata, India. She completed her primary, middle and secondary school education from Kolkata as well. Thereafter, Shreya has studied Electronics and Instrumentation Engineering in her Bachelors from India, completed in 2009. She passed Graduate Aptitude Test for Engineers (GATE 2010) and started her Masters as a GATE scholar receiving full scholarship for two years. Her first Master study was in Biomedical Engineering from Jadavpur University, Kolkata, India. Her Master thesis was signal processing and feature extraction from electrocardiograms, which was completed in 2012. She joined Philips India Ltd. as a Biomedical Service Engineer in 2012, and worked there till 2015. In late 2015, Shreya moved to Germany for further studies. Two years later in 2017, she completed her second Master also in Biomedical Engineering from Martin Luther University of Halle-Wittenberg, Germany. She was fortunate to receive the STIBET I scholarship from German Academic Exchange Service (DAAD) during the time of her thesis. Her Master thesis was about developing a low cost pulse oximetry device for rural areas using a single-board computer (Raspberry Pi).

Shreya emigrated to the Netherlands in January 2018 to join Medical UltraSound Imaging Center (MUSIC) research group in Radboudumc, Nijmegen for her PhD. She has completed her PhD in functional ultrasound imaging of female pelvic floor in 2023. Shreya also met her partner to be, Guido Huiskamp in Nijmegen and together they welcomed their daughter Siya in 2020.

E-mail: shreyads2014@gmail.com

Radboudumc
university medical center
IN DEI NOMINE FELICITER
Radboud University